Technische Universität München
TUM School of Natural Sciences

Tailoring Complexity for Catalyst Discovery Using Physically Motivated Machine Learning

Wenbin Xu

Vollständiger Abdruck der von der TUM School of Natural Sciences der Technischen Universität München zur Erlangung des akademischen Grades eines

Doktors der Naturwissenschaften (Dr. rer. nat.)

genehmigten Dissertation.

Vorsitz: Prof. Dr. Barbara Lechner

Prüfer der Dissertation:

1. Prof. Dr. Karsten Reuter
2. Prof. Dr. Ulrich K. Heiz
3. Prof. Dr. Oliver T. Hofmann

Die Dissertation wurde am 11.10.2022 bei der Technischen Universität München eingereicht und durch die TUM School of Natural Sciences am 07.11.2022 angenommen.

Preface

This dissertation is a publication-based doctoral thesis. It is based on independent articles that have been published in international peer-reviewed scientific journals.[1–3] The first chapters of this dissertation primarily serve as an introduction to the motivation and related methodological developments, followed by summaries of each published article in chapter 6. The majority of the presented work was carried out at the Chair of Theoretical Chemistry of the Technical University of Munich (TUM) between October 2018 and January 2021 and was completed between February 2021 and September 2022 at the Fritz Haber Institute (FHI) of the Max Planck Society in Berlin, both times under the supervision of Prof. Dr. Karsten Reuter.

Abstract

High-performing heterogeneous catalysts are key to a greener chemical industry and future sustainability. In-silico catalyst screening and discovery provide efficient and cost-effective solutions for finding suitable catalysts. Their implementations are commonly driven by the use of quantum mechanical calculations (density functional theory, DFT) to predict catalytic properties. Unfortunately, these calculations are prohibitively computationally demanding, thus incapable of searching the huge chemical space. As an alternative, earlier developed data-driven approaches, e.g., linear scaling relations (LSRs) that bypass fully explicit DFT calculations, have made notable advancements to expedite catalyst discovery on simple catalyst systems, e.g., transition metals (TMs) and monodentate adsorbates. However, given the intrinsic complexity of heterogeneous catalysis, such oversimplified approaches are not applicable for complex catalyst materials and reaction networks in terms of predictive accuracy. The emergence of machine learning (ML) has opened the road to tackling more realistic models of heterogeneous catalysts.

In this publication-based thesis, we seek to develop physics-motivated machine learning models to address the complexity of materials and adsorbates for screening heterogeneous catalysts with a particular focus on transition metal oxides (TMOs) and larger adsorbates that may exhibit mono-, bi- or higher-dentate adsorption motifs at TMs. The ML methods employed range from the Compressed Sensing SISSO method, which seeks descriptors in the form of analytical functions, to Gaussian Process Regression (GPR) with a physics-inspired graph representation. The resulting predictive accuracy that is on par with quantum mechanical calculations, along with great adaptability of these models, make them promising for finding high-performing catalysts across a broad class of materials and complex reaction networks.

Zusammenfassung

Leistungsstarke heterogene Katalysatoren sind der Schlüssel zu einer umweltfreundlicheren chemischen Industrie und zu künftiger Nachhaltigkeit. Dabei bietet ein in-silico Katalysatoren Screening eine effiziente und kostengünstige Lösung für die Suche nach geeigneten Katalysatoren. Ein solches Screening wird in der Regel mit Hilfe von quantenmechanischen Berechnungen (Dichtefunktionaltheorie, DFT) durchgeführt, wobei katalytische Eigenschaften vorhergesagt werden können. Bedauerlicherweise sind diese quantenmechanischen Berechnungen sehr rechenintensiv und daher meist nicht in der Lage, den riesigen vorherrschenden chemischen Raum zu erkunden. Als Alternative werden daher frühzeitig entwickelte datengesteuerte Ansätze, wie z. B. lineare Skalierungsrelationen (LSR) verwendet, welche explizite DFT-Berechnungen umgehen. Diese haben für einfache Katalysatorsysteme, wie z. B. Übergangsmetalle (TMs) und monodentate Adsorbate, bemerkenswerte Fortschritte erzielt und somit die Entdeckung von Katalysatoren vereinfacht. Angesichts der inhärenten Komplexität der heterogenen Katalyse sind solche vereinfachten Ansätze jedoch, im Hinblick auf die Vorhersagegenauigkeit, nicht für komplexe Katalysatormaterialien und deren Reaktionsnetzwerke geeignet. Mit dem Aufkommen von Methoden des maschinellen Lernens (ML) eröffneten sich Möglichkeiten, diese datengesteuerte Ansätze mit Bedacht anzupassen, um realistische Modelle von heterogenen Katalysatoren in Angriff zu nehmen.

Diese publikationsbasierte Dissertation befasst sich daher mit der Entwicklung von physikalisch motivierten Modellen des maschinellen Lernens, welche die Komplexität von Materialien und Adsorbaten für das Screening heterogener Katalysatoren erfassen. Hierbei liegt der Schwerpunkt auf Übergangsmetall Oxiden (TMOs) und größeren Adsorbaten, die ein-, zwei- oder mehrzähnige Adsorptions-Motive an TMOs aufweisen können. Die verwendeten ML-Methoden reichen von der SISSO-Methode (Compressed Sensing), die Deskriptoren in Form von analytischen Funktionen sucht, bis zur Gauß Prozess Regression (GPR), die zusammen mit einer von der Physik inspirierten Graphendarstellung verwendet wird. Die daraus resultierende Vorhersagegenauigkeit, welche mit quantenmechanischen Berechnungen vergleichbar ist und deren große Anpassungsfähigkeit, machen diese Methoden vielversprechend für die Suche nach hochleistungsfähigen Katalysatoren für eine breite Klasse an Materialien und komplexen Reaktionsnetzwerken.

Contents

1 Introduction

Enabling a sustainable energy future is one of the grand challenges that confront modern human society.[4–6] The proposed sustainable energy system by Kutscher et al. states that "sustainable development should meet the needs of the present without compromising the ability of future generations to meet their own needs".[7] Among its definitions, environmental aspects such as greenhouse gas (GHG) emissions, as well as social and economic aspects such as energy poverty, must be addressed.[7, 8]

GHG emissions such as carbon dioxide are primarily caused by burning fossil fuels for electricity, heat and chemical manufacturing. The resulting climate change has a significant effect on the environment, agriculture and human health. Energy poverty refers to the situation where households cannot access or afford essential energy services and products for day-to-day living requirements. It is typically due to the lack of energy-saving techniques and lack of modern energy infrastructure in rural areas, which drastically impacts economic development and public health.

The efficient utilization of renewable energy can address both GHG emissions and energy poverty problems through a sustainable fossil fuel-free path. As demonstrated in Fig. 1.1, such a fossil fuel-free path can be enabled by an energy infrastructure consisting of synthetic fuels and electro- and photo-powered chemical industry, both using plentiful feedstock offered from Earth's atmosphere such as H_2O, CO_2, and N_2.[9–11] In contrast to fossil fuels, renewable energy sources are replenishable, spread across large geographical areas and can reduce environmental pollution while also resulting in significant energy security and economic benefits.[12] However, one major drawback is that their generation time does not coincide with human energy demand, and intermittent power is difficult to use persistently. Therefore, efficient energy conversion and energy storage techniques are needed to enable transportation of, for example, electricity and chemical energy via key vehicles such as batteries and fuel cells.

Improving thermal-driven catalytic processes can also alleviate energy poverty. For example, Fischer-Tropsch chemical reactions[13–16] to synthesize higher alcohols and the Haber-Bosch process[17–21] to generate ammonia fertilizer typically occur under harsh conditions.[22] Enabling these processes under milder conditions makes them less energy intensive and more affordable. This also offers the prospect for decentralization of energy infrastructure, where components can be placed nearer to rural areas to meet local requirements of energy and food consumption. Nevertheless, among most of these sustainable energy processes, the holy grail to providing cost-effective and scalable solutions is undeniably high-performing heterogeneous catalysts. Their importance lies in driving these sustainable energy processes with appropriate efficiency and selectivity by reducing reaction barriers.

The development of high-performing catalysts can be achieved by a combination of theoretical and experimental studies using the following approach.[9, 23] First, theoretical investigation using *ab initio* methods such as density functional theory (DFT) coupled with thermodynamic and microkinetic models can predict the properties of several promising catalyst candidates and eliminate many other candidates. Second, experimental synthesis and performance tests are

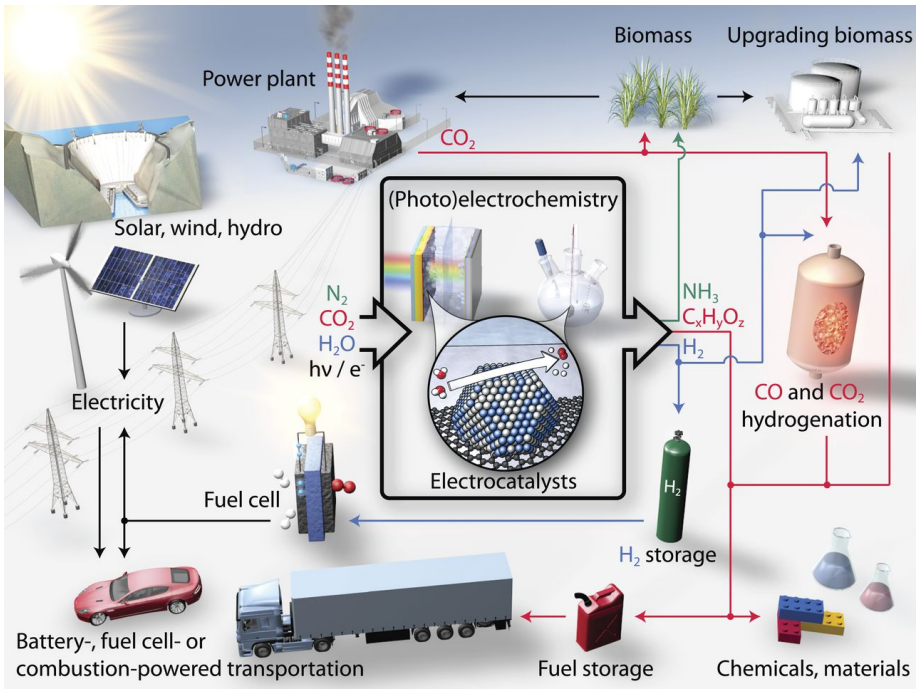

Fig. 1.1: *Schematic of a sustainable energy landscape relevant to renewable energy utilization and climate change based on heterogonous catalysis (primarily electrocatalysis). Figure reproduced with permission from ref. [9]. Copyright 2017 Nature Publishing Group.*

followed up on proposed promising catalysts. Third, the further optimization or next iteration relies on the obtained insight to improve the catalyst's composition or structure in a meaningful way. It turns out that all steps in this feedback loop, close-coupling theoretical and experimental studies, are important. However, such a protocol is only applicable for a small search space. It becomes unfeasible when considering a huge chemical space across the compositional and structural diversity, where the bottlenecks lie in computationally expensive DFT calculations at the first stage.

Of course, this limitation has been recognized for a long time, so catalysis researchers have started to utilize data-driven approaches by constructing descriptors to mitigate this increasing computational demand. Notable examples are the d−band model (a descriptor-based approach)[24–28] and linear scaling relations (LSRs).[29–37] These are based on the importance of only one or a couple of physical quantities that have made notable advancements in many studies compared to fully conducting explicit DFT calculations. However, these models are simplified and thus hard to extend to more sophisticated scenarios with complex materials and adsorbates, which are needed for many catalytic reactions in reality.

Constructing descriptors exclusively by hand and chemical intuition is a daunting task, and they are typically restricted to conceivable low dimensionality, thus hindering the development of potentially more accurate descriptors achieved in high-dimensional and non-linear forms. Fortunately, the rise of machine learning (ML) algorithms opens up opportunities, providing effective solutions to approximate sophisticated relationships, i.e., the map of input features to properties of interest by automatically learning from data.

In this regard, a recent study by Andersen and co-workers[38] in our group has demonstrated the

usefulness of the Compressed Sensing based approach, known as sure independence screening and sparsifying operator (SISSO),[39, 40] for screening transition metal (TM) and TM alloy catalysts, where the accuracy of predicted adsorption energies has been systematically improved relative to standard LSRs by using identified high dimensional descriptors. Motivated by its success, in this dissertation, we first attempt to extend this approach to address complex materials, i.e., doped rutile-type transition metal oxides (TMOs) (IrO_2 and RuO_2).[41, 42] Next to establishing a systematic first-principles database for the SISSO training, we carefully compiled a list of primary features for this class of materials. The resulting high-dimensional descriptors, identified by means of SISSO, showed high accuracy and demonstrated significant advancements in a follow-up screening study.[1] Since this SISSO-based work and most peer's frontier ML/catalysis research were limited to the scope of tackling small adsorbates, we were then asked if our method would also work well for larger, more complex adsorbates that may bind to the surface in many possible configurations. Deliberating on the important features missing from this problem, the connectivity between molecule and catalyst surface, we strive to develop a graph-based ML approach while using informative primary features.[2]

The predictive power reached and physical insights gained in these two works pave the way for efficient catalyst screening and discovery moving towards more complicated materials and reaction networks.[1, 2] Since these results have been published in peer-reviewed articles, this publication-based dissertation serves as an informative storyline for the evolution of data-driven approaches in heterogeneous catalysis and supplies a general guideline for developing and using physics-based ML models for catalyst screening and discovery.

The chapters are arranged as follows: we begin by introducing catalytic modeling techniques for predicting catalytic properties (chapter 2) and highlight adsorption enthalpies as their main input. Then, we describe how conventional data-driven approaches help quickly predict this quantity (chapter 3), followed by the intrinsic complexity in heterogeneous catalysis for which these traditional methods are not applicable (chapter 4). A detailed discussion of ML solutions, their key components and the useful toolkit for leveraging ML models are described in chapter 5.

2 Catalysis modeling and density functional theory

Modern modeling of heterogeneous catalysis relies heavily on density functional theory owing to its high accuracy in calculating electronic structures and associated energetics for a given atomic structure at a relatively low cost.[43, 44] In a dream scenario, a comprehensive theoretical investigation should be carried out by exploring the whole (ground-state) potential energy surface (PES)[45, 46] with the help of DFT calculations. Unfortunately, exploring the high-dimensional (3N dimensions where N is the no. of atoms) PES is extremely difficult and resource-consuming. Instead, one prefers to construct a whole new (reduced) PES for each elementary step in the catalytic cycle, namely based on the critical features of a PES, e.g., lowest-lying local and global minima and 1st order saddle points corresponding to (meta)stable configurations and transition states. Focusing on such critical features or even fewer elementary steps like the rate-limiting step enables efficient catalysis research on a high-throughput basis.

The fundamental responsibilities of catalyst screening and discovery include promptly assessing the stability, activity and selectivity of possible candidate catalysts in a vast chemical space. Stability will determine the active life of the catalyst, and activity and selectivity are of significant importance ecologically and economically regarding the cost of the reaction. In catalysis research, many thermodynamic- and microkinetic-based models have been used to screen these catalyst performances for solid-gas thermocatalysis[47, 48] and solid-liquid electrocatalysis.[9, 49]

2.1 Thermodynamic models

Thermodynamic properties of a system can be predicted from its chemical potential or Gibbs free energy that is in need of total (electronic) energy directly amenable to DFT calculations,[43, 50] reflecting a state that had a sufficiently long time to equilibrate fully. By leveraging thermodynamic-based models, intrinsic thermodynamic tendencies and criteria for certain chemical processes can be assessed under varying environmental conditions, e.g., temperature, pressure, pH, and applied voltage. These thermodynamic models have gained tremendous success in assessing catalytic performance, e.g., stability, activity and selectivity on a wide range of reactions and a broad class of materials.

In practice, stability of the configuration of central interest should be the property to estimate in the first place. An illustrative example in thermochemistry is the surface phase diagram which demonstrates the most stable surface structure as a function of temperature and pressure.[47, 51] Figure 2.1 depicts a surface phase diagram for CO oxidation at Pd(100) surface, where Rogal and co-workers assessed a set of 191 possible surface configurations and found only 11 to be most stable in a certain range of (T, p_{O_2}, p_{CO}) gas phase conditions and most illustrated adsorption structures have been observed in ultrahigh vacuum (UHV) experiments. The corresponding method has also been applied to TMO (RuO_2) surfaces.[48, 52] Likewise, in electrochemistry surface Pourbaix diagram serves the equivalent purpose of expressing surface stability as a function of electrode

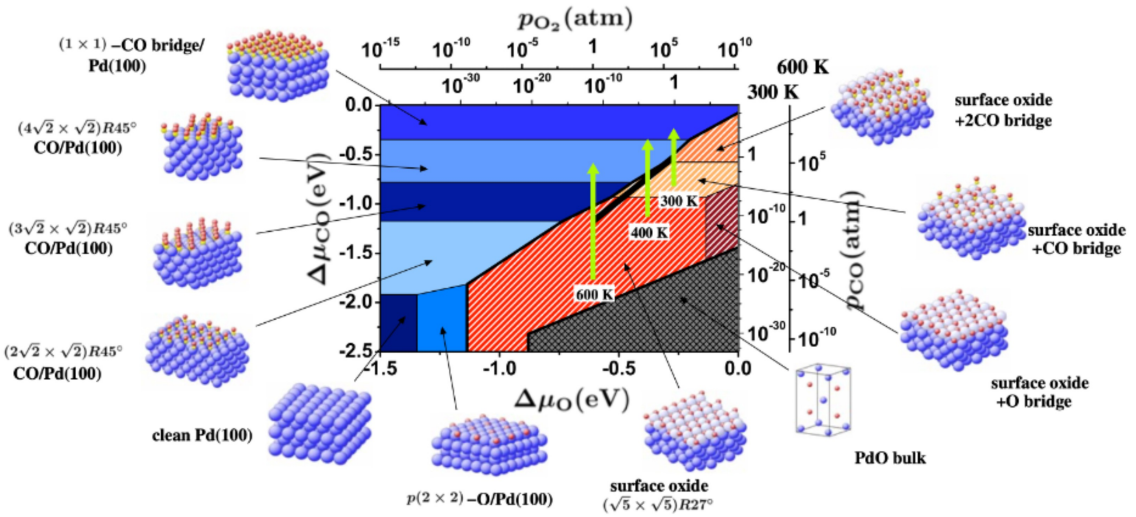

Fig. 2.1: *Ab initio thermodynamics: Surface phase diagram for the Pd(100) surface in "constrained" thermodynamic equilibrium with an environment consisting of O_2 and CO. The atomic structures underlying the various stable (co-)adsorption phases on Pd(100) and the surface oxide, as well as a thick bulklike oxide film (indicated by the bulk unit-cell), are also shown (Pd : large spheres, O : small spheres, C : white spheres). Reprinted with permission from ref. [47]. Copyright 2007 American Physical Society.*

voltage and pH. It has been used to understand many electrochemical landscapes such as TMs,[53] transition-metal carbide[54] and Li-ion battery materials.[55, 56].

Further combining this class of approaches with Wulff constructions, one is able to determine the equilibrium shape of nanoparticle shapes and dominant facets exposed.[57–59] Moreover, various reconstructive/deactivating processes, such as surface segregation, island formation, metal dissolution, and surface poisoning, can also be investigated, as exemplified in a high-throughput screening study of a variety of surface alloys.[60] It is worth noting that such thermodynamic stability evolution can help us determine the realistic surface morphology and how synthesizable the surface is, thus providing necessary information to establish an active site model for a subsequent screening study.[61]

After establishing stability, one could turn to predict the activity and selectivity of the promising candidates thermodynamically. For example, in electrochemistry, overpotential (or onset potential) is one of the vital activity metrics, often well-described by purely thermodynamic models, which can be experimentally determined by measuring the (typically small) current density as a function of applied voltage between electrodes. In theory, there is a well-established protocol to obtain it theoretically. First, one could construct a reaction free-energy diagram by including potential and pH effects via the computational hydrogen electrode (CHE) model[62] and solvent stabilization corrections to the key intermediates. Then the overpotential can be approximately gained via the thermodynamic barrier of the potential-limiting step under various applied potentials. Figure 2.2a demonstrates oxygen evolution reaction (OER) overpotentials over a wide variety of TMO surfaces from both theoretical and experimental data, and an appealing overlay can be observed, indicating reasonable prediction from theoretical thermodynamic modeling. This approach can be generalized to any electrochemical reaction with proton-coupled electron transfer (PCET) processes and has been dominating contemporary first-principles-based works on reactions such

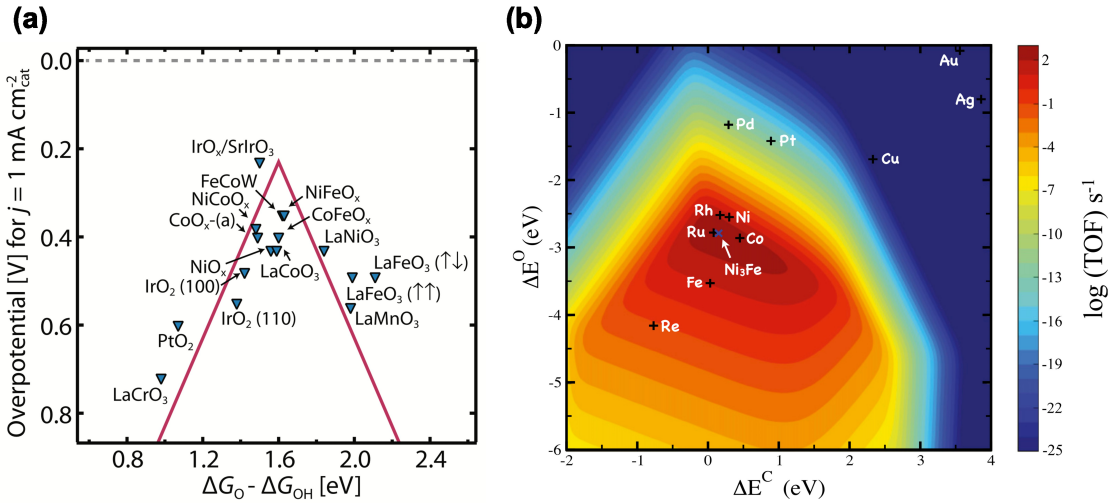

Fig. 2.2: *a) Descriptor-based activity plots: OER overpotential for a set of metal oxides combining theoretical and experimental data. Figure reproduced with permission from ref. [9]. Copyright 2017 Nature Publishing Group. b) Microkinetic modeling activity: the turnover frequency via MFA for the production of methane from syngas on stepped TMs (211) surfaces. Reproduced with permission from ref. [43]. Copyright 2011 National Academy of Sciences*

as hydrogen evolution reaction (HER),[49, 63–65] oxygen evolution reaction (OER),[1, 41, 42, 62] oxygen reduction reaction (ORR),[66, 67] and carbon dioxide reaction (CO_2RR)[68–70] on TMs and their alloys, TMOs, sulfides, and carbides etc. Note that going beyond the CHE model to include capacitative charging at the solid-liquid interface, there has been emerging interest in developing implicit solvation models within the past few years.[71]

Moreover, the selectivity can also be qualitatively evaluated. E.g., in ORR the selectivity of the two-electron pathway to produce H_2O_2 against four-electron pathways to produce H_2O was calculated based on the binding energy of key intermediates, $\Delta G_{H_2O_2} - \Delta G_{O*}$, since catalysts should have weak ΔG_{O*} as much as possible to maximize the H_2O_2 selectivity.[72] As also exemplified, the selectivity of ethanol on a number of (211) surfaces can be estimated by means of ΔE_C, depicting the different slopes of C-CO and C-H binds.[31] Despite the fact that they are not full-fledged screening methods, they may aid in highlighting some trends and locating potential materials for which more in-depth microkinetic models can be run subsequently.

2.2 Microkinetic models

Compared to thermodynamic models that are often only simplified screening studies, microkinetic models go into greater detail by explicitly taking reaction barriers into account, giving a non-equilibrium description of the reaction network, which can further be extended to include effects of surface coverage and lateral adsorbate-adsorbate interaction. In the multi-scale modeling framework, microkinetic models taking the input from quantum mechanical, electronic structure theory (e.g., DFT), can achieve a quantitative description of the reactive chemistry or charge transport at the large scale yielding first-principle microkinetic models (1pMK).[73] Such models are able to provide straightforward theoretical predictions of experimental observation, such as

the catalytic activity and selectivity in terms of the turnover frequencies (TOFs, product molecules per time and site) as a function of partial pressure and temperature in thermocatalysis, or in terms of current density (ampere per surface area) as a function of pH and applied voltage in electrocatalysis.

The popular 1pMK methods in this field include Mean-field approximation microkinetic (MFA) and spatially resolved kinetic Monte Carlo (kMC) that have shown great success in numerous heterogeneous catalysis studies, such as single atom catalysis,[74] TMs and their alloys,[75, 76] oxides[48, 77] etc. Figure 2.2b shows the output of such a MFA model for the generation of methane on several stepped (211) TMs surfaces. This technique has the advantage of being computationally efficient, but it cannot address spatial information and anisotropic systems since in MFA the spatial distribution of the adsorbates is coarse-grained into a mean coverage, ignoring coverage fluctuations, for which kMC is required. A comparison of MFA and kMC to the influence of adsorbate-adsorbate interactions in CO hydrogenation on rhodium catalysts has been explored, and it revealed that efficient modeling of lateral interactions in kMC is vital to capture subtle mechanistic insights of complicated reaction networks.[78] Without the use of a fixed lattice, adaptive kMC (on-the-fly) may be more effective at handling dynamic processes, but it is also significantly more expensive, given the current computing power.[79] Readers are referred to a recent survey and practical guidelines for the 1pMK models.[73, 80, 81]

It should be noted that in the scope of catalytic research, as a coarse-grained method, 1pMK achieves an enormous speedup over molecular dynamic (MD) simulations by the explicit treatment of the vibrational degrees of freedom of the system, and instead considering only the rare events such as adsorption/desorption, diffusion or reaction steps. However, (accelerated) MD methods could be used to gather the reaction mechanisms and rates, e.g., derived from the Arrhenius equation,[79, 82] that are required to parameterize a 1pMK model.

2.3 At the core: adsorption enthalpies

The key ingredient of thermodynamic and microkinetic models mentioned above is adsorption enthalpy. Its significance was earlier highlighted in the Sabatier principle,[83–85] a general explanatory paradigm, which states that the adsorption strength should be neither too weak which would prevent the reactants from being adsorbed and activated, nor too strong which makes the products contaminate the catalyst surface. It is also later underpinned by a well-established volcano plot,[86] a quantitative illustration of the Sabatier principle, taking the adsorption enthalpies of key intermediates as descriptors, and the catalytic activity occurs in a volcano shape whose peak presents optimal catalysts equipped with moderate binding strength. Most importantly, Brønsted–Evans–Polanyi (BEP) relations (see chapter 3.2) leverage adsorption enthalpies in the form of reaction energies that scale with kinetic barriers, thereby empowering good activity prediction from thermodynamic descriptors. These basic principles behind catalyst discovery provide key ideas on catalyst screening or design studies.

The way that adsorption enthalpies are incorporated in thermodynamics models, such as surface Pourbaix/phase diagram (if referencing to clean surface), thermodynamic deduced overpotential and selectivity, is through direct input to the calculations as introduced in chapter 2.1. However, additional derivations are needed to obtain the kinetic barriers which are further fed into the microkinetic models. Typically, such derivations are through a simple linear fitting of the adsorption enthalpies, that is BEP relations[87, 88] (as we will delineate later in chapter 3.2), which enables

an enormous reduction of the computational cost and expedites catalyst screening substantially. In contrast, an alternative explicit search of the lowest first-order saddle point on the PES at the first-principles level to get kinetic barriers using the interpolation method (nudged elastic band, NEB) [89, 90] or local method (dimer method)[91] is computationally intensive, but it is useful to define a BEP relation. One catch that has to be paid more attention to is the quality of the kinetic barrier fitted or calculated, whose error is crucial to the 1pMK models according to large error propagation. In this regard, the calculation of electrochemical kinetic barriers (including their potential dependence) is much more difficult with current techniques in comparison to the non-electrochemical steps. Thus more research effort is needed to improve the fundamental theoretical modeling of electrochemistry, e.g., developing better models for the electrified solid-liquid interface or developing constant-potential methods.

The conventional method of getting adsorption enthalpies is from explicit DFT calculations, as elaborated in chapter 2.4. Despite the steeply increasing computational power and algorithmic efficiency, this approach becomes infeasible in exploring vast chemical space in terms of the complexity source from catalyst, adsorbate and environment (the complexity of various resources will be discussed in chapter 4). To this end, the efficient prediction of adsorption enthalpies at about comparable accuracy against the first-principle level is required. Great progress has been made in the past couple of decades to get cheaper adsorption enthalpies from data-driven approaches to more sophisticated machine learning methodologies. It is encouraging to see that more and more bottlenecks have been addressed. However, some issues still persist in catalysis research in need of a thoughtful model design to handle complexity sources. A full discussion regarding the earlier employed data-driven techniques and cutting-edge machine learning is elaborated in chapters 3 and 5, respectively. This is at the heart of this thesis.

2.4 Density functional theory in a nutshell

Since the construction of data-driven/machine learning databases (including the calculations of adsorption enthalpies) relies on DFT calculations, we will briefly recapitulate the most significant ideas behind DFT in this section.

The use of conventional (electronic) wave-function-based techniques is hampered by a huge number of variables. For instance, the N-particle Schrödinger equation must handle 3N spatial coordinates where N is the number of electrons. To mitigate this issue, the Hohenberg–Kohn theorems,[92] that is the basic foundation of DFT, guarantee that there exists a functional of the (ground-state) electron density, $\rho(\mathbf{r})$, yielding the total energy. It therefore dramatically reduces the number of variables from 3N to 3 spatial coordinates described as:

$$E_{HK}[\rho(\mathbf{r})] = V_{ne}[\rho(\mathbf{r})] + T[\rho(\mathbf{r})] + V_{ee}[\rho(\mathbf{r})] \tag{2.1}$$

$V_{ne}[\rho(\mathbf{r})]$, $T[\rho(\mathbf{r})]$, and $V_{ee}[\rho(\mathbf{r})]$ denote the potential between nuclei and electrons, the kinetic energy functional, and the electron-electron interaction potential, respectively. Unfortunately, exact expressions for the $V_{ee}[\rho(\mathbf{r})]$ and $T[\rho(\mathbf{r})]$ functionals are unknown.

$$E_{KS}[\rho(\mathbf{r})] = V_{ne}[\rho(\mathbf{r})] + T_{KS}[\rho(\mathbf{r})] + J[\rho(\mathbf{r})] + E_{xc}[\rho(\mathbf{r})] \tag{2.2}$$

Within this framework, the great breakthrough afterward was achieved by Kohn and Sham (KS-DFT)[93] that leverages an imagined system of non-interacting electrons having the same electron density as the real system. In this way, they can explicitly write out these two unknown terms via classical electron-electron repulsion and non-interaction kinetic energy as shown in equation 2.2, where the (ground-state) electron density can be constructed by summing together all occupied KS orbitals (imagined), $\Phi_i(\mathbf{r})$, as:

$$\rho(\mathbf{r}) = \sum_i |\Phi_i(\mathbf{r})|^2 \tag{2.3}$$

The resulting corrections, i.e., $(V_{ee}[\rho(\mathbf{r})] - J[\rho(\mathbf{r})])$ and $(T[\rho(\mathbf{r})] - T_{KS}[\rho(\mathbf{r})])$, were lumped together into the exchange-correlation energy, $E_{xc}[\rho(\mathbf{r})]$, which is the most problematic part with unknown form, and its choice often depends on what types of physics and chemistry should be described.[94, 95] Much effort has been devoted to improving this approximation term, leading to a vast family of density functional methods that can be assigned to five rungs of the "Jacob's ladder".[96, 97] In terms of computational cost and complexity, these methods range from local density approximation (LDA), generalized gradient approximation (GGA), meta-GGA, hybrid functionals and random-phase approximation (RPA), among which GGA with Perdew–Burke–Ernzerhof (PBE)[98] functional is one of the most popular and cost-effective choices for many applications in condensed matter physics. However, the lack of van der Waals (vdW) dispersion[99] in GGA-PBE and the self-interaction error[100, 101] can be crucial that hinder the application in surface science. To this end, one notable development in general-purpose surface reactions was the Bayesian error estimation with van der Waals correlation (BEEF-vdW) functional designed by Wellendorff and co-workers.[102] The BEEF-vdW functional can provide quantitatively accurate predictions and additional error estimation based on an ensemble of functionals, making it highly popular in modern heterogeneous catalysis studies.

Next, how can we get adsorption enthalpies? By carrying out a single-point DFT calculation on a given atomic configuration of a system, the electronic energy is obtained, and atomic forces can be computed from the Hellmann-Feynman theorem.[103] The atomic force can further drive structural relaxation with the help of optimization algorithms such as the conjugate gradient (CG) method[104] and the Broyden–Fletcher–Goldfarb–Shanno (BFGS)[105] algorithm to iteratively update atomic positions until the energy of the system reaches a local minimum (on the PES). Then, the corresponding adsorption enthalpies can be routinely calculated by the energy difference between the relaxed combined surface/adsorbate system and isolated systems (clean surface and gas molecule). Unfortunately, the KS-DFT still scales as $O(\mathrm{N}^3)$ with N being the number of atoms in the system, restricting its application to calculate a system with around one hundred atoms.[106]

3 Conventional data-driven approaches in heterogeneous catalysis

Data-driven approaches seek to infer some physical laws or surrogate models (hopefully simple) from data so that the properties of interest (in this case, the adsorption enthalpy) can be directly assessed through the efficient first-principles computation of only one or a few central energetic or electronic quantities. These identified physical quantities are so-called descriptors. There has been a long history of utilizing data-driven approaches in catalysis, where most works attempt to extract chemical insight from descriptors to better understand the interplay between electronic or structural effects and material properties. This chapter is primarily meant to survey the conventional data-driven approaches in heterogeneous catalysis, some of which are still frequently utilized in this field and lay the way for the discussion of advanced machine learning methods (in chapter 5) and possible opportunities.

3.1 Descriptors

At the early stage, considerable research efforts have been put into the discovery of a single (one-dimensional) descriptor. The first representative instance is the ingenious $d-$band model,[24–28] where the binding energies of atomic species such as C and O on TM surfaces are found to be correlated with the energetic position of the $d-$band of the corresponding bulk material, as shown in Fig. 3.1a. This model links the intrinsic material property to the surface activity and underpins the fundamental understanding from the electronic structure level. Later on, the $d-$band model was extended to the active site of bare surfaces through the projected density of states (PDOS) to capture the general trend of composition and motifs of active sites. This considerably translates the catalyst design to the design of fine-tuned active sites.[1, 38, 61] It should be mentioned that the $d-$band model originated from the pure TMs and their alloys, which seldom generalize to other materials. In the case of 2D single-atom catalysts, instead, the number of electrons in the outmost $d-$shell of transition metal correlates with $G_{\mathrm{OH}*}$,[110] and for metal nitride redox materials, the number of electrons in the dopant $d-$states are found to be important.[21] Concerning TMOs, different single descriptors are judged to be crucial in emphasizing the role of e_g orbital filling [107, 111, 112] shown in Fig. 3.1b or of the O_{2p} band center[113] or of the charge transfer energy, respectively.[114, 115] These simplest single descriptors mentioned above provide valuable insights not only to the theoretical understanding but also to direct experimental synthesis.

Yet, a single descriptor maybe not necessarily dominate the catalytic performance. For complicated materials with a more intricate electronic structure it is likely governed by multiple geometric and electronic quantities. This naturally leads to the exploration of high-dimensional descriptors with more predictive power. There are some attempts in the literature to search for conceivably higher dimensional descriptors from heuristic or chemical intuition (see Fig.3.1c and d), for example, the combined role of the number of electrons in the metal ground state and their energies in metal nitride catalysts,[109] and the synergistic effect of both geometric and electronic

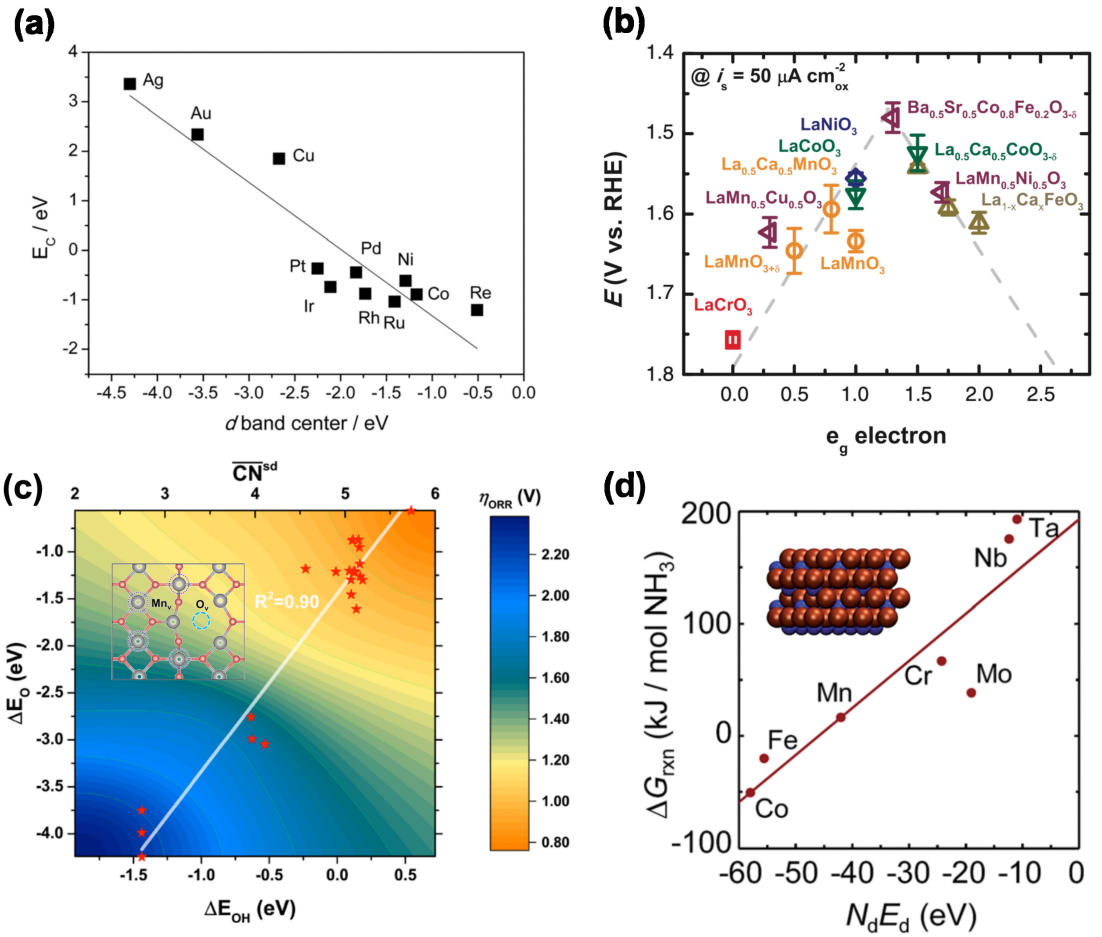

Fig. 3.1: *Single descriptor examples: a) the relation between metal d−band center and C binding energy. Adapted with permission from ref. [26]. Copyright 2000 by Academic Press. b) The relation between occupancy of the e_g−symmetry electron of the transition metal and OER overpotential. Reproduced with permission from ref. [107]. Copyright 2011 American Association for the Advancement of Science. Multi-dimensional descriptor examples: c) the relation between bond-energy-integrated orbital-wise coordination number and catalytic behavior of the β-MnO_2 surface. Adapted with permission from ref. [108]. Copyright 2018 American Chemical Society. d) The relation between N_dE_d (the number of d electrons and their energies) and the free energy of the NH_3 evolution via metal nitride. Adapted with permission from ref. [109]. Copyright 2015 The Royal Society of Chemistry.*

structures around the active site yielding the bond-energy-integrated orbital-wise coordination number to the prediction of TMOs.[108] These approaches highly relying on human intuition are apparently inefficient, when going for even higher dimensions to obtain better predictive performance. In this regard, one could ask for the help of an advanced ML algorithm to construct a huge descriptor space and identify sparse solutions or reduce the dimensionality through a compressed sensing-based method or principle component analysis (PCA) as will be discussed in detail in chapter 5.

It should be emphasized that descriptor-based methods belong to so-called discrete models, i.e., bypassing construction of the entire PES, not limited to predicting catalytic activity but also other chemical properties. Due to the inclusion of more physics, these methods merit great generalization across elements, giving somewhat of interpretability through mathematically analytic equations.

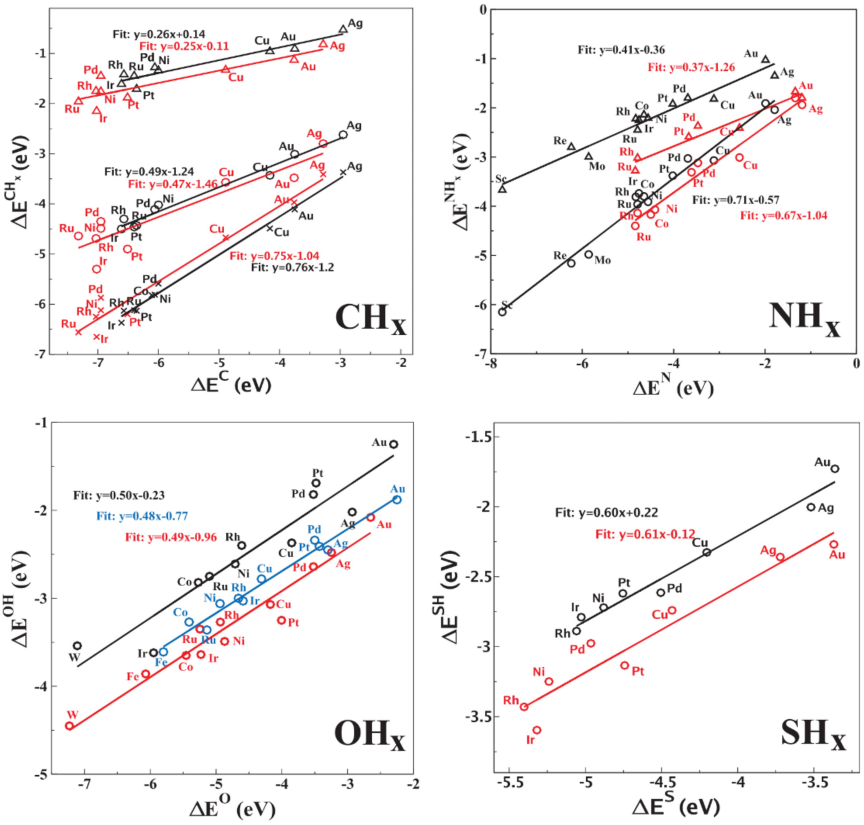

Fig. 3.2: *Binding energy linear scaling relations: adsorption energies of CH_x intermediates (crosses: x = 1; circles: x = 2; triangles: x = 3), NH_x intermediates (circles: x = 1; triangles: x = 2), OH, and SH intermediates plotted against adsorption energies of C, N, O, and S, respectively. The adsorption energy of molecule A is defined as the total energy of A adsorbed in the lowest energy position outside the surface minus the sum of the total energies of A in vacuum and the clean surface. The data points represent results for close-packed (black) and stepped (red) surfaces on various transition-metal surfaces. In addition, data points for metals in the fcc(100) structure (blue) have been included for OH_x. Adapted with permission from ref. [29]. Copyright 2007 American Physical Society.*

3.2 Linear scaling relations

Another widely used subset of conventional data-driven techniques is linear scaling relations (LSRs). Its primary input is adsorption enthalpies rather than fundamental physical quantities, i.e., electronic and geometric properties. In terms of their goals, there are two classes of LSRs used in catalysis research: a) extending the adsorption enthalpies of simple atomic species to larger fragments, namely binding energy linear scaling relations (BELSRs) shown in Fig. 3.2 and b) approximating the kinetic barrier by fitting the adsorption enthalpies of key intermediates, that is Brønsted-Evans-Polanyi (BEP) relations displayed in Fig. 3.3b. In the former class, the concept was initialized on reactions involving hydrogenation of rather inert species like the Haber-Bosch process and methanation, where NH_x and CH_x binding energies are found to be linearly correlated to that of their central atoms, N and C.[29, 116, 117] This can be attributed to the valency considerations of the number of hydrogens relative to their atomic species being a unique descriptor. Despite its simplicity, a similar linear trend has also been found for many surface adsorbates like C_2 hydrocarbon species, where the binding energy of C_2H-type adsorbates on Cu, Ag and Au surfaces show a scaling relation with their atomic C counterpart.[118] From there, one could rapidly construct a reaction network including many intermediates by means of exclusively calculating the simplest atomic species. This elegant protocol has been used extensively in modern catalysis research to access favorable reaction thermochemistry. For instance, selective hydrogenation of acetylene to ethylene on various transition metal alloy surfaces has been investigated by leveraging merely the binding energy of CH,[37] and the conversion of synthesis gas to higher alcohols on a number of 211 surfaces is studied by Medford and co-workers on the basis of two parameters, binding energies of C and O.[31]

Despite the enormous success, it should be noted that BELSRs are likely to fail in a variety of circumstances. Similar to the $d-$band model, which was first developed on pure TMs, BELSRs are difficult to apply to other complex compound materials, and additional refinements are needed. A notable example is TMOs[1, 41] with intricate electronic structures resulting in many outliers of larger than 1 eV deviation by applying standard BELSRs. It has been found that additional correction (features) related to local charge transfer to the adsorption energies could further refine the predictive power of BELSRs. The binding geometry of adsorbates is another major factor giving rise to non-linear behavior. It has been suggested that BELSRs are site-specific, e.g., the association between the binding energy of C and CH_3 depends on whether they were constructed on optimal binding sites or on top sites,[29] and similarly, extraordinary adsorption geometry of CH_2O results in non-linear relations of CHO vs. CH_2O on $Mo_2C(100)$ surfaces.[57] Yet, more factors such as alloying,[119] strains[120] and external fields[121–123] are also able to break scaling relations. This is a frontier in catalysis as it enables overcoming the inherent law, that is, adsorption enthalpies of adsorbates with the same binding atoms to the surface are changing proportionally to produce high-performance catalysts. The interested readers are recommended to a recent review for in-depth discussion.[124]

In the latter class of LSRs, as its importance already mentioned in chapter 2.3, BEP relations serve as a useful "glue" to closely tie together thermodynamics and kinetics, thus providing cheaper rate constants to the microkinetic models as compared to calculating barriers and rates from first principles. Its original idea is to express the activation energy of a given class of elementary steps as a linear function of the reaction energy, ΔE, and the coefficient of ΔE is 0.5 for symmetric reactions and approaches 0 or 1 depending on whether the transition state structure resembles initial or final states respectively.[126–129] The subsequent development is to construct the transition state

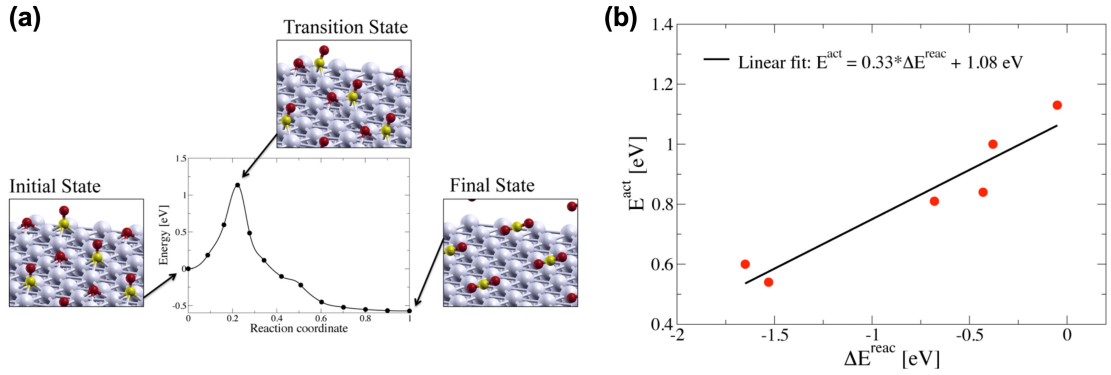

Fig. 3.3: *(a) Nudged elastic band calculation of the minimum energy path for CO oxidation on Pd(111). The figure shows the energy profile along the reaction coordinate and the geometries of initial, transition, and final states in a (3 × 3) unit cell. (b) Linear fit of the dependence of the activation energy on the reaction energy (based on BEP relations). Figure adapted with permission from ref. [125]. Copyright 2014 American Chemical Society.*

energy as a function of initial (E_{IS}) or final (E_{FS}) states with the factors multiplying E_{IS} or E_{FS} to be 1 to remain universal, namely independent on the chosen energy references.[130]

Coupling BEP relations with microkinetic modeling has shown great promise in many catalytic reactions such as CO hydrogenation on rhodium,[78] CO methanation reaction on stepped TMs and binary TM alloy catalysts,[75] as well as CO_2 reduction to CO on Ag.[131] On the downside, the application of BEP relations is limited in that the parameters are, in principle, only transferable to the site types similar to those used in the fitting. Recent work demonstrated a vast underestimation of the TOF on layered $FePd_3$ or $FePd_3$ catalysts, as these surfaces exhibit a reversed energetic ordering of step and terrace sites for OH adsorption. The latter happens because the step sites are composed of the more noble metal (Pt or Pd), whereas the terrace sites are composed of a highly reactive metal (Fe).[75] Thereby, all types of adsorption sites (step, terrace, top, bridge etc.) for all adsorbates have to be considered. Moreover, a criterion for the application of BEP relations for catalytic dissociation reactions has been developed and assessed, thus providing an estimation of when to trust BEP relations in the exploration of complex reaction networks.[132]

As a whole, the introduced BELSRs and BEP relations, capable of quickly obtaining cheaper thermodynamic and kinetic data, are undoubtedly invaluable tools in computational screening that have been used up to now. Unfortunately, the internal error is inconsistent across catalytic systems. Therefore, adopting hierarchical refinement, i.e., predicting maps using BELSRs and BEP relations and refining the essential thermochemistry solely using DFT, is desired.[133] More effort should be placed on the development of new methods with improved predictions.

4 Complexity in heterogeneous catalysis

As discussed in chapter 3, conventional data-driven approaches in heterogeneous catalysis behave well mostly for simple systems such as pure TM catalysts and monodentate adsorbates. Given that real catalytic systems are usually far from simple, it is apparent that further methodological development should account for such complexities that generally arise from three sources: the catalyst, adsorbate and external environment, as sketched in Fig. 4.1. In the following, we will briefly discuss each of these sources of complexity and underline challenges to the development of new methodologies.

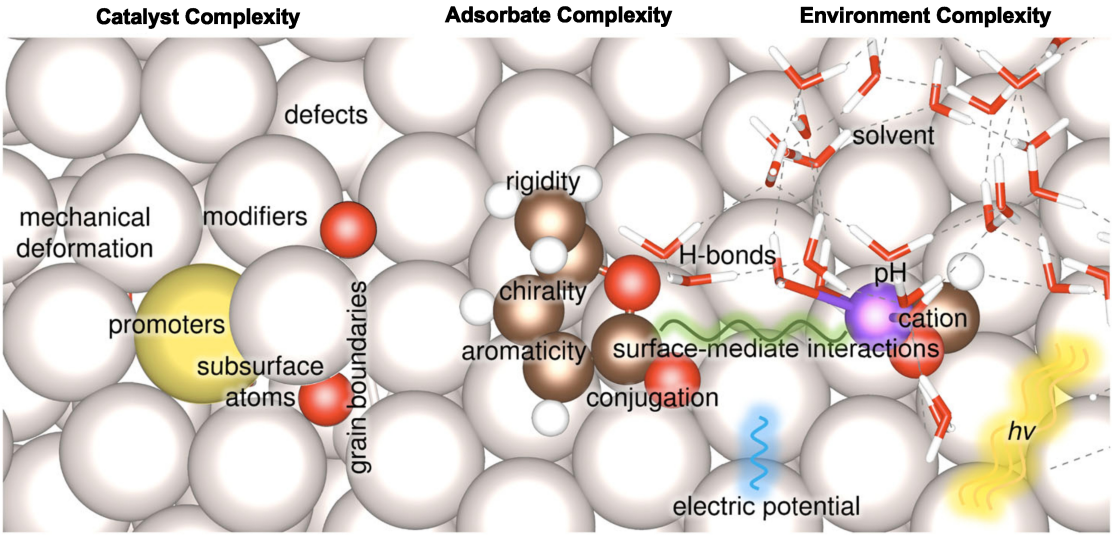

Fig. 4.1: *Sources of complexity in heterogeneous catalysis at the levels of the material, the molecule, and the external factors. Adapted with permission from ref. [134]. Copyright 2021 Wiley Periodicals LLC.*

4.1 Catalyst complexity

The catalyst drives the catalytic process forward by effectively reducing the activation barrier that converts reactants to products. Important solid heterogeneous catalysts include TMs and their alloys,[38] TMOs,[1, 9] zeolites,[135] graphitic carbon,[136, 137] etc., which spans a broad inorganic materials space. In general, the complexity of these catalysts can be categorized into the electronic structure or geometric complexity.

Electronic structure complexity comes either from the intrinsic complicated electronic structure arising from, e.g., composition, or additional modifications. Already a large variety of chemical compositions spanning the entire periodic table are daunting at first glance, and the combination of element species with largely different chemical natures is becoming more formidable. For

instance, compared to TMs, TMOs have more localized and intricate electronic structures where the intact $d-$orbital of the host metal is split up into T_{2g} and E_g orbital based on crystal field theory.[138] Furthermore, the O_{2p} band of coordinated oxygen should also be carefully taken into account, as its overlap with E_g could dramatically affect the local charge transfer between the host metal and coordinated oxygen. TMOs could also be metallic or semiconductors in origin due to the electron alignment around the Fermi level.[139, 140] The additional modifications through dopants, host substrates or promoters can make things even more complicated.[1, 141] These effects together reflect the difficulty of coming up with a single or a few physical quantities, that is, the idea of conventional descriptor-based approaches to govern the behavior of such compound materials.

Geometrical complexity can come from many aspects, such as the geometry of a catalyst, the introduction of a vacancy, strain, defect etc., whose effects one can primarily understand as the role of the active site motifs where the reaction actually happens.[61] Much evidence in the literature has confirmed that changing the size of catalysts, e.g., nanoparticle, affects the ratio of edge sites vs. corner sites that are introduced, therefore leading to variable catalytic performance.[142, 143] The strain engineering technique[144, 145] might potentially build thin films and nanostructured materials beyond their bulk or powder form in terms of coordination numbers. The defect engineering[146] allows for the production of unsaturated active site motifs giving rise to better activating chemical bonds. Therefore, many corresponding works aiming to control surface morphology and active site exposure toward rational catalyst design can be observed in this field. Of course, the size and geometry of catalysts may not be fixed. Realistic catalyst materials are often not well-defined but exhibit an abundance of varied geometric shapes, surface terminations, and non-regular forms, resulting in various active sites responsible for the catalytic action.[147–152] Furthermore, geometric evolution is crucial during operating conditions. For instance, previously unidentified surface reconstructing mechanisms of Pd islands on Ag have been revealed under various temperatures by Lim and co-workers,[153] and recent work suggested that IrO_2 exhibits a dramatic surface reconstruction under different applied voltages. Theoretical studies on a rigid lattice often ignore such operando response.[154]

It should be emphasized that geometric and electronic structures typically have strong relationships and do not change independently. Therefore, rather than focusing on just one of them, it is important to carefully explore the synergistic effect of electronic structure and geometric factors. In this regard, the goal is often to devise an advanced algorithm that can efficiently find multi-dimensional descriptors of these different features.

4.2 Adsorbate complexity

The adsorbate complexity not only relates to the reactants and products but also includes all possible intermediates that could potentially be engaged in reactions. The foremost aspect is the chemical complexity of adsorbates, e.g., composition and functional group. Although there are not many kinds of elements (typically, C, H, O and N) present in organic molecules, the nature of chemical bonds such as C-H single bond, C-C double bond, and N-N triple bonds could be very different to activate. In the presence of several alcohols and amines functional groups, the number of conformations increases exponentially,[155] and the repelling between functional groups may be mediated by the surface (similar results can be obtained due to the covering effect), breaking the thermochemical additivity rule.

The second aspect is underlying diverse binding motifs due to the inclusion of larger adsorbates, which is more crucial. Even for the reaction yielding C_{2+} products, some larger fragments may show a wide range of mono-, bi- and higher-dentate adsorption modes. As exemplified in a pioneering case study, for syngas conversion on a pure Rh(211) surface, the C_2 and oxygenated C_1 and C_2 fragments prefer to adsorb on the surface in a bidentate and, in some cases, tridentate manner, resulting in many thousands of possible intermediates per surface termination.[156] Accordingly, the previously reported catalytic properties constructed by a multitude of, in principle, conceivable intermediates are likely to be misestimated, and the intrinsic reaction mechanism is elusive. We recall that LSRs developed for the oversimplified molecular system, i.e., monodentate, rarely containing more than two central atoms. Thus deviation errors are exacerbated when increasing the size of the adsorbate.[157, 158]

The difficulty of handling larger adsorbates is very often associated with the assembly of a massive reaction network. An instance of a reaction network for the reaction of syngas with intermediates with up to two carbons and two oxygens (C_1/C_2 chemistries) on Rh(111) surface has already demonstrated that there are more than 100 species and 2000 pathways possible.[159] Determining the dominant pathway requires calculations on all adsorbates involved. In this regard, it is highly desirable to have an efficient method to treat these larger fragments and the tools for generating better initial placement of adsorbates and reaction networks. For example, CatKit can only provide adequate initial configurations up to conditioned bidentate motifs,[160] and hence further improvements are needed.

4.3 Environment complexity

Apart from the internal catalyst and adsorbate complexity, the external environment is another source of complexity, including but not limited to temperature, pressure, solvent effect and applied voltage, that can change both catalyst and adsorbate in the course of a catalytic reaction.

High temperature and pressure drive the making and breaking of chemical bonds in thermocatalysis, but may also dynamically change the surface morphology. For instance, the Haber-Bosch process does not proceed at a detectable rate at room temperature due to the high energy needed for activating N–N triple bonds but becomes favorable at high pressure (200 - 400 bar) and temperature (400 - 650 °C). A recent study revisited this reaction using ML-accelerated MD simulations and demonstrated a mobile surface morphology under operation conditions indicating an ensemble effect of the polytropic active surfaces.[161] Moreover, for CO oxidation on RuO_2(100) surfaces, different oxidation states can be identified from both experiments and theoretical predictions.[48, 52]

In electrocatalysis, the effect of the solvent can be equally important. First of all, the presence of solvent may change the diffusion of critical reactants and products, therefore changing their local concentration around the surface and local pH.[162–164] Water solvent can also act as a proton donor, stabilizing important reaction intermediates and thus e.g. tuning the resulting electrocatalytic selectivity. Other solvents, such as ionic liquids, can promote catalytic reactions like CO_2 reduction by altering the saturation of CO_2 and conductivity.[165, 166] The further introduction of additives into solvent could also drastically impact the catalytic performance through interaction with the adsorbate via a functional group or adjust the surface's electronic structure.[167, 168] Moreover, dissolution behavior can be observed on electrocatalyst surfaces under applied voltage. The sum of all these effects makes it difficult to understand catalytic

processes, some of which have simple stages that are either hardly perceptible or buried in the surrounding environment. Therefore, the use of in-situ experiments to offer experimental information to assist us in understanding the chemical process is a popular topic.

At this stage, it is not difficult to imagine that the real catalytic process takes place under a mixed complexity from many of the aforementioned sources. That said, it is, however, also clear that the conventional data-driven approaches necessarily have limitations in addressing these complexities despite their current success. Thus it is our hope that the rise of ML methodologies gives opportunities to circumvent this quandary.

5 Machine learning in heterogeneous catalysis

In the past decades, ML methods have witnessed unprecedented technological breakthroughs enabling a plethora of applications, such as natural language processing,[169] computer vision,[170] automated driving[171] and drug design,[172] some of which have become daily companions in our lives. In parallel, a transformative impact on modern computational chemistry research has also been made by dramatically accelerating computational algorithms and amplifying the available insights. As a result, atomic simulation nowadays is able to break the traditional trade-off between accuracy and speed and can be extended to an unprecedented time and length scale. Notably, one recent effort focusing on length scale has accomplished reactive molecular dynamics of 0.5 trillion atoms concomitantly with quantum-mechanical accuracy for the heterogeneous catalytic system of H_2/Pt(111).[173]

Zooming in the field of heterogeneous catalysis, most predictive ML models are supervised learning-based regression models, which strive to map the structural space or feature space, e.g., structural representation and fingerprint, to property space, e.g., energy (including adsorption energies) and force. This class of predictive models is of great utility for catalyst screening and material discovery.[174–178] Moreover, depending on the fact that whether the aim is to learn the continuous (or entire) region of the PES or only the critical points, these models can be classified into continuous and discrete ML models, respectively. Continuous ML models are generally combined with molecular dynamic or structural relaxation to drive atomic simulation, while discrete ML models can directly give predictions on properties of interest. In this chapter, we will firstly elaborate in-depth on continuous and discrete ML models and then move on to their key elements concerning database, representation and regression methods. Finally, to help ML applications, useful tools will also be discussed.

This chapter is not only intended to introduce certain ML methods but rather serve as guidance on how to use ML to solve scientific problems in heterogeneous catalysis, more specifically, how to address the various levels of complexity discussed in chapter 4.

5.1 Continuous and discrete ML methods.

Continuous ML methods are also known as machine learning (interatomic) potentials (MLPs) or ML force fields. The key idea is to learn a continuous statistical relation between chemical structure and potential energy without relying on a preconceived notion of fixed chemical bonds of knowledge about the relevant interactions, therefore driving molecular dynamic or structural relaxation.[177, 187] As shown in equation 5.1, its general ansatz is to decompose the total energy of the system (E_{total}) as a sum of atomic contributions (E_i) which are based on the atoms' local environments ($\mathbf{R}_i$) within a predefined cutoff. In this way, the resulting ML model is size-extensive and readily extended to large length simulations.

Tab. 5.1: *Overview of recent literature works on the prediction of adsorption enthalpies using machine learning methods.*

Ref	Material	Adsorbate[a]	Features[b]	Methods	Regression[c]	Dataset size
Andersen et al. (2019)[38]	metals	monodentate	electronic, atomic	discrete	linear (CS)	884
Xu et al. (2021)[1]	oxides	monodentate	electronic, geometry, atomic	discrete	linear (CS)	684
Noh et al. (2018)[179]	metals	CO*	electronic	discrete	kernel (KRR)	263
Xu et al. (2022)[2]	metals	multidentate	electronic, geometry, atomic, connectivity	discrete	kernel (GPR)	1,679
Mamun et al. (2020)[180]	metals	monodentate	connectivity	discrete	kernel (GPR)	43,834
Li et al. (2017)[181]	metals	CO*, OH*	electronic	discrete	NN (ANN)	1,032
Fung et al. (2021)[182]	metals	monodentate	electronic	discrete	NN (CNN)	37,000
Back et al. (2019)[183]	metals	CO*, H*	connectivity, atomic	discrete	NN (GCN)	43,247
Wang et al. (2021)[184]	metals	OH*	connectivity, atomic	discrete	NN (GCN)	748
Chanussot et al. (2021)[185]	intermetallics, nonmetals	multidentate	learned representation	discrete	NN (MPNN)	460,328
Chanussot et al. (2021)[185]	intermetallics, nonmetals	multidentate	learned representation	continuous	NN (MPNN)	133,934,018
Tran et al. (2022)[186]	oxides	monodentate	learned representation	discrete	NN (MPNN)	31,244
Tran et al. (2022)[186]	oxides	monodentate	learned representation	continuous	NN (MPNN)	6,642,168

[a] Adsorbate type considered in the work. Apart from a couple of adsorbates specified, "monodentate" refers to many simple adsorbates with only monodentate adsorption motifs, and "multidentate" refers to many simple and complex adsorbates with multidentate adsorption motifs included.
[b] Main type of features used as input to the model. "Electronic" is DFT-calculated electronic structure features related to surface and adsorbates. "Geometry" is local environment-based descriptors, and "learned from geometry" is specific for message passing neural networks where features are randomly initialized and updated based on geometry. "Atomic" covers features of atoms or ions in the material (physical constants). "Connectivity" covers (generalized) coordination numbers and graphs.
[c] Machine learning abbreviations. CS: compressed sensing, KRR: kernel ridge regression, GPR: gaussian process regression, ANN: Artificial (basic) neural networks, CNN: convolutional neural networks, GCN: graph convolutional neural networks, MPNN: message passing graph neural networks.

$$E_{total} = \sum_{i=1}^{N_{atoms}} E_i(\{\mathbf{R}_i\}) \tag{5.1}$$

MLPs seek to narrow the gap between the accuracy of the *ab initio* method and the efficiency of the classical force field to go beyond the traditional speed/accuracy trade-off. Unlike the continuous ML methods, the discrete ML methods are devoted to exclusively learning critical points instead of the entire PES, for example, local minima, global minima and 1st saddle point, or to learning (discrete) property space. These methods have also been applied to many other chemical property predictions, such as reaction mechanism,[188] protein structure,[189] band gaps[190] etc.

In order to obtain cheaper adsorption enthalpies, whose importance in catalyst screening and material discovery has already been highlighted in chapter 2, continuous ML methods require a structural relaxation of the initial structure to the local minima, while discrete ML methods can straightforwardly predict adsorption enthalpies of optimized structure (in some cases without the need of initial structure). In this regard, discrete ML methods can largely tailor target space, thus providing a quick assessment of possible reaction patterns and desirable catalyst compositions.

The development of both continuous and discrete ML models in computational chemistry is a rapidly growing field with many new advances presented on a daily basis. A comprehensive overview of recent literature aimed at predicting adsorption enthalpies using ML methods is compiled in Tab. 5.1, with targeting materials, adsorbates, algorithms, as well as dataset size underlined. According to these current methodological cornerstones, there is a tendency for ML methods to undertake systems of increasing complexity, e.g., oxides materials and multidentate adsorbates, and meanwhile, the size of datasets becomes larger and larger. Continuous ML models

can handle cases where the adsorbate dissociates or the surface reconstructs after the adsorption event. However, they are more expensive and data-hungry since less physical information is included, e.g., electronic structure information is generally not included in the model, and they have difficulty handling many elements. This can be observed in Open Catalyst (OC20)[185] and OC22[186] projects, where the number of training data of continuous ML models is 200-300 times larger than discrete ML models (see Tab. 5.1). Discrete ML models, on the other hand, have the advantage of extrapolation to different elements and are faster, but they are confined to working with rigid systems. It is also worth noting that the traditional data-driven approaches in heterogeneous catalysis, particularly $d-$band model, descriptors, and LSRs, all belong to the family of discrete methods, which is one of the reasons why discrete models are popular in heterogeneous catalysis.

Furthermore, from the standpoint of catalyst screening and discovery, discrete ML models will benefit from rapid predictions, making this procedure considerably faster. They could also be partially interpretable in terms of the solution in the form of analytic equations, e.g., SISSO descriptors or the ranking of primary features, e.g., decision trees, thus providing further chemical insights. We also note that continuous ML methods can validate these predicted properties of discrete ML models and facilitate the construction of databases through ML-accelerated structure optimization.[191]

In the following, we will briefly describe essential components of building ML models and review the methodological cornerstones of existing approaches and ongoing developments.

5.2 Dataset and representations

In any data-driven approach, the assembly of a dataset is the first and vital task to conduct. For constructing MLPs, suitably labeled data from *ab initio* calculations is needed to learn the relevant structure-property interplay to perform ML-based atomic simulations. This could be the most computationally expensive part. A representative database should ideally cover as many different structures as possible, acting as a representative sample of all likely structures on a global PES. In order to escape the local basin of the PES to exploit unknown regions, sampling strategies such as basin hopping,[192] parallel tempering,[193] umbrella sampling,[194, 195] and stochastic surface walking (SSW)[196, 197] method etc., are normally employed. The thorough descriptions of any/all of these methods are not in the scope of this work, and the readers are referred to corresponding literature. As to discrete ML models, the number of data points needed is often less than the one for generating continuous ML models, partially since only discrete points on PES are learned and partially due to the inclusion of more physics in primary features. Its great ability to tackle databases comprising multiple elements makes it intriguing in the context of catalyst screening.

There is no need to construct a database in a brute-force manner. Methods such as similarity measurement and active learning enable to efficiently compile a database from scratch which can reduce computational costs to a large extent. The exemplified similarity measurement such as farthest point sampling,[198, 199] based on kernel distance calculated in smooth overlap of atomic positions (SOAP), is able to detect relevant new structures with large dissimilarity to already labeled datapoints. In comparison, the acquisition function in the active learning approach[200, 201] suggests a sample of interest on the fly (more discussion will be provided in chapter 5.4).

Once a good quality database has been established, the next step is to represent data points

based on certain data structures and descriptors. Widely used data structures in computational chemistry are vector- and graph-based representations. The former is most commonly used in many ML and consists of a series of features relevant to the target properties encoded to a vector representation [202]. In heterogeneous catalysis included features could be global quantities of the entire surface and the molecule, e.g., work functions and frontier orbitals (HOMO/LUMO energy levels), and local quantities concerning active site atoms by average or sum. It should be noted that the vector-based representation does not contain any information about detailed connectivity. In contrast, graph representation is a more versatile method for representing molecular structures where every atom in the structure is a node with edges representing chemical bonds to neighboring atoms, and their character can be further augmented by node and edges attributions, respectively. Graph representation has detailed information on every atom, chemical bonds and how atoms are connected and has been successfully applied in isolated molecules,[203] crystal structures[190] or the combined surface-adsorbate systems.[160] Due to the constraints applied to the input form, graph representation resorts to the use of graph neural networks or graph kernels and has experienced a surge in interest in developing cutting-edge ML algorithms in many fields.

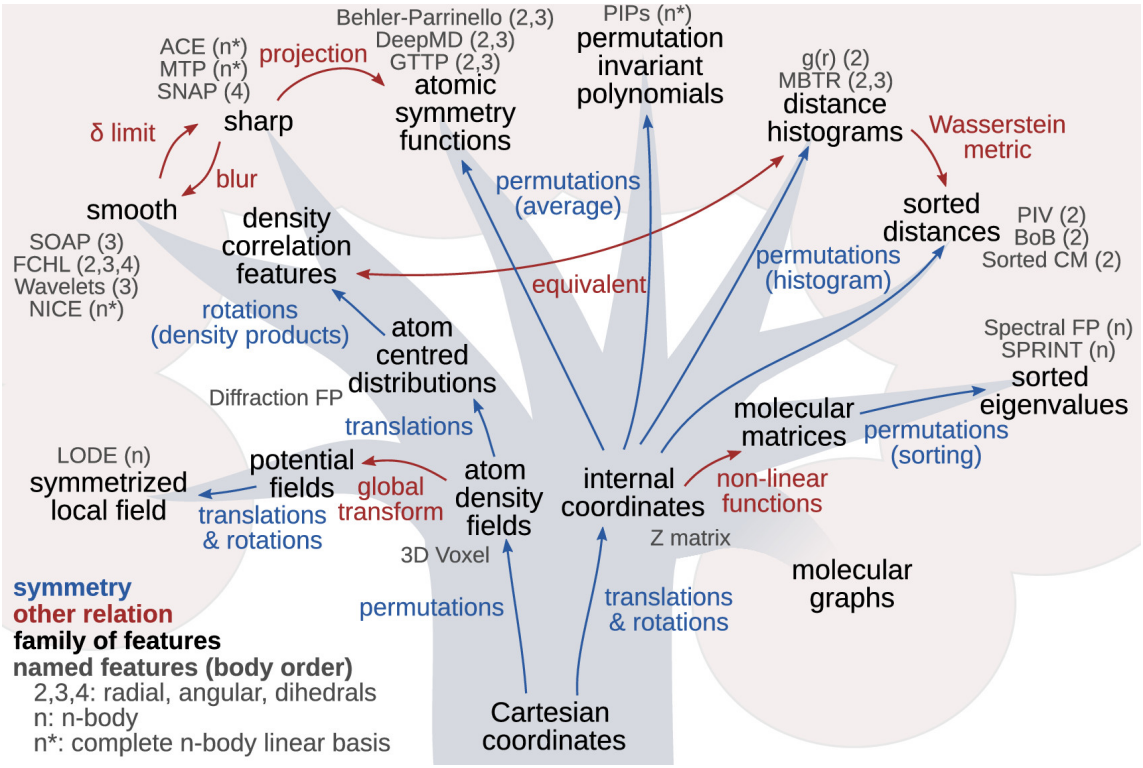

Fig. 5.1: *Examples of structural descriptors considered in continuous ML models. Arrows indicate the relationship between different groups of features. Lists of names, in gray, indicate the most common implementations for each class. Classes that appear as "leaves" of the tree are fully symmetric. Reproduced with permission from ref. [202]. 2021 Copyright American Chemical Society.*

Embedded in the data structure, the second essential component are the descriptors that are relevant to properties of interest. There have been considerable research efforts devoted to developing physically motivated descriptors. In the scope of continuous ML models, the objective is to represent the chemical structure, i.e., geometry, by transforming the Cartesian coordinates of the

atoms.[202] It is highly important to incorporate physical symmetry with respect to translations, rotations, inversion and atom permutation into the descriptors for the sake of data efficiency. Further, the descriptors need to fulfill smoothness, locality and additivity, thus ensuring transferability and extensivity for large scale simulation. Fig.5.1 nicely displays a broad class of descriptors for presenting local environments, such as atom-centered symmetry functions (ACSFs),[204] many-body tensor representation (MBTR)[205] and SOAP, which have been extensively used in many MLPs models.[202] Recently, some of the atom-centered environment descriptors have been unified into the framework of atom-centered density correlations.[206] We refer readers to the relevant literature cited above since understanding these structural descriptors is crucial for building a model. Of course, it is also possible to include features from electronic structure calculations, such as the charge density, the electron density of states or the elements of the Fock matrix to increase the transferability and accuracy of the models.[207, 208] However, this may greatly lead to additional computational efforts. We also note that reliable density-functional tight-binding methods for the simultaneous treatment of many different adsorbates and/or alloy surfaces are still difficult to obtain.[209]

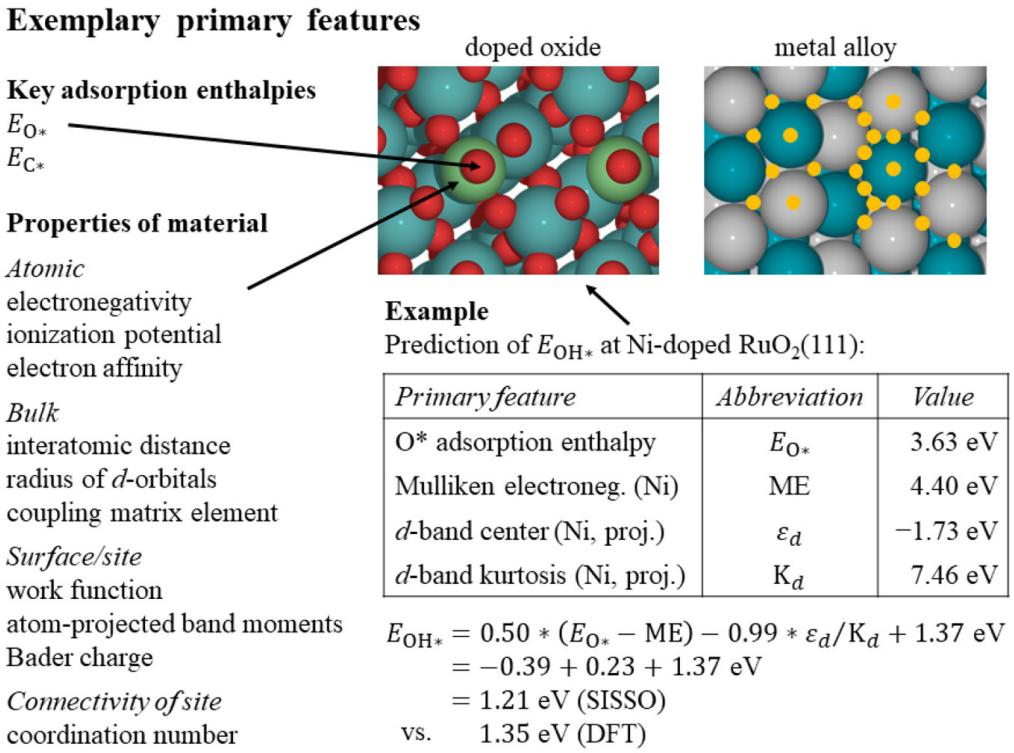

Fig. 5.2: *Examples of primary features considered in discrete ML models in the studies of TMs and TMOs systems. Symmetry-inequivalent adsorption sites (top, bridge, and threefold- and fourfold-coordinated sites) on the stepped metal alloy are marked in yellow. In case the adsorption site is made up of several atoms (all but top sites), the primary features are averaged over these atoms. Reproduced with the permission from ref. [210]. 2021 Copyright American Chemical Society.*

From the perspective of discrete ML models, adhering to the basic idea of well-established, d−band model and LSRs (see chapter 3), they invariably leverage readily obtained physical quantities from bulk or isolated clean surface and gas phase molecules. As a demonstration, Fig. 5.2

displays some physical quantities which can be key for the description of surface adsorption. These include electronegativity (atomic or ionic property), coupling matrix element (bulk property), work function and atom-projected band moments (surface property) and are capable of capturing more information than geometric descriptors found in continuous ML models. We note that adsorbate related features are not included in this example because they are less important for simple adsorbates. Instead only the active site on the surface is crucial. One should also keep in mind that the choice of these physical quantities is typically specific to the material, as the adsorption is likely governed by a different part of the density of states (DOS). In this scenario, one presumably would choose more and more primary features to train a model, but this could be problematic for computationally intense codes. Alternatively, given the entire DOS[182] one could let the ML model itself isolate and learn the important part of DOS by taking advantage of feature extraction techniques like in conventional neural networks.

5.3 Regression models

With the dataset and representation having been constructed, the next stage is the regression models, which capture relations via linear or non-linear functions between the dependent variable (material properties) and the independent variable (structural space or feature space) inferred from the dataset. In terms of model complexity, these models are typically ranging from linear regressions, kernel methods, to neural networks. We note that decision tree-based methods such as random forest[211] and XGboost[212] are another family of ML algorithms. However, they are not topic of this dissertation and therefore not further addressed. In general, there is no way to say which one is the best. The choice of ML models highly depends on the application in terms of computational cost, accuracy, and interpretability.

5.3.1 Linear models

Linear regression is one of the most basic classes of regression models in machine learning in which the target value, $\mathbf{y}$, is expected to be a linear combination of the features, $\mathbf{x}$, as shown in equation 5.2, where $(w_1, \cdots, w_n)$ and w_0 denoted as coefficients and intercept, respectively.

$$\hat{y}(\mathbf{w}, \mathbf{x}) = w_0 + w_1 x_1 + \cdots + w_n x_n \tag{5.2}$$

In this formalism, the leading function form is linear, but the feature itself could be non-linear, e.g., a non-linear combination of single features, resembling the case of polynomial regression that uses linear models trained on non-linear functions of the data $(1, x, x^2, \cdots, x^n)$.

The commonly used linear model is ordinary least squares that minimizes the residual sum of squares between observed targets (Y) in the dataset and model predictions ($\mathbf{Xw}$) as displayed in equation 5.3. Furthermore, least absolute shrinkage and selection operator (LASSO)[213, 214] and ridge regression[215] impose a penalty on the size of the coefficients through L1 ($\|\mathbf{w}\|_1$) and L2 ($\|\mathbf{w}\|_2^2$) regularization to overcome overfitting problem.

$$\min_{\mathbf{w}} \|\mathbf{Xw} - \mathbf{Y}\|_2^2 \tag{5.3}$$

It should be noted that L1 regularization favors solutions with fewer non-zero coefficients, hence lowering the number of features. For this reason, LASSO is fundamental to the field of compressed sensing. Hereby, we would like to introduce a recently developed compressed sensing-based SISSO method that goes beyond LASSO, aiming to tackle huge feature space while retaining the effectiveness of compressed sensing, providing some intrinsically interpretable descriptors, i.e., analytic formulas. As a linear model (specifically by the use of symbolic regression), SISSO makes the ansatz that the property of interest $\mathbf{P}$ can be expressed as

$$\mathbf{P} = \sum_{i}^{M} c_i \mathbf{f}_i \tag{5.4}$$

where c_i are free parameters (coefficients) and $\mathbf{f}_i$ are a small number of selected features, i.e., the sparse solution, constructed by a set of algebraic/functional operators to a list of predefined primary features (see exemplified SISSO descriptor in Fig. 5.2). Two hyperparameters in SISSO, dimensionality (M) and rung (Φ_N), control the complexity of final descriptor and selected features, $\mathbf{f}_i$. In contrast to chemical intuition-driven linear models,[30, 114, 126, 216] SISSO is able to autonomously find the best high-dimensional descriptor from a huge feature space, e.g., 10^{12} candidates at Φ_3, which is well-suited to find sophisticated descriptors to address material complexity given many geometric and electronic structure quantities likely at play. Note that the predictive performance of the resulting descriptor crucially depends on a set of initial primary features, and they are typically different for various classes of materials. The readers are referred to our recent work using the SISSO method to screen dopant TMOs electrocatalysts for water splitting.[1]

5.3.2 Kernel methods

In contrast to linear models, kernel methods provide an efficient way to achieve nonlinearity by implicitly transforming the input space into higher dimensional space, and then the inner product in high dimensional space equals the calculation of kernel function in the original low dimensional space. The combination of a non-linear transformation and an implicit calculation through the kernel function are the so-called "kernel trick", which alleviates the computational complexity of dealing with high-dimensional feature spaces. As its ansatz demonstrated in equation 5.5, ϕ is the map: $\mathcal{X} \rightarrow \mathcal{H}$, where $\mathcal{X}$ and $\mathcal{H}$ are the input space and high-dimensional feature space, respectively.

$$k(\mathbf{x_1}, \mathbf{x_2}) = \left\langle \phi(\mathbf{x_1}), \phi(\mathbf{x_2}) \right\rangle, \forall \mathbf{x_1}, \mathbf{x_2} \in \mathcal{X} \tag{5.5}$$

There is no need to know ϕ and $\mathcal{H}$, and their existence is sufficient. The key to the kernel methods is the choice of the kernel function that must be positive definite. The leading kernel values can be readily interpreted as a similarity measure over different input samples, e.g., the value (kernel distance) of SOAP kernel offers the structural similarity measurement, and the value of graph kernels indicates graph similarity.[217] Many kernel functions have been proposed up until now. Scalar- and vector-valued data is routinely handled using, e.g., radial basis function (RBF) kernel, linear kernel or Laplacian kernel, whereas graph-valued data requires a graph kernel, e.g., message-passing graph kernel[218] or Weisfeiler-Lehman subtree kernel.[219, 220] The choice of kernel function largely depends on the learning task and the form of the input and can therefore

dramatically affect the performance. The development of new kernel functions for emerging applications is an ongoing topic in computer science.[221]

The use of kernel functions has to be coupled with suitable algorithms such as support vector machine (SVM), kernel ridge regression (KRR) and gaussian processes regression (GPR). Among them, GPR is one of the most popular methodologies in computational chemistry, as it provides additional uncertainty estimates on the predictions, which is essential in the context of outlier detection and active learning. The matured GPR-based methods include both continuous and discrete ML methods proposed in literature. For continuous ML models, Gaussian approximation potential (GAP) is a framework using SOAP descriptors which provides straightforward access to scalable MLPs for atomic structures. FLARE is an on-the-fly training framework for molecular dynamic simulations invoking the internal uncertainty of a GPR model to decide when to perform first principle calculations.[222] Bayesian optimization structure search (BOSS)[223] is an active learning technique for global exploration of energy and property phase space. Regarding discrete ML models, the Bayesian framework is designed for the model selection and model averaging for efficient and robust prediction of chemisorption energies of a few important multi-atom monodentate adsorbates on a bimetallic alloy dataset.[180] WWL-GPR models utilize graph kernel and GPR to address multi-dentate adsorbates on TMs and their alloys.[2]

5.3.3 Neural networks

Another approach to achieving nonlinearity is neural networks. Let's consider a simple and special case of a feedforward neural network that is a multilayer perceptron with only one hidden layer, whose mathematical formulation is presented in equation 5.6:

$$f(\mathbf{x}) = \mathbf{w_2} g(\mathbf{w_1}^T \mathbf{x} + \mathrm{b}_1) + \mathrm{b}_2, \tag{5.6}$$

$\mathbf{w_1}$, $\mathbf{w_2}$, b_1 and b_2 are model parameters where the first two represent the weights of the input layer and hidden layer, and the last two represent the bias added to the hidden layer and the output layer. $g(\cdot)$ is the activation function which may be a non-linear function for the sake of nonlinearity constructions. Furthermore, under the scope of deep neural networks, when many multilayers exist between the input and output layers, the number of learnable parameters grows exponentially, making its function much more flexible than linear models and kernel methods which have stronger mathematical constraints. Beneficial from the recent algorithm advances, many promising neural network architectures, including convolutional neural networks (CNN), graph convolutional neural networks (GCN), and message passing neural networks (MPNN), have been successfully adapted to computational chemistry.

Looking back, the first high-dimensional neural network potential (HDNNP) is the so-called Behler-Parrinello neural network or 2G-HDNNP, proposed in 2007.[224] Due to the locality of the MLPs in terms of their general definition (see equation 5.1) based on local environments, the lack of long-range interaction can be crucial for certain materials and scenarios.[187] Later development hence focuses on including long-range and nonlocal effects leading to 3G-HDNNP[225] in 2011 and 4G-HDNNP[226] in 2021. More specifically, 3G-HDNNP is designed by environment-dependent electrostatic interactions using Coulomb's law so that it cannot describe nonlocal charge transfer, whereas 4G-HDNNP was built on a charge equilibration scheme, therefore taking the global charge distribution into account. We note that these MLPs perfectly fall into descriptor-based continuous ML models by leveraging ACSFs, which are analogous to GAP potentials in connection with SOAP descriptors. Until recently, another family of MLPs emerged based on MPNN that

does not require input descriptors, instead, learning representation during the training process, thus substantially reducing human interaction.[227] MPNN is a specific graph neural network, and the key components behind MPNN are the message functions defining how to propagate messages between neighbor nodes and the update function defining how to update node attributes accordingly. Furthermore, according to the different message passing schemes a variety of MPNNs has been proposed with an early designed SchNet,[228] which is a purely invariant model and later developed DimNet incorporating some angular information to achieve a directional message.[229] The state-of-the-art MPNNs are equivariant-based models such as NequIP,[230] GemNet[231] and PaiNN,[232] which have shown more data efficiency due to the inclusion of rotationally equivariant representations. In the context of discrete ML methods, given various input features, DOSnet is a convolutional neural network-based model taking the whole density of state as input and does not need additional partitions.[182] CGCNN is graph convolutional neural network built on some readily obtained atomic features.[183, 233] It is also possible to use MPNN based discrete ML models, but the input would largely rely on the geometry.[185, 186]

With more and more databases being publically available, neural network models are likely to be more effective because of the capabilities of handling large databases and readily adapted architectures. The representative databases such as Aflow,[234] Material Project,[235] NOMAD,[236] QM9,[237] MD17,[198] catalysis hub,[238] and OC20[185] are motivated by specific domain usage or database size and complexity, many of which have become standard baseline that allows consecutive improvement of the ML models. It should be underlined that OC20 is the largest dataset with a particular focus on heterogeneous catalysis, having more than 400k relaxed structures and 200 million single-point calculations. The OC20 dataset reflects a daunting challenge with a goal of creating universal MLPs. Last year, merging efforts from computational chemistry and computer science fields achieved remarkable progress on OC20 in terms of the predictive accuracy of ML models. Although it is still a far cry from the targeted accuracy, we can already observe that in order to construct a universal ML model for heterogeneous catalysis, both the size of the database and ML models with respect to the number of hyperparameters has expanded dramatically. This trend can also be seen in the industry, where steeply rising computing demands have forced training on tens of thousands of GPUs with trillions of parameters in ML models. Large-scale simulation and distributed training of large models will, therefore, undoubtedly become increasingly significant in the coming years.

Now let's recap current advances in both continuous and discrete ML models on how to incorporate physics, also known as "domain knowledge" and "bias inductive", behind ML algorithms. The general strategies cover the design of physics-inspired representation, ML architectures and physical regularization. Specifically, the physics-inspired presentation includes symmetry descriptions of the structure or electronic structure-based features, which can increase data efficiency.[202] The ML architectures mainly refer to explicit physics modules such as Ewald summation, charge equilibration, charge-dependent dispersion, and physically motivated hyperparameters.[2, 226, 239, 240] Ultimately, the loss function is the place to enforce physic constraints and get rid of overfitting problems, e.g., introducing auxiliary tasks into the loss.[241]

Nevertheless, infusing physics into the ML model has demonstrated great indispensability for addressing the problem of chemical domains. For instance, high-dimensional and non-linear ML models made up of multiple electronic structures and geometrical descriptors can accurately describe complex materials.[1] The physics-inspired graph representation in connection with surface adsorption-motivated hyperparameters can help treat complex adsorbates with numerous binding motifs.[2] Moreover, there are very limited works aiming to address the external environment,

for which a second neural network could help drive the convergence of external electric field iteratively,[242] yet further development is required.

5.4 Useful tools towards ML applications

Many of the ML models mentioned above have demonstrated a satisfactory predictive performance with root-mean-square errors (RMSE) around 0.1–0.2 eV for adsorption enthalpies. However, from the perspective of ML application, it is also crucial to couple these models with some useful tools in order to automate workflow, quantify uncertainty, and visualize data.

5.4.1 Automated workflow

An automated workflow is crucially important to assist many stages of ML applications covering structure generation, database construction, and iterative on-the-fly training to considerably reduce human interactions in heterogeneous catalysis. This allows us to go beyond chemical intuition and tedious manual work to refine model predictions and accelerate catalyst screening. Its underlying procedures can be described as follows:

First, initial structure generations resort to considering as many active sites and binding motifs of a given adsorbate/surface as possible in order to end up with a correct reaction mechanism. Current structure construction tools such as Catkit can only provide reasonable initial configurations up to bidentate adsorption motifs by enumerating the surface.[160] In this regard, further improvements in this class of generation tools are needed, and ML-accelerated adsorbate replacement seems promising to find global and local minima, which are useful for structure generations.

Second, regarding subsequent DFT calculations for the construction of database or on-the-fly training, workflows should be able to connect to DFT code, MD code, and high-performance computing (HPC) clusters for which the use of infrastructures tools such as FireWorks[243] and AIIDA[244] seems straightforward.

Finally, in order to train ML models with iteratively enlarged databases and find optimal catalysts, workflows need to communicate with advanced ML architecture like PyTorch,[245] TensorFlow,[246] and GPyTorch[247] on GPU facility.

Some immediate instances are starting to become available.[222, 248] We noted that continuous ML models typically need to be constructed for every material of interest. Therefore the use of such workflows is much more rewarding without worthless repeating. Ultimately, extending to a cloud-based research environment to enable sharing of databases and models from any device immediately and cloud computing is promising.

5.4.2 Uncertainty quantification and active learning

Uncertainty quantification can provide valuable estimates of the residual error or uncertainty (e.g., standard deviation), associated with a certain input, to decide whether to trust the predictions. In thermodynamic and microkinetic-based catalyst screening, large outliers give rise to significant error propagation from unsatisfactory predicted adsorption enthalpies, so they need to be precisely identified and followed up with explicit DFT calculations. Well-studied methods offering uncertainty predictions are Bayesian methods and ensemble methods with various sampling strategies, e.g., subsampling and bootstrapping. Bayesian methods include GPR, Bayesian neural network, convolution-fed gaussian process regressions etc.[249] Bayesian methods demonstrated a great

calibration ability. Unfortunately, they are not sensitive to large outliers.[2, 250] For detecting large outliers, ensemble methods with bootstrapping sampling strategies are best-suited.

Apart from commonly used standard deviation, metrics such as calibration, sharpness and dispersion are also proposed in the literature.[249] A useful uncertainty quantification method should have a small miscalibration area (that is, a good match between the expected and observed cumulative error distribution), a small sharpness value (small error estimates) and a large dispersion value (dispersion error estimates). As a whole, next to accuracy metric (RMSE or MAE) and uncertainty metric (standard deviation), it is also important to assess distribution-based metrics, e.g., calibration and sharpness. Furthermore, a better uncertainty calibration can be obtained by suitable recalibration methods, known as the postprocessing step of the uncertainty, as proposed in recent papers, either by isotonic regression[251] or linear regression.[250]

On top of uncertainty prediction, active learning is known as the optimal experimental design, a class of approaches to iteratively query a user to label new data points with the desired output.[169] In the scope of catalyst screening, this entails iteratively performing DFT calculations on the queried data to enlarge the database and find promising candidates. The usefulness of this approach has been exemplified in the discovery of electrocatalysts for CO_2 reduction and H_2 evolution by Tran and co-workers.[201] Candidate materials either are highly promising in terms of a predicted target property (adsorption enthalpy) or exhibit a high uncertainty.

Since the emphasis herein is on the assistance to ML applications, we would like to draw attention to the fact that active learning is often used to enlarge the database and search for optimal hyperparameters intelligently. For the former, as discussed in chapter 5.2, efficient continuous ML models require a database covering representative samples on PES that should span various local basins. The acquisition function in active learning can control whether to explore or exploit, thus possibly escaping local basins to search unknown regions. For the latter, given the fact that many ML models are expensive or have no gradients to train, or their evaluations may be noisy, methods like Bayesian optimization are rewarding to efficiently find optimal hyperparameters compared to grid search and random search, which have been implemented in many toolkit packages for ease of use.[252]

5.4.3 Data visualization

Data visualization typically uses dimensional reduction techniques such as PCA (kernel PCA),[253, 254] t-SNE,[255] and UMAP,[256] mapping the input high dimensional features space to typically 2D or 3D space while retaining the relations (for example, distance) among data points in high dimensional space. Furthermore, depending on the choice of input features, they can be used to reveal structure-property relations[257, 258] or the most relevant features to the targeted property.[2, 201] Thus, it is of great utility for data analysis, pattern recognition, and providing valuable insights for materials design.

6 Publications

6.1 Data-Driven Descriptor Engineering and Refined Scaling Relations for Predicting Transition Metal Oxide Reactivity

Wenbin Xu, Mie Andersen and Karsten Reuter

ACS Catal. 11, 2, 734–742 (2021)

Summary: For the sake of addressing the complexity at the level of the material, this project aims to identify high-dimensional descriptors for transition metal oxides (TMOs). As already discussed in chapter 4.1, although conventional descriptor-based and linear scaling relations (LSRs) methods have made great progress on screening transition metals (TMs), they are ill-posed to extend to more complicated compound materials. To this end, we follow a compressed sensing approach that has been demonstrated to be of great usefulness for TM and TM alloy catalysts in our recent work. The corresponding SISSO (sure independence screening and sparsifying operator) approach allows for predicting the adsorption energies from descriptors that are expressed as nonlinear functions of intrinsic properties of the clean catalyst surface (so-called primary features), e.g., coordination numbers, $d-$band moments, and density of states at the Fermi level.

Given the promising rutile-type TMOs that are IrO_2 and RuO_2 electrocatalysts for water splitting (i.e., oxygen evolution reaction), we are particularly interested in identifying descriptors for their TM dopants and further screening them with enhanced activities. This work starts with a database construction to include O*, OH* and OOH* adsorption enthalpies of all five low-index facts of IrO_2 and RuO_2 when doping them with a variety of TMs (Ti, Mn, Fe, Co, Ni, Cu, Zn, Mo, Ru, Ag, W, and Ir). Then, we carefully compile a list of primary features from general physicochemical considerations as well as previously highlighted descriptors in the literature. By carrying out systematic SISSO training, we are able to iteratively identify multidimensional descriptors with a best-performance of root-mean-square error of 0.18 eV which is on par with DFT uncertainty, and inferior primary features turn out to be significant when they are combined with the others, thus can not be disregarded. Furthermore, the SISSO-refined LSRs study points out local charge transfer as the missing ingredient in standard LSRs for this class of materials. Ultimately, we set up a thermodynamic model to predict the theoretical overpotential through the computational hydrogen electrode approach. The SISSO-based screening clearly identified Co- and Fe-doped surface with the lowest overpotential in agreement with experimental works, but the LSRs-based approach likely disregarded them. Thus, this approach provides a reliable computational screening and general guideline to tailor complicated compound materials.

Individual contributions: The initial idea was conceived by Karsten Reuter and Mie Andersen. I manually construct the oxides database via the quantum-espresso python interface. Compiling primary features is a daunting task because it is crucial for predictive performance, and it is unclear which features are important. Karsten Reuter kindly gave me many valuable suggestions on possible features for trial-error tests. To systematically train a SISSO model, fruitful discussions with Mie Andersen and Martin Deimel helped me arrive at a full-blown training protocol. The idea

of SISSO-refined scaling relations originates from Karsten Reuter, and I perform a thermodynamic model for catalyst screening. The manuscript was jointly written and edited by all authors.

6.2 Predicting Binding Motifs of Complex Adsorbates Using Machine Learning with a Physics-inspired Graph Representation

Wenbin Xu, Karsten Reuter and Mie Andersen
Nat. Comput. Sci. 2, 443–450 (2022)

Summary: While finishing up the first SISSO project, several emerging ML approaches can routinely achieve RMSE of 0.1 - 0.2 eV for predicting adsorption enthalpies of simple adsorbates but are unfortunately not applicable to complex adsorbates. However, the handling of complex adsorbates is highly important for many surface catalytic processes such as Fischer-Tropsch reactions, higher oxygenate syntheses and CO_2 reduction. Therefore, in this project, we aim to address the complexity at the level of adsorbates, specifically to tackle numerous possible bonding motifs relevant to the adsorption of larger adsorbates. We note that graph representations seem promising due to the inclusion of more detailed information about each atom and how they connect, while relying solely on connectivity-based features has exhibited poor data efficiency.

Accordingly, we developed a data-efficient graph ML model leveraging physics-inspired graph representations, a customized Wasserstein Weisfeiler–Lehman graph kernel and Gaussian process regression. The physics part of the developed WWL-GPR model lies on the physics-based primary features related to d−band moments (surfaces), HOMO/LUMO frontier orbital (adsorbate) and local geometry. More importantly, we incorporate surface adsorption-motivated hyperparameters under the graph kernel architecture to emphasize the role of various atom shells and chemical bonds. This work considers 41 different small and large adsorbates on multiple TM and alloy surfaces as they are of great interest for ethanol synthesis. Foremost, we realize that the construction of a complex adsorbates dataset is non-trivial since as many multidentate adsorption motifs as possible should be considered, for which an automated workflow has been developed to link structure generation toolkit (CatKit), DFT code, and workflow manager altogether. Then, based on this complex adsorbates dataset and another simple adsorbates dataset from our previous works, we compare the WWL-GPR model with three vector-based ML models: SISSO, radial basis function (RBF)-GPR, and XGBoost. As expected, we found no added value in using a graph model for handling simple adsorbates since the averaged surface atom features already govern their adsorption. However, the WWL-GPR model significantly outperforms other vector-based ML models in handling complex adsorbates with an RMSE of about 0.2 eV. The insight gained from KPCA analysis and ML-learned hyperparameters tells us that graph representation is indispensable for distinguishing binding motifs of complex adsorbates, and it is crucial to consider more atom shells for the sake of better predictive performance. Ultimately, we show its good extrapolation ability and uncertainty estimate based on an ensemble model to reliably capture outliers, which makes it promising for exploring complex reaction networks.

Individual contributions: The question of how we can utilize ML to predict adsorption enthalpies of complex adsorbate was initially proposed by Karsten Reuter and Mie Andersen. Graph representations look promising, but it is unclear how to construct a data-efficient and accurate graph model for this challenging problem. After brainstorming and surveying the literature, we found kernelized ML methods and physics-enhanced graph representations are possible solutions. I began by developing an automated workflow based on the Aiida-py plugin that was initially made by Simeon Beinlich and Nicolas Bergmann in our group. With this workflow, we can reduce human interaction and accelerate the training of ML models. Then, I developed

methodological details of WWL-GPR and the ensemble model. Mie Andersen, Karsten Reuter and me wrote the manuscript.

6.3 Further work

The following article was published during my time working at the Chair of Theoretical Chemistry as a side project. We collaborated with Prof. Jan Knudsen's group at Lund University on oxygen evolution reaction on graphene at room temperature, which is relevant to the chemical reaction investigated in my first project. This work is only mentioned here for completeness and reference because it is not forming a part of this dissertation.

Graphene as an Adsorption Template for Studying Double Bond Activation in Catalysis
Virginia Boix, Wenbin Xu, Giulio D'Acunto, Johannes Stubbe, Tamires Gallo, Marie Døvre Strømsheim, Suyun Zhu, Mattia Scardamaglia, Andrey Shavorskiy, Karsten Reuter, Mie Andersen, and Jan Knudsen
J. Phys. Chem. C 126, 33, 14116–14124 (2022)

7 Summary, Conclusions and Outlook

Efficient heterogeneous catalysts are a key pillar of sustainable energy processes and their discovery relies on combining theoretical and experimental insights. From the standing point of catalysis modeling, remarkable progress has been made in the development of both thermodynamic and microkinetic models that can provide accurate predictions of catalytic performance, e.g., stability, activity and selectivity. Such models are therefore heavily relied upon for catalyst screening and material discovery. However, merely depending on standard quantum mechanical calculations, i.e., for the calculation of adsorption enthalpies, becomes a bottleneck if wanting to test hundreds or even thousands of candidate structures in the vast chemical space available. We have seen many conventional data-driven approaches, e.g., $d-$band model and linear scaling relations, help alleviate some of these problems. However, the oversimplified physics involved cannot address the complexity presented in realistic catalytic processes. With machine learning tools becoming increasingly popular in computational chemistry, there is an opportunity to develop more flexible models to fulfill predictive accuracy and computational efficiency simultaneously. Such models, however, must be carefully designed or adapted to heterogeneous catalysis in order to really address the different sources of existing complexity.

In this work, we have focused on developing data-efficient and physically motivated ML models for the prediction of adsorption enthalpies on two strands of complexity relevant to the computational screening of heterogeneous catalyst materials. One strand is the computational screening of TMOs to address catalyst complexity, where we constructed a database of key OER intermediates including O*, OH*, and OOH* at doped IrO_2 and RuO_2 electrocatalysts. In a second step, we used the compressed sensing method SISSO to identify descriptors for the prediction of adsorption enthalpies at these surfaces. The descriptors were constructed as algebraic formulations of electronic and geometric primary features. By incorporating the O* adsorption enthalpy into the training data, we identified so-called SISSO-refined scaling relations. Their compositions help us to identify primary features related to the local charge transfer as the primary correction (and thereby missing ingredient) to standard LSRs. For the showcased screening of dopants, these corrections turn out as crucial to reliably identify Co and Fe in accordance with recent experimental findings.[1]

The second strand is developing a graph ML model to address adsorbate complexity with their mon-, bi-, and multi-dentate adsorption motifs that are likely at play. More specifically, next to the construction of a database that includes 41 different small to large adsorbates on TM surfaces relevant to ethanol synthesis, we develop a data-efficient and physics-inspired ML approach based on a customized Wasserstein Weisfeiler-Lehman graph kernel (WWL) and GPR. The ML task is to directly predict the relaxed adsorption enthalpies corresponding to a variety of plausible initial guesses of the adsorption motif based on graph representation. Therefore, for a given surface/adsorbate combination of interest, both the most stable and all meta-stable adsorption motifs, as well as their concomitant adsorption enthalpies, can be predicted. Rather than relying solely on graph representation, as is commonly done in more data-greedy approaches implemented with deep neural networks, our WWL-GPR model is augmented with physically inspired node

attributes representing local geometric or electronic information about each atom in the structure, as well as surface adsorption motivated hyperparameters emphasizing the role of atoms near the active site and the surface/adsorbate interface. The model achieves an in-domain prediction of adsorption enthalpies with an RMSE of 0.18 eV on par with the expected inherent uncertainty in DFT.[2]

The presented works in this dissertation only begin to scratch the enormous complexity of heterogeneous catalysis to some extent. In practice, one can envision that a combined complexity could come from catalysts, adsorbates and the external environment altogether. Furthermore, dynamic changes in working catalysts are likely to happen during operating conditions, only becoming observable with simulations of large length scales and long-term catalyst operation.[73] On the one hand, fundamental theories need to be further developed. For example, in the context of electrocatalysis, accurate calculation of potential-dependent adsorption enthalpies calls for better models to describe the electrified solid-liquid interface.[71] In order to account for operando evolution away from crystalline lattices,[73, 79] off-lattice adaptive kMC has to be implemented in connection with ML interatomic potentials and recognition of local atomic environments. On the other hand, ML methods should be developed that can account for these mixed complexities introduced. Since the OC20 database was launched, containing many components of complexity, we have observed consecutive advances for the time being. It may still be tough to conceive that a universal ML model works for all materials, but pre-trained ML models based on this large database could be helpful for training on a small database for specific domain materials through transfer learning.[259] In the meantime, we cannot overlook simplified ML models constructed on a small and homogeneous database as the reduced complexity may shed light on important fundamental principles and provide crucial understanding for designing large ML models.

In the scope of catalyst discovery, the focused predictive ML models that go from initial structure to property prediction in this dissertation are just one choice among data-driven methods. One apparent drawback is that the search is limited by the user-selected library, either the experimental database or computational database. Possible high-performing catalysts are thus likely to be missed if not in the library, and the efficiency can be low since the screening is run over the database blindly without directions to search. Alternatively, inverse design (here generative ML models) is conceptually advanced in that taking the target property asks for the structure of interest by learning their distribution in the continuous space so that it can generate new materials, not in the existing database. There are already some promising deep generative architectures such as variational autoencoders (VAEs),[260] generative adversarial networks (GANs),[261] invertible neural networks (INNs)[262] at present. Their application to heterogeneous catalysis, however, still faces many challenges such as the lack of invertible representation, diversity database, and well-defined models, so that further methodological development is needed.

Nevertheless, with the advent of ML methods in heterogeneous catalysts, we do actually see a theory-headed catalyst discovery becoming more mature. This is a new, exciting direction for computational catalysis. It is my hope that my research work could provide guidelines on how to incorporate domain knowledge in ML methods used in the context of heterogeneous catalysis and pave the path toward accelerating catalyst discovery. Ultimately, identified catalysts could be leveraged to improve everyone's quality of life.

Acknowledgments / Danksagung

First and foremost, I would like to thank Prof. Karsten Reuter for giving me this opportunity to conduct my Ph.D. in his group. I can't express how lucky I am to pursue research in such a wonderful family with a great working environment and many lovely colleagues. Prof. Karsten Reuter supplies not only academic and strategic guidance but also influences my thoughts on how to conduct self-motivated and high-quality research work. Particularly, I would like to thank his support in extending my research experiences, covering my visit to Carnegie Mellon University, external collaborations at Lund University, as well as the chances of attending many conferences, from which I gained a lot of rewarding experiences to work and discuss with a diverse team of other researchers.

Likewise, I would like to thank my direct supervisor and mentor, Prof. Mie Andersen, for her tremendous efforts in my Ph.D. study, including scientific input, support and advice. Especially, I sincerely appreciate her continuous concerns and patience during her pregnancy. Although, at the last stage of my Ph.D., she moved to a new position at Aarhus University and performed supervision remotely, she was always there whenever needed and very helpful to the progress of my projects.

A big thank you to my colleagues who enabled the efficient work of my Ph.D. For example, Simeon Beinlich, Nicolas Bergmann, and the IT team for their contribution to the group wiki helped me initialize my Ph.D. and adjust to the IT infrastructure. I would like to thank my officemates Simiam Ghan, Elias Diesen, Sina Stocker, Yonghyuk Lee and Alexandra Dudzinski for all their support and friendship. I would also like to acknowledge fruitful discussions from Johannes Margraf, Christian Kunkel, Frederic Felsen, Carsten Staacke, and Martin Deimel, for which the progress of these challenging projects cannot happen within my endeavors alone. I would also like to express gratitude to Vanessa Jane Bukas, Hendrik Heenen, Elias Diesen and Olga Vinogradova for proofreading my thesis. In addition, much appreciation goes to our secretaries, Julia Pach and Ruth Mösch, and the rest of the group for a pleasant atmosphere during my time here.

Besides our group, I would like to thank our collaborators Prof. Zachary Ulissi, Adeesh Kolluru, and Muhammed Shuabi at Carnegie Mellon University and Prof. Jan Knudsen, Virginia Boix at Lund University, for invaluable discussion and help extend the breadth and depth of my research.

I would like to acknowledge the support from the China Scholarship Council and computing time at the Jülich Supercomputing Centre, Max Planck Computing and Data Facility, as well as Leibniz Supercomputing Centre. The financial support from the international graduate school of the Technical University of Munich is further gratefully acknowledged.

Ultimately, I would like to thank my parents, who always give their unconditional support and have helped me in every conceivable way. I would like to express my sincere appreciation to my girlfriend Jun for her companionship and sacrifices, encouraging me to become better myself. Without their care and love, this journey would have been much bumpy, not even possible.

Bibliography

[1] W. Xu, M. Andersen, and K. Reuter, *Data-Driven Descriptor Engineering and Refined Scaling Relations for Predicting Transition Metal Oxide Reactivity*, ACS Catalysis **11**, 734 (2021) (cit. on pp. i, 3, 7, 11, 14, 17, 18, 22, 27, 29, 39).

[2] W. Xu, K. Reuter, and M. Andersen, *Predicting binding motifs of complex adsorbates using machine learning with a physics-inspired graph representation*, Nature Computational Science **2**, 443 (2022) (cit. on pp. i, 3, 22, 28, 29, 31, 40).

[3] V. Boix, W. Xu, G. D'Acunto, J. Stubbe, T. Gallo, M. Døvre Strømsheim, S. Zhu, M. Scardamaglia, A. Shavorskiy, K. Reuter, M. Andersen, and J. Knudsen, *Graphene as an Adsorption Template for Studying Double Bond Activation in Catalysis*, The Journal of Physical Chemistry C **126**, 14116 (2022) (cit. on p. i).

[4] J. A. Turner, *Sustainable hydrogen production*, Science **305**, 972 (2004) (cit. on p. 1).

[5] S. Chu and A. Majumdar, *Opportunities and challenges for a sustainable energy future*, nature **488**, 294 (2012) (cit. on p. 1).

[6] S. LewisN and N. G. Poweringtheplanet, *Chemicalchallengesinsolarenergyutilization*, Proceedingofthe NationalAcademyofSciences **103**, 15729 (2006) (cit. on p. 1).

[7] C. F. Kutscher, J. B. Milford, and F. Kreith, *Principles of sustainable energy systems* (CRC Press, 2018) (cit. on p. 1).

[8] I. Gunnarsdóttir, B. Davidsdottir, E. Worrell, and S. Sigurgeirsdóttir, *Sustainable energy development: history of the concept and emerging themes*, Renewable and Sustainable Energy Reviews **141**, 110770 (2021) (cit. on p. 1).

[9] Z. W. Seh, J. Kibsgaard, C. F. Dickens, I. Chorkendorff, J. K. Nørskov, and T. F. Jaramillo, *Combining theory and experiment in electrocatalysis: Insights into materials design*, Science **355**, eaad4998 (2017) (cit. on pp. 1, 2, 5, 7, 17).

[10] S. Chu, Y. Cui, and N. Liu, *The path towards sustainable energy*, Nature Materials **16**, 16 (2017) (cit. on p. 1).

[11] S. Chu and A. Majumdar, *Opportunities and challenges for a sustainable energy future*, Nature **488**, 294 (2012) (cit. on p. 1).

[12] J. Gong and R. Luque, *Catalysis for production of renewable energy*, Chemical Society Reviews **43**, 7466 (2014) (cit. on p. 1).

[13] O. O. James, B. Chowdhury, M. A. Mesubi, and S. Maity, *Reflections on the chemistry of the fischer–tropsch synthesis*, Rsc Advances **2**, 7347 (2012) (cit. on p. 1).

[14] Q. Zhang, J. Kang, and Y. Wang, *Development of novel catalysts for fischer–tropsch synthesis: tuning the product selectivity*, ChemCatChem **2**, 1030 (2010) (cit. on p. 1).

[15] N. E. Tsakoumis, M. Rønning, Ø. Borg, E. Rytter, and A. Holmen, *Deactivation of cobalt based fischer–tropsch catalysts: a review*, Catalysis Today **154**, 162 (2010) (cit. on p. 1).

[16] R. G. dos Santos and A. C. Alencar, *Biomass-derived syngas production via gasification process and its catalytic conversion into fuels by fischer tropsch synthesis: a review*, International Journal of Hydrogen Energy **45**, 18114 (2020) (cit. on p. 1).

[17] A. Vojvodic, A. J. Medford, F. Studt, F. Abild-Pedersen, T. S. Khan, T. Bligaard, and J. Nørskov, *Exploring the limits: a low-pressure, low-temperature haber–bosch process*, Chemical Physics Letters **598**, 108 (2014) (cit. on p. 1).

[18] T. Kandemir, M. E. Schuster, A. Senyshyn, M. Behrens, and R. Schlögl, *The haber–bosch process revisited: on the real structure and stability of "ammonia iron" under working conditions*, Angewandte Chemie International Edition **52**, 12723 (2013) (cit. on p. 1).

[19] B. M. Hoffman, D. Lukoyanov, Z.-Y. Yang, D. R. Dean, and L. C. Seefeldt, *Mechanism of nitrogen fixation by nitrogenase: the next stage*, Chemical reviews **114**, 4041 (2014) (cit. on p. 1).

[20] S. L. Foster, S. I. P. Bakovic, R. D. Duda, S. Maheshwari, R. D. Milton, S. D. Minteer, M. J. Janik, J. N. Renner, and L. F. Greenlee, *Catalysts for nitrogen reduction to ammonia*, Nature Catalysis **1**, 490 (2018) (cit. on p. 1).

[21] R. Michalsky, P. H. Pfromm, and A. Steinfeld, *Rational design of metal nitride redox materials for solar-driven ammonia synthesis*, Interface Focus **5**, 20140084 (2015) (cit. on pp. 1, 11).

[22] X. Jia, W. Khan, Z. Wu, J. Choi, and A. C. Yip, *Modern synthesis strategies for hierarchical zeolites: bottom-up versus top-down strategies*, Advanced Powder Technology **30**, 467 (2019) (cit. on p. 1).

[23] S. Hammes-Schiffer and G. Galli, *Integration of theory and experiment in the modelling of heterogeneous electrocatalysis*, Nature Energy **6**, 700 (2021) (cit. on p. 1).

[24] S. Bhattacharjee, U. V. Waghmare, and S.-C. Lee, *An improved d-band model of the catalytic activity of magnetic transition metal surfaces*, Scientific Reports **6**, 35916 (2016) (cit. on pp. 2, 11).

[25] B. Hammer and J. Nørskov, *Electronic factors determining the reactivity of metal surfaces*, Surface Science **343**, 211 (1995) (cit. on pp. 2, 11).

[26] B. Hammer and J. Nørskov, in *Advances in Catalysis*, Vol. 45 (Elsevier, 2000), pp. 71–129 (cit. on pp. 2, 11, 12).

[27] I. Takigawa, K.-i. Shimizu, K. Tsuda, and S. Takakusagi, *Machine-learning prediction of the d-band center for metals and bimetals*, RSC Advances **6**, 52587 (2016) (cit. on pp. 2, 11).

[28] A. Vojvodic, J. K. Nørskov, and F. Abild-Pedersen, *Electronic Structure Effects in Transition Metal Surface Chemistry*, Topics in Catalysis **57**, 25 (2014) (cit. on pp. 2, 11).

[29] F. Abild-Pedersen, J. Greeley, F. Studt, J. Rossmeisl, T. R. Munter, P. G. Moses, E. Skúlason, T. Bligaard, and J. K. Nørskov, *Scaling Properties of Adsorption Energies for Hydrogen-Containing Molecules on Transition-Metal Surfaces*, Physical Review Letters **99**, 016105 (2007) (cit. on pp. 2, 13, 14).

[30] E. M. Fernández, P. G. Moses, A. Toftelund, H. A. Hansen, J. I. Martínez, F. Abild-Pedersen, J. Kleis, B. Hinnemann, J. Rossmeisl, T. Bligaard, and J. K. Nørskov, *Scaling Relationships for Adsorption Energies on Transition Metal Oxide, Sulfide, and Nitride Surfaces*, Angewandte Chemie International Edition **47**, 4683 (2008) (cit. on pp. 2, 27).

[31] A. J. Medford, A. C. Lausche, F. Abild-Pedersen, B. Temel, N. C. Schjødt, J. K. Nørskov, and F. Studt, *Activity and Selectivity Trends in Synthesis Gas Conversion to Higher Alcohols*, Top Catal, 8 (2014) (cit. on pp. 2, 7, 14).

[32] F. Calle-Vallejo, J. I. Martínez, and J. Rossmeisl, *Density functional studies of functionalized graphitic materials with late transition metals for oxygen reduction reactions*, Physical Chemistry Chemical Physics **13**, 15639 (2011) (cit. on p. 2).

[33] A. O. Elnabawy, J. A. Herron, J. Scaranto, and M. Mavrikakis, *Structure Sensitivity of Formic Acid Electrooxidation on Transition Metal Surfaces: A First-Principles Study*, Journal of The Electrochemical Society **165**, J3109 (2018) (cit. on p. 2).

[34] X. Hong, K. Chan, C. Tsai, and J. K. Nørskov, *How Doped MoS_2 Breaks Transition-Metal Scaling Relations for CO_2 Electrochemical Reduction*, ACS Catalysis **6**, 4428 (2016) (cit. on p. 2).

[35] A. J. Medford, A. Vojvodic, J. S. Hummelshøj, J. Voss, F. Abild-Pedersen, F. Studt, T. Bligaard, A. Nilsson, and J. K. Nørskov, *From the Sabatier principle to a predictive theory of transition-metal heterogeneous catalysis*, Journal of Catalysis **328**, 36 (2015) (cit. on p. 2).

[36] J. H. Montoya, C. Tsai, A. Vojvodic, and J. K. Nørskov, *The Challenge of Electrochemical Ammonia Synthesis: A New Perspective on the Role of Nitrogen Scaling Relations*, ChemSusChem **8**, 2180 (2015) (cit. on p. 2).

[37] F. Studt, F. Abild-Pedersen, T. Bligaard, R. Z. Sørensen, C. H. Christensen, and J. K. Nørskov, *Identification of Non-Precious Metal Alloy Catalysts for Selective Hydrogenation of Acetylene*, Science **320**, 1320 (2008) (cit. on pp. 2, 14).

[38] M. Andersen, S. V. Levchenko, M. Scheffler, and K. Reuter, *Beyond Scaling Relations for the Description of Catalytic Materials*, ACS Catalysis **9**, 2752 (2019) (cit. on pp. 2, 11, 17, 22).

[39] R. Ouyang, S. Curtarolo, E. Ahmetcik, M. Scheffler, and L. M. Ghiringhelli, *SISSO: A compressed-sensing method for identifying the best low-dimensional descriptor in an immensity of offered candidates*, Physical Review Materials **2**, 083802 (2018) (cit. on p. 3).

[40] R. Ouyang, E. Ahmetcik, C. Carbogno, M. Scheffler, and L. M. Ghiringhelli, *Simultaneous learning of several materials properties from incomplete databases with multi-task SISSO*, Journal of Physics: Materials **2**, 024002 (2019) (cit. on p. 3).

[41] I. C. Man, H.-Y. Su, F. Calle-Vallejo, H. A. Hansen, J. I. Martínez, N. G. Inoglu, J. Kitchin, T. F. Jaramillo, J. K. Nørskov, and J. Rossmeisl, *Universality in Oxygen Evolution Electrocatalysis on Oxide Surfaces*, ChemCatChem **3**, 1159 (2011) (cit. on pp. 3, 7, 14).

[42] J. Rossmeisl, Z.-W. Qu, H. Zhu, G.-J. Kroes, and J. Nørskov, *Electrolysis of water on oxide surfaces*, Journal of Electroanalytical Chemistry **607**, 83 (2007) (cit. on pp. 3, 7).

[43] J. K. Nørskov, F. Abild-Pedersen, F. Studt, and T. Bligaard, *Density functional theory in surface chemistry and catalysis*, Proceedings of the National Academy of Sciences **108**, 937 (2011) (cit. on pp. 5, 7).

[44] B. W. J. Chen, L. Xu, and M. Mavrikakis, *Computational Methods in Heterogeneous Catalysis*, Chemical Reviews **121**, 1007 (2021) (cit. on p. 5).

[45] A. D. McNaught, A. Wilkinson, et al., *Compendium of chemical terminology*, Vol. 1669 (Blackwell Science Oxford, 1997) (cit. on p. 5).

[46] E. G. Lewars, in *Computational chemistry* (Springer, 2016), pp. 9–49 (cit. on p. 5).

[47] J. Rogal, K. Reuter, and M. Scheffler, *First-Principles Statistical Mechanics Study of the Stability of a Subnanometer Thin Surface Oxide in Reactive Environments: CO Oxidation at Pd(100)*, Physical Review Letters **98**, 046101 (2007) (cit. on pp. 5, 6).

[48] K. Reuter and M. Scheffler, *First-principles kinetic Monte Carlo simulations for heterogeneous catalysis: Application to the CO oxidation at Ru O 2 (110)*, Physical Review B **73**, 045433 (2006) (cit. on pp. 5, 8, 19).

[49] Y. Jiao, Y. Zheng, M. Jaroniec, and S. Z. Qiao, *Design of electrocatalysts for oxygen- and hydrogen-involving energy conversion reactions*, Chemical Society Reviews **44**, 2060 (2015) (cit. on pp. 5, 7).

[50] J. Rogal and K. Reuter, *Ab Initio Atomistic Thermodynamics for Surfaces: A Primer*, 18 (cit. on p. 5).

[51] T. Lee, Y. Lee, S. Piccinin, and A. Soon, Ab Initio *Thermodynamics of Surface Oxide Structures under Controlled Growth Conditions*, The Journal of Physical Chemistry C **121**, 2228 (2017) (cit. on p. 5).

[52] K. Reuter and M. Scheffler, *First-Principles Atomistic Thermodynamics for Oxidation Catalysis: Surface Phase Diagrams and Catalytically Interesting Regions*, Physical Review Letters **90**, 046103 (2003) (cit. on pp. 5, 19).

[53] H. A. Hansen, J. Rossmeisl, and J. K. Nørskov, *Surface Pourbaix diagrams and oxygen reduction activity of Pt, Ag and Ni(111) surfaces studied by DFT*, Physical Chemistry Chemical Physics **10**, 3722 (2008) (cit. on p. 6).

[54] C. Griesser, H. Li, E.-M. Wernig, D. Winkler, N. Shakibi Nia, T. Mairegger, T. Götsch, T. Schachinger, A. Steiger-Thirsfeld, S. Penner, D. Wielend, D. Egger, C. Scheurer, K. Reuter, and J. Kunze-Liebhäuser, *True Nature of the Transition-Metal Carbide/Liquid Interface Determines Its Reactivity*, ACS Catalysis **11**, 4920 (2021) (cit. on p. 6).

[55] K. S. Exner, *A short perspective of modeling electrode materials in lithium-ion batteries by the ab initio atomistic thermodynamics approach*, Journal of Solid State Electrochemistry **22**, 3111 (2018) (cit. on p. 6).

[56] *Constrained Ab Initio Thermodynamics: Transferring the Concept of Surface Pourbaix Diagrams in Electrocatalysis to Electrode Materials in Lithium-Ion Batteries*, 7 (2017) (cit. on p. 6).

[57] H. Li and K. Reuter, *Active-Site Computational Screening: Role of Structural and Compositional Diversity for the Electrochemical CO $_2$ Reduction at Mo Carbide Catalysts*, ACS Catalysis **10**, 11814 (2020) (cit. on pp. 6, 14).

[58] D. Opalka, C. Scheurer, and K. Reuter, *Ab Initio Thermodynamics Insight into the Structural Evolution of Working IrO $_2$ Catalysts in Proton-Exchange Membrane Electrolyzers*, ACS Catalysis **9**, 4944 (2019) (cit. on p. 6).

[59] M. Bajdich, M. García-Mota, A. Vojvodic, J. K. Nørskov, and A. T. Bell, *Theoretical Investigation of the Activity of Cobalt Oxides for the Electrochemical Oxidation of Water*, Journal of the American Chemical Society **135**, 13521 (2013) (cit. on p. 6).

[60] J. Greeley, T. F. Jaramillo, J. Bonde, I. Chorkendorff, and J. K. Nørskov, *Computational high-throughput screening of electrocatalytic materials for hydrogen evolution*, Nature Materials **5**, 909 (2006) (cit. on p. 6).

[61] K. Reuter, C. P. Plaisance, H. Oberhofer, and M. Andersen, *Perspective: On the active site model in computational catalyst screening*, The Journal of Chemical Physics **146**, 040901 (2017) (cit. on pp. 6, 11, 18).

[62] J. K. Nørskov, J. Rossmeisl, A. Logadottir, L. Lindqvist, J. R. Kitchin, T. Bligaard, and H. Jónsson, *Origin of the Overpotential for Oxygen Reduction at a Fuel-Cell Cathode*, The Journal of Physical Chemistry B **108**, 17886 (2004) (cit. on pp. 6, 7).

[63] J. D. Benck, T. R. Hellstern, J. Kibsgaard, P. Chakthranont, and T. F. Jaramillo, *Catalyzing the Hydrogen Evolution Reaction (HER) with Molybdenum Sulfide Nanomaterials*, ACS Catalysis **4**, 3957 (2014) (cit. on p. 7).

[64] Y. Zheng, Y. Jiao, L. H. Li, T. Xing, Y. Chen, M. Jaroniec, and S. Z. Qiao, *Toward Design of Synergistically Active Carbon-Based Catalysts for Electrocatalytic Hydrogen Evolution*, ACS Nano **8**, 5290 (2014) (cit. on p. 7).

[65] X. Zou and Y. Zhang, *Noble metal-free hydrogen evolution catalysts for water splitting*, Chemical Society Reviews **44**, 5148 (2015) (cit. on p. 7).

[66] S. Siahrostami, A. Verdaguer-Casadevall, M. Karamad, D. Deiana, P. Malacrida, B. Wickman, M. Escudero-Escribano, E. A. Paoli, R. Frydendal, T. W. Hansen, I. Chorkendorff, I. E. L. Stephens, and J. Rossmeisl, *Enabling direct H2O2 production through rational electrocatalyst design*, Nature Materials **12**, 1137 (2013) (cit. on p. 7).

[67] A. Verdaguer-Casadevall, D. Deiana, M. Karamad, S. Siahrostami, P. Malacrida, T. W. Hansen, J. Rossmeisl, I. Chorkendorff, and I. E. L. Stephens, *Trends in the Electrochemical Synthesis of H_2O_2: Enhancing Activity and Selectivity by Electrocatalytic Site Engineering*, Nano Letters **14**, 1603 (2014) (cit. on p. 7).

[68] K. P. Kuhl, T. Hatsukade, E. R. Cave, D. N. Abram, J. Kibsgaard, and T. F. Jaramillo, *Electrocatalytic Conversion of Carbon Dioxide to Methane and Methanol on Transition Metal Surfaces*, Journal of the American Chemical Society **136**, 14107 (2014) (cit. on p. 7).

[69] A. A. Peterson, F. Abild-Pedersen, F. Studt, J. Rossmeisl, and J. K. Nørskov, *How copper catalyzes the electroreduction of carbon dioxide into hydrocarbon fuels*, Energy & Environmental Science **3**, 1311 (2010) (cit. on p. 7).

[70] C. Shi, H. A. Hansen, A. C. Lausche, and J. K. Nørskov, *Trends in electrochemical CO2 reduction activity for open and close-packed metal surfaces*, Physical Chemistry Chemical Physics **16**, 4720 (2014) (cit. on p. 7).

[71] S. Ringe, N. G. Hörmann, H. Oberhofer, and K. Reuter, *Implicit Solvation Methods for Catalysis at Electrified Interfaces*, Chemical Reviews **122**, 10777 (2022) (cit. on pp. 7, 40).

[72] S. Back, J. Na, and Z. W. Ulissi, *Efficient Discovery of Active, Selective, and Stable Catalysts for Electrochemical H_2O_2 Synthesis through Active Motif Screening*, ACS Catalysis **11**, 2483 (2021) (cit. on p. 7).

[73] A. Bruix, J. T. Margraf, M. Andersen, and K. Reuter, *First-principles-based multiscale modelling of heterogeneous catalysis*, Nature Catalysis **2**, 659 (2019) (cit. on pp. 7, 8, 40).

[74] M. Rebarchik, S. Bhandari, T. Kropp, and M. Mavrikakis, *How Noninnocent Spectator Species Improve the Oxygen Reduction Activity of Single-Atom Catalysts: Microkinetic Models from First-Principles Calculations*, ACS Catalysis **10**, 9129 (2020) (cit. on p. 8).

[75] M. Deimel, K. Reuter, and M. Andersen, *Active Site Representation in First-Principles Microkinetic Models: Data-Enhanced Computational Screening for Improved Methanation Catalysts*, ACS Catalysis **10**, 13729 (2020) (cit. on pp. 8, 15).

[76] S. Linic, *Construction of a reaction coordinate and a microkinetic model for ethylene epoxidation on silver from DFT calculations and surface science experiments*, Journal of Catalysis **214**, 200 (2003) (cit. on p. 8).

[77] S. Pogodin and N. López, *A More Accurate Kinetic Monte Carlo Approach to a Monodimensional Surface Reaction: The Interaction of Oxygen with the RuO $_2$ (110) Surface*, ACS Catalysis **4**, 2328 (2014) (cit. on p. 8).

[78] M. Deimel, H. Prats, M. Seibt, K. Reuter, and M. Andersen, *Selectivity Trends and Role of Adsorbate–Adsorbate Interactions in CO Hydrogenation on Rhodium Catalysts*, ACS Catalysis **12**, 7907 (2022) (cit. on pp. 8, 15).

[79] S. T. Chill and G. Henkelman, *Molecular dynamics saddle search adaptive kinetic Monte Carlo*, The Journal of Chemical Physics **140**, 214110 (2014) (cit. on pp. 8, 40).

[80] M. Andersen, C. Panosetti, and K. Reuter, *A Practical Guide to Surface Kinetic Monte Carlo Simulations*, Frontiers in Chemistry **7**, 202 (2019) (cit. on p. 8).

[81] S. Matera, W. F. Schneider, A. Heyden, and A. Savara, *Progress in Accurate Chemical Kinetic Modeling, Simulations, and Parameter Estimation for Heterogeneous Catalysis*, ACS Catalysis **9**, 6624 (2019) (cit. on p. 8).

[82] V. Dufour-Décieux, R. Freitas, and E. J. Reed, *Atomic-Level Features for Kinetic Monte Carlo Models of Complex Chemistry from Molecular Dynamics Simulations*, The Journal of Physical Chemistry A **125**, 4233 (2021) (cit. on p. 8).

[83] A. B. Laursen, A. S. Varela, F. Dionigi, H. Fanchiu, C. Miller, O. L. Trinhammer, J. Rossmeisl, and S. Dahl, *Electrochemical Hydrogen Evolution: Sabatier's Principle and the Volcano Plot*, Journal of Chemical Education **89**, 1595 (2012) (cit. on p. 8).

[84] J. K. Nørskov, T. Bligaard, J. Rossmeisl, and C. H. Christensen, *Towards the computational design of solid catalysts*, Nature Chemistry **1**, 37 (2009) (cit. on p. 8).

[85] M. Che, *Nobel Prize in chemistry 1912 to Sabatier: Organic chemistry or catalysis?* Catalysis Today **218–219**, 162 (2013) (cit. on p. 8).

[86] A. J. Medford, A. Vojvodic, J. S. Hummelshøj, J. Voss, F. Abild-Pedersen, F. Studt, T. Bligaard, A. Nilsson, and J. K. Nørskov, *From the Sabatier principle to a predictive theory of transition-metal heterogeneous catalysis*, Journal of Catalysis **328**, 36 (2015) (cit. on p. 8).

[87] J. N. Bbonsted, *Acid and Basic Catalysis.* 108 (cit. on p. 8).

[88] H. Eyring, *INERTIA AND DRIVING FORCE OF CHEMICAL REACTIONS. BY M. G. EVANSAND M. POLANYI.* 14 (cit. on p. 8).

[89] G. Henkelman and H. Jónsson, *Improved tangent estimate in the nudged elastic band method for finding minimum energy paths and saddle points*, The Journal of Chemical Physics **113**, 9978 (2000) (cit. on p. 9).

[90] H. Jónsson, G. Mills, and K. W. Jacobsen, "Nudged elastic band method for finding minimum energy paths of transitions," in Classical and Quantum Dynamics in Condensed Phase Simulations (June 1998), pp. 385–404 (cit. on p. 9).

[91] G. Henkelman and H. Jónsson, *A dimer method for finding saddle points on high dimensional potential surfaces using only first derivatives*, The Journal of Chemical Physics **111**, 7010 (1999) (cit. on p. 9).

[92] P. Hohenberg and W. Kohn, *Inhomogeneous Electron Gas*, Physical Review **136**, B864 (1964) (cit. on p. 9).

[93] W. Kohn and L. J. Sham, *Self-Consistent Equations Including Exchange and Correlation Effects*, Physical Review **140**, A1133 (1965) (cit. on p. 10).

[94] A. J. Cohen, P. Mori-Sánchez, and W. Yang, *Challenges for Density Functional Theory*, Chemical Reviews **112**, 289 (2012) (cit. on p. 10).

[95] K. Burke and L. O. Wagner, *DFT in a nutshell*, International Journal of Quantum Chemistry **113**, 96 (2013) (cit. on p. 10).

[96] J. P. Perdew, "Jacob's ladder of density functional approximations for the exchange-correlation energy," in AIP Conference Proceedings, Vol. 577 (2001), pp. 1–20 (cit. on p. 10).

[97] I. Y. Zhang and X. Xu, *On the top rung of Jacob's ladder of density functional theory: Toward resolving the dilemma of SIE and NCE*, WIREs Computational Molecular Science **11**, `10.1002/wcms.1490` (2021) (cit. on p. 10).

[98] J. P. Perdew, K. Burke, and M. Ernzerhof, *Generalized Gradient Approximation Made Simple*, Physical Review Letters **77**, 3865 (1996) (cit. on p. 10).

[99] C. D. Sherrill, *Frontiers in electronic structure theory*, The Journal of Chemical Physics **132**, 110902 (2010) (cit. on p. 10).

[100] I. Dabo, A. Ferretti, N. Poilvert, Y. Li, N. Marzari, and M. Cococcioni, *Koopmans' condition for density-functional theory*, Physical Review B **82**, 115121 (2010) (cit. on p. 10).

[101] O. A. Vydrov, G. E. Scuseria, and J. P. Perdew, *Tests of functionals for systems with fractional electron number*, The Journal of Chemical Physics **126**, 154109 (2007) (cit. on p. 10).

[102] J. Wellendorff, K. T. Lundgaard, A. Møgelhøj, V. Petzold, D. D. Landis, J. K. Nørskov, T. Bligaard, and K. W. Jacobsen, *Density functionals for surface science: Exchange-correlation model development with Bayesian error estimation*, Physical Review B **85**, 235149 (2012) (cit. on p. 10).

[103] P. Politzer and J. S. Murray, *The Hellmann-Feynman theorem: a perspective*, Journal of Molecular Modeling **24**, 266 (2018) (cit. on p. 10).

[104] J. L. Nazareth, *Conjugate gradient method*, WIREs Computational Statistics **1**, 348 (2009) (cit. on p. 10).

[105] J. D. Head and M. C. Zerner, *A BROYDEN-FLETCHER-GOLDFARB-SHANNO FOR MOLECULAR GEOMETRIES*, **122**, 7 (1985) (cit. on p. 10).

[106] H. S. Yu, S. L. Li, and D. G. Truhlar, *Perspective: Kohn-Sham density functional theory descending a staircase*, The Journal of Chemical Physics **145**, 130901 (2016) (cit. on p. 10).

[107] J. Suntivich, K. J. May, H. A. Gasteiger, J. B. Goodenough, and Y. Shao-Horn, *A Perovskite Oxide Optimized for Oxygen Evolution Catalysis from Molecular Orbital Principles*, Science **334**, 1383 (2011) (cit. on pp. 11, 12).

[108] D. Wu, C. Dong, H. Zhan, and X.-W. Du, *Bond-Energy-Integrated Descriptor for Oxygen Electrocatalysis of Transition Metal Oxides*, The Journal of Physical Chemistry Letters **9**, 3387 (2018) (cit. on pp. 12, 13).

[109] R. Michalsky, A. M. Avram, B. A. Peterson, P. H. Pfromm, and A. A. Peterson, *Chemical looping of metal nitride catalysts: low-pressure ammonia synthesis for energy storage*, Chemical Science **6**, 3965 (2015) (cit. on pp. 11, 12).

[110] H. Yuan, Z. Li, X. C. Zeng, and J. Yang, *Descriptor-Based Design Principle for Two-Dimensional Single-Atom Catalysts: Carbon Dioxide Electroreduction*, The Journal of Physical Chemistry Letters **11**, 3481 (2020) (cit. on p. 11).

[111] Y. Zhou, S. Sun, S. Xi, Y. Duan, T. Sritharan, Y. Du, and Z. J. Xu, *Superexchange Effects on Oxygen Reduction Activity of Edge-Sharing [$Co_x Mn_{1-x} O_6$] Octahedra in Spinel Oxide*, Advanced Materials **30**, 1705407 (2018) (cit. on p. 11).

[112] J. Suntivich, H. A. Gasteiger, N. Yabuuchi, H. Nakanishi, J. B. Goodenough, and Y. Shao-Horn, *Design principles for oxygen-reduction activity on perovskite oxide catalysts for fuel cells and metal–air batteries*, Nature Chemistry **3**, 546 (2011) (cit. on p. 11).

[113] C. F. Dickens, J. H. Montoya, A. R. Kulkarni, M. Bajdich, and J. K. Nørskov, *An electronic structure descriptor for oxygen reactivity at metal and metal-oxide surfaces*, Surface Science **681**, 122 (2019) (cit. on p. 11).

[114] W. T. Hong, K. A. Stoerzinger, Y.-L. Lee, L. Giordano, A. Grimaud, A. M. Johnson, J. Hwang, E. J. Crumlin, W. Yang, and Y. Shao-Horn, *Charge-transfer-energy-dependent oxygen evolution reaction mechanisms for perovskite oxides*, Energy & Environmental Science **10**, 2190 (2017) (cit. on pp. 11, 27).

[115] I. Yamada, A. Takamatsu, K. Asai, T. Shirakawa, H. Ohzuku, A. Seno, T. Uchimura, H. Fujii, S. Kawaguchi, K. Wada, H. Ikeno, and S. Yagi, *Systematic Study of Descriptors for Oxygen Evolution Reaction Catalysis in Perovskite Oxides*, The Journal of Physical Chemistry C **122**, 27885 (2018) (cit. on p. 11).

[116] E. Skúlason, T. Bligaard, S. Gudmundsdóttir, F. Studt, J. Rossmeisl, F. Abild-Pedersen, T. Vegge, H. Jónsson, and J. K. Nørskov, *A theoretical evaluation of possible transition metal electro-catalysts for N_2 reduction*, Phys. Chem. Chem. Phys. **14**, 1235 (2012) (cit. on p. 14).

[117] M. M. Montemore and J. W. Medlin, *A Unified Picture of Adsorption on Transition Metals through Different Atoms*, J. Am. Chem. Soc., 4 (2014) (cit. on p. 14).

[118] G. Jones, *Scaling relationships for adsorption energies of C2 hydrocarbons on transition metal surfaces*, Chemical Engineering Science, 6 (2011) (cit. on p. 14).

[119] T. A. Batchelor, J. K. Pedersen, S. H. Winther, I. E. Castelli, K. W. Jacobsen, and J. Rossmeisl, *High-Entropy Alloys as a Discovery Platform for Electrocatalysis*, Joule **3**, 834 (2019) (cit. on p. 14).

[120] A. Khorshidi, J. Violet, J. Hashemi, and A. A. Peterson, *How strain can break the scaling relations of catalysis*, Nature Catalysis **1**, 263 (2018) (cit. on p. 14).

[121] F. A. Garcés-Pineda, M. Blasco-Ahicart, D. Nieto-Castro, N. López, and J. R. Galán-Mascarós, *Direct magnetic enhancement of electrocatalytic water oxidation in alkaline media*, Nature Energy **4**, 519 (2019) (cit. on p. 14).

[122] S. Linic, P. Christopher, and D. B. Ingram, *Plasmonic-metal nanostructures for efficient conversion of solar to chemical energy*, Nature Materials **10**, 911 (2011) (cit. on p. 14).

[123] J. C. Robertson, M. L. Coote, and A. C. Bissember, *Synthetic applications of light, electricity, mechanical force and flow*, Nature Reviews Chemistry **3**, 290 (2019) (cit. on p. 14).

[124] J. Pérez-Ramírez and N. López, *Strategies to break linear scaling relationships*, Nature Catalysis **2**, 971 (2019) (cit. on p. 14).

[125] S. Piccinin and M. Stamatakis, *CO Oxidation on Pd(111): A First-Principles-Based Kinetic Monte Carlo Study*, ACS Catalysis **4**, 2143 (2014) (cit. on p. 15).

[126] F. Calle-Vallejo, J. I. Martínez, J. M. García-Lastra, P. Sautet, and D. Loffreda, *Fast Prediction of Adsorption Properties for Platinum Nanocatalysts with Generalized Coordination Numbers*, Angewandte Chemie International Edition **53**, 8316 (2014) (cit. on pp. 14, 27).

[127] R. Garcıa-Muelas, Q. Li, and N. López, *Density Functional Theory Comparison of Methanol Decomposition and Reverse Reactions on Metal Surfaces*, ACS Catalysis **5**, 1027 (2015) (cit. on p. 14).

[128] J. E. Sutton, W. Guo, M. A. Katsoulakis, and D. G. Vlachos, *Effects of correlated parameters and uncertainty in electronic-structure-based chemical kinetic modelling*, Nature Chemistry **8**, 331 (2016) (cit. on p. 14).

[129] D. Loffreda, F. Delbecq, F. Vigné, and P. Sautet, *Fast Prediction of Selectivity in Heterogeneous Catalysis from Extended Brønsted-Evans-Polanyi Relations: A Theoretical Insight*, Angewandte Chemie **121**, 9140 (2009) (cit. on p. 14).

[130] Q. Li, R. García-Muelas, and N. López, *Microkinetics of alcohol reforming for H2 production from a FAIR density functional theory database*, Nature Communications **9**, 526 (2018) (cit. on p. 15).

[131] X. Zhu, J. Huang, and M. Eikerling, *Electrochemical CO_2 Reduction at Silver from a Local Perspective*, ACS Catalysis **11**, 14521 (2021) (cit. on p. 15).

[132] Z.-B. Ding and M. Maestri, *Development and Assessment of a Criterion for the Application of Brønsted–Evans–Polanyi Relations for Dissociation Catalytic Reactions at Surfaces*, Industrial & Engineering Chemistry Research **58**, 9864 (2019) (cit. on p. 15).

[133] J. E. Sutton and D. G. Vlachos, *Effect of errors in linear scaling relations and Brønsted–Evans–Polanyi relations on activity and selectivity maps*, Journal of Catalysis **338**, 273 (2016) (cit. on p. 15).

[134] S. Pablo-García, R. García-Muelas, A. Sabadell-Rendón, and N. López, *Dimensionality reduction of complex reaction networks in heterogeneous catalysis: From l INEAR-SCALING relationships to statistical learning techniques*, WIREs Computational Molecular Science **11**, 10.1002/wcms.1540 (2021) (cit. on p. 17).

[135] J. Li, H. Chang, L. Ma, J. Hao, and R. T. Yang, *Low-temperature selective catalytic reduction of NOx with NH3 over metal oxide and zeolite catalysts—A review*, Catalysis Today **175**, 147 (2011) (cit. on p. 17).

[136] T. O. Ajiboye, A. T. Kuvarega, and D. C. Onwudiwe, *Graphitic carbon nitride-based catalysts and their applications: A review*, Nano-Structures & Nano-Objects **24**, 100577 (2020) (cit. on p. 17).

[137] J. Zhu, P. Xiao, H. Li, and S. A. C. Carabineiro, *Graphitic Carbon Nitride: Synthesis, Properties, and Applications in Catalysis*, ACS Applied Materials & Interfaces **6**, 16449 (2014) (cit. on p. 17).

[138] H. Wang, K. H. L. Zhang, J. P. Hofmann, V. A. de la Peña O'Shea, and F. E. Oropeza, *The electronic structure of transition metal oxides for oxygen evolution reaction*, Journal of Materials Chemistry A **9**, 19465 (2021) (cit. on p. 18).

[139] M. T. Greiner and Z.-H. Lu, *Thin-film metal oxides in organic semiconductor devices: their electronic structures, work functions and interfaces*, NPG Asia Materials **5**, e55 (2013) (cit. on p. 18).

[140] Z. Zhang and J. T. Yates, *Band Bending in Semiconductors: Chemical and Physical Consequences at Surfaces and Interfaces*, Chemical Reviews **112**, 5520 (2012) (cit. on p. 18).

[141] Z. Yao and K. Reuter, *First-Principles Computational Screening of Dopants to Improve the Deacon Process over RuO_2*, ChemCatChem **10**, 465 (2018) (cit. on p. 18).

[142] X. Cui, J. Wang, B. Liu, S. Ling, R. Long, and Y. Xiong, *Turning Au Nanoclusters Catalytically Active for Visible-Light-Driven CO_2 Reduction through Bridging Ligands*, Journal of the American Chemical Society **140**, 16514 (2018) (cit. on p. 18).

[143] J.-X. Liu, I. A. W. Filot, Y. Su, B. Zijlstra, and E. J. M. Hensen, *Optimum Particle Size for Gold-Catalyzed CO Oxidation*, The Journal of Physical Chemistry C **122**, 8327 (2018) (cit. on p. 18).

[144] M. Luo and S. Guo, *Strain-controlled electrocatalysis on multimetallic nanomaterials*, Nature Reviews Materials **2**, 17059 (2017) (cit. on p. 18).

[145] M. Mavrikakis, B. Hammer, and J. K. Nørskov, *Effect of Strain on the Reactivity of Metal Surfaces*, Physical Review Letters **81**, 2819 (1998) (cit. on p. 18).

[146] M. Moser, I. Czekaj, N. López, and J. Pérez-Ramírez, *Frontispiece: The Virtue of Defects: Stable Bromine Production by Catalytic Oxidation of Hydrogen Bromide on Titanium Oxide*, Angewandte Chemie International Edition **53**, `10.1002/anie.201483371` (2014) (cit. on p. 18).

[147] C. T. Campbell, S. C. Parker, and D. E. Starr, *The Effect of Size-Dependent Nanoparticle Energetics on Catalyst Sintering*, Science **298**, 811 (2002) (cit. on p. 18).

[148] L. Foppa, T. Margossian, S. M. Kim, C. Müller, C. Copéret, K. Larmier, and A. Comas-Vives, *Contrasting the Role of Ni/Al_2O_3 Interfaces in Water–Gas Shift and Dry Reforming of Methane*, Journal of the American Chemical Society **139**, 17128 (2017) (cit. on p. 18).

[149] S. S. Grønborg, N. Salazar, A. Bruix, J. Rodríguez-Fernández, S. D. Thomsen, B. Hammer, and J. V. Lauritsen, *Visualizing hydrogen-induced reshaping and edge activation in MoS2 and Co-promoted MoS2 catalyst clusters*, Nature Communications **9**, 2211 (2018) (cit. on p. 18).

[150] M. Jørgensen and H. Grönbeck, *Scaling Relations and Kinetic Monte Carlo Simulations To Bridge the Materials Gap in Heterogeneous Catalysis*, ACS Catalysis **7**, 5054 (2017) (cit. on p. 18).

[151] M.-C. Silaghi, A. Comas-Vives, and C. Copéret, *CO_2 Activation on Ni/γ–Al_2O_3 Catalysts by First-Principles Calculations: From Ideal Surfaces to Supported Nanoparticles*, ACS Catalysis **6**, 4501 (2016) (cit. on p. 18).

[152] B. Zugic, L. Wang, C. Heine, D. N. Zakharov, B. A. J. Lechner, E. A. Stach, J. Biener, M. Salmeron, R. J. Madix, and C. M. Friend, *Dynamic restructuring drives catalytic activity on nanoporous gold–silver alloy catalysts*, Nature Materials **16**, 558 (2017) (cit. on p. 18).

[153] J. S. Lim, J. Vandermause, M. A. van Spronsen, A. Musaelian, Y. Xie, L. Sun, C. R. O'Connor, T. Egle, N. Molinari, J. Florian, K. Duanmu, R. J. Madix, P. Sautet, C. M. Friend, and B. Kozinsky, *Evolution of Metastable Structures at Bimetallic Surfaces from Microscopy and Machine-Learning Molecular Dynamics*, Journal of the American Chemical Society **142**, 15907 (2020) (cit. on p. 18).

[154] J. Timmermann, F. Kraushofer, N. Resch, P. Li, Y. Wang, Z. Mao, M. Riva, Y. Lee, C. Staacke, M. Schmid, C. Scheurer, G. S. Parkinson, U. Diebold, and K. Reuter, *IrO 2 Surface Complexions Identified through Machine Learning and Surface Investigations*, Physical Review Letters **125**, 206101 (2020) (cit. on p. 18).

[155] R. García-Muelas and N. López, *Collective Descriptors for the Adsorption of Sugar Alcohols on Pt and Pd(111)*, The Journal of Physical Chemistry C **118**, 17531 (2014) (cit. on p. 18).

[156] I. A. W. Filot, R. J. P. Broos, J. P. M. van Rijn, G. J. H. A. van Heugten, R. A. van Santen, and E. J. M. Hensen, *First-Principles-Based Microkinetics Simulations of Synthesis Gas Conversion on a Stepped Rhodium Surface*, ACS Catalysis **5**, 5453 (2015) (cit. on p. 19).

[157] A. Cao, J. Schumann, T. Wang, L. Zhang, J. Xiao, P. Bothra, Y. Liu, F. Abild-Pedersen, and J. K. Nørskov, *Mechanistic Insights into the Synthesis of Higher Alcohols from Syngas on CuCo Alloys*, ACS Catalysis **8**, 10148 (2018) (cit. on p. 19).

[158] T. Gu, B. Wang, S. Chen, and B. Yang, *Automated Generation and Analysis of the Complex Catalytic Reaction Network of Ethanol Synthesis from Syngas on Rh(111)*, ACS Catalysis **10**, 6346 (2020) (cit. on p. 19).

[159] Z. W. Ulissi, A. J. Medford, T. Bligaard, and J. K. Nørskov, *To address surface reaction network complexity using scaling relations machine learning and DFT calculations*, Nature Communications **8**, 14621 (2017) (cit. on p. 19).

[160] J. R. Boes, O. Mamun, K. Winther, and T. Bligaard, *Graph Theory Approach to High-Throughput Surface Adsorption Structure Generation*, The Journal of Physical Chemistry A **123**, 2281 (2019) (cit. on pp. 19, 24, 30).

[161] M. Parrinello, *Complex chemistry*, `https://www.youtube.com/watch?v=c0ouIW5lhRA`, May 2022 (cit. on p. 19).

[162] M. Garcia-Ratés, R. García-Muelas, and N. López, *Solvation Effects on Methanol Decomposition on Pd(111), Pt(111), and Ru(0001)*, J. Phys. Chem. C, 7 (2017) (cit. on p. 19).

[163] M. Garcia-Ratés and N. López, *Multigrid-Based Methodology for Implicit Solvation Models in Periodic DFT*, Journal of Chemical Theory and Computation **12**, 1331 (2016) (cit. on p. 19).

[164] Q. Li, R. García-Muelas, and N. López, *Microkinetics of alcohol reforming for H2 production from a FAIR density functional theory database*, Nature Communications **9**, 526 (2018) (cit. on p. 19).

[165] M. Alvarez-Guerra, J. Albo, E. Alvarez-Guerra, and A. Irabien, *Ionic liquids in the electrochemical valorisation of CO $_2$*, Energy & Environmental Science **8**, 2574 (2015) (cit. on p. 19).

[166] Y. Oh and X. Hu, *Ionic liquids enhance the electrochemical CO $_2$ reduction catalyzed by MoO $_2$*, Chemical Communications **51**, 13698 (2015) (cit. on p. 19).

[167] Y. Qiu, H. Zhong, W. Xu, T. Zhang, X. Li, and H. Zhang, *Tuning the electrocatalytic properties of a Cu electrode with organic additives containing amine group for CO $_2$ reduction*, Journal of Materials Chemistry A **7**, 5453 (2019) (cit. on p. 19).

[168] W. Xu, Y. Qiu, T. Zhang, X. Li, and H. Zhang, *The Effect of Organic Additives on the Activity and Selectivity of CO $_2$ Electroreduction: The Role of Functional Groups*, ChemSusChem **11**, 2904 (2018) (cit. on p. 19).

[169] F. Olsson, *A literature survey of active machine learning in the context of natural language processing*, 59 (cit. on pp. 21, 31).

[170] A. Voulodimos, N. Doulamis, A. Doulamis, and E. Protopapadakis, *Deep Learning for Computer Vision: A Brief Review*, Computational Intelligence and Neuroscience **2018**, 1 (2018) (cit. on p. 21).

[171] J. Stilgoe, *Machine learning, social learning and the governance of self-driving cars*, Social Studies of Science, 32 (cit. on p. 21).

[172] L. Zhang, J. Tan, D. Han, and H. Zhu, *From machine learning to deep learning: progress in machine intelligence for rational drug discovery*, Drug Discovery Today **22**, 1680 (2017) (cit. on p. 21).

[173] A. Johansson, Y. Xie, C. J. Owen, J. S. Lim, L. Sun, J. Vandermause, and B. Kozinsky, *Micron-scale heterogeneous catalysis with Bayesian force fields from first principles and active learning*, Apr. 26, 2022 (cit. on p. 21).

[174] B. R. Goldsmith, J. Esterhuizen, J.-X. Liu, C. J. Bartel, and C. Sutton, *Machine learning for heterogeneous catalyst design and discovery*, AIChE Journal **64**, 2311 (2018) (cit. on p. 21).

[175] O. T. Unke, S. Chmiela, H. E. Sauceda, M. Gastegger, I. Poltavsky, K. T. Schütt, A. Tkatchenko, and K.-R. Müller, *Machine Learning Force Fields*, Chemical Reviews **121**, 10142 (2021) (cit. on p. 21).

[176] J. Xu, X.-M. Cao, and P. Hu, *Perspective on computational reaction prediction using machine learning methods in heterogeneous catalysis*, Physical Chemistry Chemical Physics **23**, 11155 (2021) (cit. on p. 21).

[177] E. Kocer, T. W. Ko, and J. Behler, *Neural Network Potentials: A Concise Overview of Methods*, July 8, 2021 (cit. on p. 21).

[178] P. Schlexer Lamoureux, K. T. Winther, J. A. Garrido Torres, V. Streibel, M. Zhao, M. Bajdich, F. Abild-Pedersen, and T. Bligaard, *Machine Learning for Computational Heterogeneous Catalysis*, ChemCatChem **11**, 3581 (2019) (cit. on p. 21).

[179] J. Noh, S. Back, J. Kim, and Y. Jung, *Active learning with non-* ab initio *input features toward efficient CO $_2$ reduction catalysts*, Chemical Science **9**, 5152 (2018) (cit. on p. 22).

[180] O. Mamun, K. T. Winther, J. R. Boes, and T. Bligaard, *A Bayesian framework for adsorption energy prediction on bimetallic alloy catalysts*, npj Computational Materials **6**, 177 (2020) (cit. on pp. 22, 28).

[181] Z. Li, S. Wang, W. S. Chin, L. E. Achenie, and H. Xin, *High-throughput screening of bimetallic catalysts enabled by machine learning*, Journal of Materials Chemistry A **5**, 24131 (2017) (cit. on p. 22).

[182] V. Fung, G. Hu, P. Ganesh, and B. G. Sumpter, *Machine learned features from density of states for accurate adsorption energy prediction*, Nature Communications **12**, 88 (2021) (cit. on pp. 22, 26, 29).

[183] S. Back, J. Yoon, N. Tian, W. Zhong, K. Tran, and Z. W. Ulissi, *Convolutional Neural Network of Atomic Surface Structures To Predict Binding Energies for High-Throughput Screening of Catalysts*, The Journal of Physical Chemistry Letters **10**, 4401 (2019) (cit. on pp. 22, 29).

[184] S.-H. Wang, H. S. Pillai, S. Wang, L. E. K. Achenie, and H. Xin, *Infusing theory into deep learning for interpretable reactivity prediction*, Nature Communications **12**, 5288 (2021) (cit. on p. 22).

[185] L. Chanussot, A. Das, S. Goyal, T. Lavril, M. Shuaibi, M. Riviere, K. Tran, J. Heras-Domingo, C. Ho, W. Hu, A. Palizhati, A. Sriram, B. Wood, J. Yoon, D. Parikh, C. L. Zitnick, and Z. Ulissi, *Open Catalyst 2020 (OC20) Dataset and Community Challenges*, ACS Catalysis **11**, 6059 (2021) (cit. on pp. 22, 23, 29).

[186] R. Tran, J. Lan, M. Shuaibi, S. Goyal, B. M. Wood, A. Das, J. Heras-Domingo, A. Kolluru, A. Rizvi, N. Shoghi, A. Sriram, Z. Ulissi, and C. L. Zitnick, *The Open Catalyst 2022 (OC22) Dataset and Challenges for Oxide Electrocatalysis*, June 17, 2022 (cit. on pp. 22, 23, 29).

[187] T. W. Ko, J. A. Finkler, S. Goedecker, and J. Behler, *General-Purpose Machine Learning Potentials Capturing Nonlocal Charge Transfer*, Accounts of Chemical Research **54**, 808 (2021) (cit. on pp. 21, 28).

[188] M. H. S. Segler, M. Preuss, and M. P. Waller, *Planning chemical syntheses with deep neural networks and symbolic AI*, Nature **555**, 604 (2018) (cit. on p. 22).

[189] Jianlin Cheng, A. Tegge, and P. Baldi, *Machine Learning Methods for Protein Structure Prediction*, IEEE Reviews in Biomedical Engineering **1**, 41 (2008) (cit. on p. 22).

[190] T. Xie and J. C. Grossman, *Crystal Graph Convolutional Neural Networks for an Accurate and Interpretable Prediction of Material Properties*, Physical Review Letters **120**, 145301 (2018) (cit. on pp. 22, 24).

[191] J. Musielewicz, X. Wang, T. Tian, and Z. Ulissi, *FINETUNA: Fine-tuning Accelerated Molecular Simulations*, July 1, 2022 (cit. on p. 23).

[192] D. J. Wales and J. P. K. Doye, *Global Optimization by Basin-Hopping and the Lowest Energy Structures of Lennard-Jones Clusters Containing up to 110 Atoms*, The Journal of Physical Chemistry A **101**, 5111 (1997) (cit. on p. 23).

[193] M. Sambridge, *A Parallel Tempering algorithm for probabilistic sampling and multimodal optimization*, Geophysical Journal International **196**, 357 (2014) (cit. on p. 23).

[194] J. Kästner, *Umbrella sampling: Umbrella sampling*, Wiley Interdisciplinary Reviews: Computational Molecular Science **1**, 932 (2011) (cit. on p. 23).

[195] G. Torrie and J. Valleau, *Nonphysical sampling distributions in Monte Carlo free-energy estimation: Umbrella sampling*, Journal of Computational Physics **23**, 187 (1977) (cit. on p. 23).

[196] P.-L. Kang, C. Shang, and Z.-P. Liu, *Large-Scale Atomic Simulation via Machine Learning Potentials Constructed by Global Potential Energy Surface Exploration*, Accounts of Chemical Research **53**, 2119 (2020) (cit. on p. 23).

[197] S. Ma, C. Shang, and Z.-P. Liu, *Heterogeneous catalysis from structure to activity via SSW-NN method*, The Journal of Chemical Physics **151**, 050901 (2019) (cit. on p. 23).

[198] A. P. Bartók, S. De, C. Poelking, N. Bernstein, J. R. Kermode, G. Csányi, and M. Ceriotti, *Machine learning unifies the modeling of materials and molecules*, Science Advances **3**, e1701816 (2017) (cit. on pp. 23, 29).

[199] S. Stocker, G. Csányi, K. Reuter, and J. T. Margraf, *Machine learning in chemical reaction space*, Nature Communications **11**, 5505 (2020) (cit. on p. 23).

[200] C. Kunkel, J. T. Margraf, K. Chen, H. Oberhofer, and K. Reuter, *Active discovery of organic semiconductors*, Nature Communications **12**, 2422 (2021) (cit. on p. 23).

[201] K. Tran and Z. W. Ulissi, *Active learning across intermetallics to guide discovery of electrocatalysts for CO2 reduction and H2 evolution*, Nature Catalysis **1**, 696 (2018) (cit. on pp. 23, 31).

[202] F. Musil, A. Grisafi, A. P. Bartók, C. Ortner, G. Csányi, and M. Ceriotti, *Physics-Inspired Structural Representations for Molecules and Materials*, Chemical Reviews **121**, 9759 (2021) (cit. on pp. 24, 25, 29).

[203] M. Wen, S. M. Blau, E. W. C. Spotte-Smith, S. Dwaraknath, and K. A. Persson, *BonDNet: a graph neural network for the prediction of bond dissociation energies for charged molecules*, Chemical Science **12**, 1858 (2021) (cit. on p. 24).

[204] J. Behler, *Atom-centered symmetry functions for constructing high-dimensional neural network potentials*, The Journal of Chemical Physics **134**, 074106 (2011) (cit. on p. 25).

[205] H. Huo and M. Rupp, *Unified Representation of Molecules and Crystals for Machine Learning*, Jan. 2, 2018 (cit. on p. 25).

[206] J. Nigam, S. Pozdnyakov, G. Fraux, and M. Ceriotti, *Unified theory of atom-centered representations and message-passing machine-learning schemes*, The Journal of Chemical Physics **156**, 204115 (2022) (cit. on p. 25).

[207] Z. Qiao, M. Welborn, A. Anandkumar, F. R. Manby, and T. F. Miller, *OrbNet: Deep learning for quantum chemistry using symmetry-adapted atomic-orbital features*, The Journal of Chemical Physics **153**, 124111 (2020) (cit. on p. 25).

[208] Z. Qiao, A. S. Christensen, M. Welborn, F. R. Manby, A. Anandkumar, and T. F. Miller III, *Informing Geometric Deep Learning with Electronic Interactions to Accelerate Quantum Chemistry*, Apr. 1, 2022 (cit. on p. 25).

[209] C. Chang and A. J. Medford, *Application of Density Functional Tight Binding and Machine Learning to Evaluate the Stability of Biomass Intermediates on the Rh(111) Surface*, The Journal of Physical Chemistry C **125**, 18210 (2021) (cit. on p. 25).

[210] M. Andersen and K. Reuter, *Adsorption Enthalpies for Catalysis Modeling through Machine-Learned Descriptors*, Accounts of Chemical Research **54**, 2741 (2021) (cit. on p. 25).

[211] M. Pal, *Random forest classifier for remote sensing classification*, International Journal of Remote Sensing **26**, 217 (2005) (cit. on p. 26).

[212] T. Chen and C. Guestrin, "XGBoost: A Scalable Tree Boosting System," in Proceedings of the 22nd ACM SIGKDD International Conference on Knowledge Discovery and Data Mining (Aug. 13, 2016), pp. 785–794 (cit. on p. 26).

[213] R. Muthukrishnan and R. Rohini, "LASSO: A feature selection technique in predictive modeling for machine learning," in 2016 IEEE International Conference on Advances in Computer Applications (ICACA) (Oct. 2016), pp. 18–20 (cit. on p. 26).

[214] J. Ranstam and J. A. Cook, *LASSO regression*, British Journal of Surgery **105**, 1348 (2018) (cit. on p. 26).

[215] A. E. Hoerl and R. W. Kennard, *Ridge Regression: Applications to Nonorthogonal Problems*, Technometrics **12**, 69 (1970) (cit. on p. 26).

[216] F. Calle-Vallejo, N. G. Inoglu, H.-Y. Su, J. I. Martínez, I. C. Man, M. T. M. Koper, J. R. Kitchin, and J. Rossmeisl, *Number of outer electrons as descriptor for adsorption processes on transition metals and their oxides*, Chemical Science **4**, 1245 (2013) (cit. on p. 27).

[217] M. Rupp, *Machine learning for quantum mechanics in a nutshell*, International Journal of Quantum Chemistry **115**, 1058 (2015) (cit. on p. 27).

[218] G. Nikolentzos and M. Vazirgiannis, *Message Passing Graph Kernels*, Aug. 7, 2018 (cit. on p. 27).

[219] N. Shervashidze, *Weisfeiler-Lehman Graph Kernels*, 23 (cit. on p. 27).

[220] M. Togninalli, E. Ghisu, F. Llinares-López, B. Rieck, and K. Borgwardt, *Wasserstein Weisfeiler-Lehman Graph Kernels*, 11 (cit. on p. 27).

[221] G. Nikolentzos, G. Siglidis, and M. Vazirgiannis, *Graph Kernels: A Survey*, Journal of Artificial Intelligence Research **72**, 943 (2021) (cit. on p. 28).

[222] J. Vandermause, S. B. Torrisi, S. Batzner, Y. Xie, L. Sun, A. M. Kolpak, and B. Kozinsky, *On-the-fly active learning of interpretable Bayesian force fields for atomistic rare events*, npj Computational Materials **6**, 20 (2020) (cit. on pp. 28, 30).

[223] M. Todorović, M. U. Gutmann, J. Corander, and P. Rinke, *Bayesian inference of atomistic structure in functional materials*, npj Computational Materials **5**, 35 (2019) (cit. on p. 28).

[224] J. Behler and M. Parrinello, *Generalized Neural-Network Representation of High-Dimensional Potential-Energy Surfaces*, Physical Review Letters **98**, 146401 (2007) (cit. on p. 28).

[225] N. Artrith, T. Morawietz, and J. Behler, *High-dimensional neural-network potentials for multicomponent systems: Applications to zinc oxide*, Physical Review B **83**, 153101 (2011) (cit. on p. 28).

[226] T. W. Ko, J. A. Finkler, S. Goedecker, and J. Behler, *A fourth-generation high-dimensional neural network potential with accurate electrostatics including non-local charge transfer*, Nature Communications **12**, 398 (2021) (cit. on pp. 28, 29).

[227] J. Gilmer, S. S. Schoenholz, P. F. Riley, O. Vinyals, and G. E. Dahl, *Neural Message Passing for Quantum Chemistry*, June 12, 2017 (cit. on p. 29).

[228] K. T. Schütt, H. E. Sauceda, P.-J. Kindermans, A. Tkatchenko, and K.-R. Müller, *SchNet – A deep learning architecture for molecules and materials*, The Journal of Chemical Physics **148**, 241722 (2018) (cit. on p. 29).

[229] J. Gasteiger, J. Groß, and S. Günnemann, *Directional Message Passing for Molecular Graphs*, Apr. 5, 2022 (cit. on p. 29).

[230] S. Batzner, A. Musaelian, L. Sun, M. Geiger, J. P. Mailoa, M. Kornbluth, N. Molinari, T. E. Smidt, and B. Kozinsky, *E(3)-equivariant graph neural networks for data-efficient and accurate interatomic potentials*, Nature Communications **13**, 2453 (2022) (cit. on p. 29).

[231] J. Gasteiger, F. Becker, and S. Günnemann, *GemNet: Universal Directional Graph Neural Networks for Molecules*, Apr. 5, 2022 (cit. on p. 29).

[232] K. T. Schütt, O. T. Unke, and M. Gastegger, *Equivariant Message Passing for the Prediction of Tensorial Properties and Molecular Spectra*, 12 (cit. on p. 29).

[233] G. H. Gu, J. Noh, S. Kim, S. Back, Z. Ulissi, and Y. Jung, *Practical Deep-Learning Representation for Fast Heterogeneous Catalyst Screening*, The Journal of Physical Chemistry Letters **11**, 3185 (2020) (cit. on p. 29).

[234] C. E. Calderon, J. J. Plata, C. Toher, C. Oses, O. Levy, M. Fornari, A. Natan, M. J. Mehl, G. Hart, M. Buongiorno Nardelli, and S. Curtarolo, *The AFLOW standard for high-throughput materials science calculations*, Computational Materials Science **108**, 233 (2015) (cit. on p. 29).

[235] A. Jain, S. P. Ong, G. Hautier, W. Chen, W. D. Richards, S. Dacek, S. Cholia, D. Gunter, D. Skinner, G. Ceder, and K. A. Persson, *Commentary: The Materials Project: A materials genome approach to accelerating materials innovation*, APL Materials **1**, 011002 (2013) (cit. on p. 29).

[236] C. Draxl and M. Scheffler, *The NOMAD laboratory: from data sharing to artificial intelligence*, Journal of Physics: Materials **2**, 036001 (2019) (cit. on p. 29).

[237] R. Ramakrishnan, P. O. Dral, M. Rupp, and O. A. von Lilienfeld, *Quantum chemistry structures and properties of 134 kilo molecules*, Scientific Data **1**, 140022 (2014) (cit. on p. 29).

[238] K. T. Winther, M. J. Hoffmann, J. R. Boes, O. Mamun, M. Bajdich, and T. Bligaard, *Catalysis-Hub.org, an open electronic structure database for surface reactions*, Scientific Data **6**, 75 (2019) (cit. on p. 29).

[239] C. G. Staacke, S. Wengert, C. Kunkel, G. Csányi, K. Reuter, and J. T. Margraf, *Kernel charge equilibration: efficient and accurate prediction of molecular dipole moments with a machine-learning enhanced electron density model*, Machine Learning: Science and Technology **3**, 015032 (2022) (cit. on p. 29).

[240] R. Zubatyuk, J. S. Smith, B. T. Nebgen, S. Tretiak, and O. Isayev, *Teaching a neural network to attach and detach electrons from molecules*, Nature Communications **12**, 4870 (2021) (cit. on p. 29).

[241] Z. Liu, L. Lin, Q. Jia, Z. Cheng, Y. Jiang, Y. Guo, and J. Ma, *Transferable Multilevel Attention Neural Network for Accurate Prediction of Quantum Chemistry Properties via Multitask Learning*, Journal of Chemical Information and Modeling **61**, 1066 (2021) (cit. on p. 29).

[242] A. Gao and R. C. Remsing, *Self-consistent determination of long-range electrostatics in neural network potentials*, Nature Communications **13**, 1572 (2022) (cit. on p. 30).

[243] A. Jain, S. P. Ong, W. Chen, B. Medasani, X. Qu, M. Kocher, M. Brafman, G. Petretto, G.-M. Rignanese, G. Hautier, D. Gunter, and K. A. Persson, *FireWorks: a dynamic workflow system designed for high-throughput applications*, Concurrency and Computation: Practice and Experience **27**, 5037 (2015) (cit. on p. 30).

[244] S. P. Huber, S. Zoupanos, M. Uhrin, L. Talirz, L. Kahle, R. Häuselmann, D. Gresch, T. Müller, A. V. Yakutovich, C. W. Andersen, F. F. Ramirez, C. S. Adorf, F. Gargiulo, S. Kumbhar, E. Passaro, C. Johnston, A. Merkys, A. Cepellotti, N. Mounet, N. Marzari, B. Kozinsky, and G. Pizzi, *AiiDA 1.0, a scalable computational infrastructure for automated reproducible workflows and data provenance*, Scientific Data **7**, 300 (2020) (cit. on p. 30).

[245] A. Paszke, S. Gross, F. Massa, A. Lerer, J. Bradbury, G. Chanan, T. Killeen, Z. Lin, N. Gimelshein, L. Antiga, A. Desmaison, A. Köpf, E. Yang, Z. DeVito, M. Raison, A. Tejani, S. Chilamkurthy, B. Steiner, L. Fang, J. Bai, and S. Chintala, *PyTorch: An Imperative Style, High-Performance Deep Learning Library*, Dec. 3, 2019 (cit. on p. 30).

[246] M. Abadi, A. Agarwal, P. Barham, E. Brevdo, Z. Chen, C. Citro, G. S. Corrado, A. Davis, J. Dean, M. Devin, S. Ghemawat, I. Goodfellow, A. Harp, G. Irving, M. Isard, Y. Jia, R. Jozefowicz, L. Kaiser, M. Kudlur, J. Levenberg, D. Mane, R. Monga, S. Moore, D. Murray, C. Olah, M. Schuster, J. Shlens, B. Steiner, I. Sutskever, K. Talwar, P. Tucker, V. Vanhoucke, V. Vasudevan, F. Viegas, O. Vinyals, P. Warden, M. Wattenberg, M. Wicke, Y. Yu, and X. Zheng, *TensorFlow: Large-Scale Machine Learning on Heterogeneous Distributed Systems*, Mar. 16, 2016 (cit. on p. 30).

[247] J. R. Gardner, G. Pleiss, D. Bindel, K. Q. Weinberger, and A. G. Wilson, *GPyTorch: Blackbox Matrix-Matrix Gaussian Process Inference with GPU Acceleration*, June 29, 2021 (cit. on p. 30).

[248] J. Timmermann, Y. Lee, C. G. Staacke, J. T. Margraf, C. Scheurer, and K. Reuter, *Data-efficient iterative training of Gaussian approximation potentials: Application to surface structure determination of rutile IrO_2 and RuO_2*, The Journal of Chemical Physics **155**, 244107 (2021) (cit. on p. 30).

[249] K. Tran, W. Neiswanger, J. Yoon, Q. Zhang, E. Xing, and Z. W. Ulissi, *Methods for comparing uncertainty quantifications for material property predictions*, Machine Learning: Science and Technology **1**, 025006 (2020) (cit. on pp. 30, 31).

[250] G. Palmer, S. Du, A. Politowicz, J. P. Emory, X. Yang, A. Gautam, G. Gupta, Z. Li, R. Jacobs, and D. Morgan, *Calibration after bootstrap for accurate uncertainty quantification in regression models*, npj Computational Materials **8**, 115 (2022) (cit. on p. 31).

[251] V. Kuleshov, N. Fenner, and S. Ermon, *Accurate Uncertainties for Deep Learning Using Calibrated Regression*, 9 (cit. on p. 31).

[252] T. Head, G. L. MechCoder, I. Shcherbatyi, et al., *Scikit-optimize/scikit-optimize: v0. 5.2*, Zenodo (2018) (cit. on p. 31).

[253] H. Abdi and L. J. Williams, *Principal component analysis: Principal component analysis*, Wiley Interdisciplinary Reviews: Computational Statistics **2**, 433 (2010) (cit. on p. 31).

[254] B. Schölkopf, A. Smola, and K.-R. Müller, in *Artificial Neural Networks — ICANN'97*, Vol. 1327, edited by W. Gerstner, A. Germond, M. Hasler, and J.-D. Nicoud, red. by G. Goos, J. Hartmanis, and J. van Leeuwen, Lecture Notes in Computer Science (Springer Berlin Heidelberg, Berlin, Heidelberg, 1997), pp. 583–588 (cit. on p. 31).

[255] A. Gisbrecht, A. Schulz, and B. Hammer, *Parametric nonlinear dimensionality reduction using kernel t-SNE*, Neurocomputing **147**, 71 (2015) (cit. on p. 31).

[256] L. McInnes, J. Healy, and J. Melville, *UMAP: Uniform Manifold Approximation and Projection for Dimension Reduction*, Sept. 17, 2020 (cit. on p. 31).

[257] B. Cheng, R.-R. Griffiths, S. Wengert, C. Kunkel, T. Stenczel, B. Zhu, V. L. Deringer, N. Bernstein, J. T. Margraf, K. Reuter, and G. Csanyi, *Mapping Materials and Molecules*, Accounts of Chemical Research **53**, 1981 (2020) (cit. on p. 31).

[258] B. A. Helfrecht, R. K. Cersonsky, G. Fraux, and M. Ceriotti, *Structure-property maps with Kernel principal covariates regression*, Machine Learning: Science and Technology **1**, 045021 (2020) (cit. on p. 31).

[259] A. Kolluru, N. Shoghi, M. Shuaibi, S. Goyal, A. Das, C. L. Zitnick, and Z. Ulissi, *Transfer learning using attentions across atomic systems with graph neural networks (TAAG)*, The Journal of Chemical Physics **156**, 184702 (2022) (cit. on p. 40).

[260] D. P. Kingma and M. Welling, *Auto-Encoding Variational Bayes*, May 1, 2014 (cit. on p. 40).

[261] I. J. Goodfellow, J. Pouget-Abadie, M. Mirza, B. Xu, D. Warde-Farley, S. Ozair, A. Courville, and Y. Bengio, *Generative Adversarial Networks*, June 10, 2014 (cit. on p. 40).

[262] L. Ardizzone, J. Kruse, S. Wirkert, D. Rahner, E. W. Pellegrini, R. S. Klessen, L. Maier-Hein, C. Rother, and U. Köthe, *Analyzing Inverse Problems with Invertible Neural Networks*, Feb. 6, 2019 (cit. on p. 40).

Appendix

A Paper # 1

Data-Driven Descriptor Engineering and Refined Scaling Relations for Predicting Transition Metal Oxide Reactivity

Wenbin Xu, Mie Andersen,* and Karsten Reuter

ACS Catal. 11, 734742 (2021).
DOI:10.1021/acscatal.0c04170

ACS Catalysis

pubs.acs.org/acscatalysis

Research Article

Data-Driven Descriptor Engineering and Refined Scaling Relations for Predicting Transition Metal Oxide Reactivity

Wenbin Xu, Mie Andersen,* and Karsten Reuter

Cite This: *ACS Catal.* 2021, 11, 734−742

Read Online

ACCESS | Metrics & More | Article Recommendations | Supporting Information

ABSTRACT: Computational screening of metal oxide catalysts is challenging due to their more localized and intricate electronic structure as compared to metal catalysts and the resulting lack of suitable activity descriptors to replace expensive density functional theory (DFT) calculations. By using a compressed sensing approach, we here identify descriptors in the form of algebraic expressions of surface-derived features for predicting adsorption enthalpies of oxygen evolution reaction (OER) intermediates at doped RuO_2 and IrO_2 electrocatalysts. Our descriptors significantly outperform previously highlighted single descriptors both in terms of accuracy and computational cost. Compared to standard scaling relations that employ the oxygen adsorption enthalpy as a unique reactivity descriptor, our analysis reveals that the consideration of features related to the local charge transfer leads to significantly improved refined scaling relations. These allow us to screen for improved OER electrocatalysts with an uncertainty in the theoretical overpotential similar to the expected intrinsic DFT error of 0.2 V.

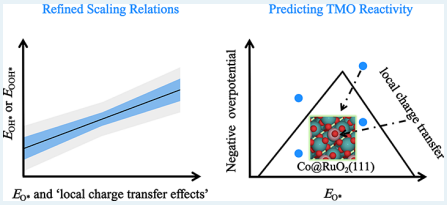

KEYWORDS: *computational screening, heterogeneous catalysis, ab initio calculation, oxygen evolution reaction, transition metal oxides, compressed sensing, machine learning*

INTRODUCTION

Adsorption enthalpies are core quantities for the understanding and modeling of numerous surface-related applications, not the least including heterogeneous catalysis.[1−6] Over the last decades, density functional theory (DFT) has become the prevalent approach to compute such adsorption enthalpies with the required predictive quality.[7] Thanks to steeply increasing computational power and algorithmic efficiency, these calculations can nowadays quite readily be performed.[8] Nevertheless, this progress still cannot keep up with the exploding demand, in particular, of computational screening or design studies that need vast numbers of adsorption enthalpies in their exploration of extensive materials or feature spaces.[2−5] This fuels approaches that allow us to efficiently predict adsorption enthalpies at about comparable accuracy from simpler to compute quantities or from already calculated other adsorption enthalpies. For transition metals (TMs) and their alloys, the *d*-band model[9] and related scaling relations[10] constitute a highly successful such approach that has dramatically impacted the capabilities especially of modern catalysis research.[11−13] Ultimately, this approach draws its performance from the comparatively simple electronic structure of extended TM surfaces, which allows us to describe adsorption enthalpies to the largest extent through just one base quantity: the energetic position of the *d*-band (ε_d). Unfortunately, this simplicity does not extend to other materials classes where scaling relations generally do not hold that well or are completely broken. This concerns notably TM oxides with their more localized, intricate electronic structure.[14,15] Multiple geometric and electronic quantities could then in principle govern the adsorption enthalpies, with recent work, e.g., emphasizing the role of the e_g orbital filling[16,17] or of the charge transfer energy (CTE) as the energetic difference between unoccupied metal d and filled oxygen 2p bands. However, with multiple quantities likely at play, it is unrealistic to expect that a final descriptor that allows us to reliably predict adsorption enthalpies should be a linear function of just a single one of them. In this work, we therefore pursue a data-driven approach to identify the best-performing descriptor in the form of the most general algebraic expression of possible base quantities. Starting from an extensive list of such quantities, we tackle the search for this best multidimensional descriptor out of billions of possible candidates through the compressed sensing method SISSO (sure independence screening and sparsifying operator).[20−22] As a showcase, we focus on the simultaneous learning of dopant-dependent adsorption enthalpies for key intermediates in the oxygen evolution reaction (OER) at different facets of state-of-the-art rutile-structured IrO_2 and RuO_2 electrocatalysts.[23−26] The SISSO analysis generates a descriptor that allows us to predict all adsorption enthalpies with a root-mean-square error

Received: September 23, 2020
Revised: December 16, 2020
Published: December 31, 2020

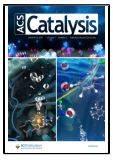

https://dx.doi.org/10.1021/acscatal.0c04170
ACS Catal. 2021, 11, 734−742

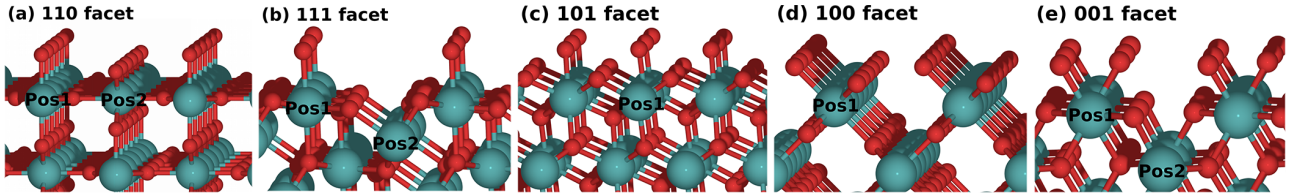

Figure 1. (a–e) Perspective side views of oxygen-rich terminations of low-index facets of rutile-structured oxides. The TM atoms (Ru or Ir) are shown in green, and O atoms are shown in red. The considered substitutional doping positions are indicated.

(RMSE) of 0.18 eV. This is on par with the best-performing descriptor approaches for adsorption at the simpler TMs[22,27] and suggests SISSO as a suitable and systematic avenue to efficiently generate adsorption enthalpies for complex compound materials. The analysis also reveals the primary shortcoming of standard scaling relations in the form of simple correction terms. It is only through these correction terms that a number of dopants are correctly identified as promising in the computational screening, for which recent experiments have indeed indicated strong OER activity increases.

METHODS

Structural Description. O*, OH*, and OOH* are established key OER intermediates, and the linear scaling of O* and OH* (or O* and OOH*) adsorption enthalpies on TM oxide surfaces poses well-known limitations to OER performance for this materials class.[23,24] TM doping to further enhance the activity of stable rutile IrO_2 and RuO_2 electrocatalysts is therefore of high interest and spans a typical materials space for which efficient adsorption enthalpy prediction would be of value. To generate a database for the learning, we therefore use DFT (Quantum ESPRESSO code[28] and BEEF-vdW functional[29]) to compute O*, OH*, and OOH* adsorption enthalpies at the coordinatively unsaturated (cus) sites of all five symmetry-inequivalent low-index facets of both oxides (see Figure 1), when doping them with a wide range of TMs (Ti, Mn, Fe, Co, Ni, Cu, Zn, Mo, Ru, Ag, W, and Ir). The used criteria for selecting these specific dopant atoms were (i) that they should cover a representative part of the periodic table from early to late 3d, 4d, and 5d TMs in order to increase the chance of finding a dopant that would lead to a high activity and (ii) that they should be relatively cheap and abundant in order to bring down the cost of state-of-the-art Ir- and Ru-based electrocatalysts. Considering all symmetry-inequivalent substitutional doping positions in the topmost layers in surface unit cells, this yields a total of 684 cases with stable cus site adsorption of the intact intermediate, cf. Section S1 of the Supporting Information for all details. As shown in the here constructed linear scaling relations in Figure 2, the calculated adsorption enthalpies extend over a wide range of ∼5 eV (O*), ∼3 eV (OH*), and ∼2 eV (OOH*). More importantly, they scatter widely around the scaling relation line with multiple outliers deviating significantly from the linear prediction. This reflects the tuning prospects of TM doping by breaking the scaling-imposed OER performance limitations (see below). Yet, it equally reflects the challenge for a reliable adsorption enthalpy prediction with a targeted uncertainty not exceeding typical DFT uncertainties of about ∼±0.2 eV.

Primary Features. The starting point for our SISSO search for an optimum descriptor is an extensive list of 31 base quantities that are potential factors determining the reactivity

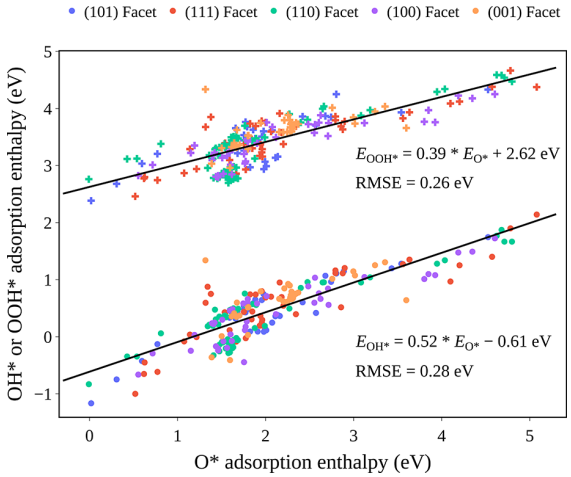

Figure 2. OOH* vs O* (top) and OH* vs O* (bottom) linear scaling relations (fitted black lines). The data points (pluses for OOH* and circles for OH*) are for adsorption at the cus site of the five low-index facets of rutile-structured IrO_2 and RuO_2 shown in Figure 1 with substitutional doping.

of oxide surfaces and therewith the adsorption enthalpies. We assemble this list of so-called primary features from general physicochemical considerations, as well as from previously emphasized descriptors in the literature.[2,16−19,22,30−34] As detailed in the Supporting Information, these features divide into geometric and electronic properties and can be classified into features characterizing the entire surface, the local adsorption site, or the specific cus metal atom to which the adsorbates coordinate to. We specifically refer to Sections S1.2 and S2 and Figure S3 of the Supporting Information for further details on how the features are calculated. Since the primary features considered crucially determine the predictive performance of the resulting descriptor, the most extensive initial list appears desirable at first sight. On the other hand, additional primary features that are highly correlated with other features render the problem ill-posed. While SISSO is precisely constructed to handle correlated features, it is still preferable to filter out obvious correlations *a priori* to mitigate the steeply increasing computational cost of SISSO approaches with the number of primary features. We therefore evaluate the Pearson correlation coefficient between every pair of primary features for our database and cross out primary features that exhibit more than around 90% correlation with one or more other primary features. As further discussed in Section S2 of the Supporting Information, this intriguingly eliminates prominent base quantities like the tabulated adsorbate coupling matrix element or the atomic radius of the cus atom, which are both found to be highly correlated with the CTE.

https://dx.doi.org/10.1021/acscatal.0c04170
ACS Catal. 2021, 11, 734−742

After this initial filtering, we arrive at the set of the 24 least-correlated primary features compiled in Table 1. Additionally

Table 1. A Set of the 24 Least-Correlated Primary Features Used for the Descriptor Construction[a]

abbreviation	correlation	name	class
W_d	0.744	width of the *d*-band (site projected)	site
CTE	0.734	charge transfer energy (site projected)	site
f_{e_g}	0.643	filling of the e_g *d*-band (site projected)	site
K_d	0.604	kurtosis of the *d*-band (site projected)	site
q_{Bader}	0.567	Bader charge (site projected)	site
f_d	0.521	filling of the *d*-band (site projected)	site
$\varepsilon_{O_{2p}}$	0.490	center of the O_{2p}-band (coordinated O atoms)	site
S_d	0.470	skewness of the *d*-band (site projected)	site
ε_d	0.438	center of the *d*-band (site projected)	site
FE	0.392	dopant formation energy	site
$DOS_{O_{2p}}$	0.378	O_{2p} density of states (DOS) at the Fermi level (coordinated O atoms)	site
Q_1	0.346	angular-resolved local order parameter (l = 1)	site
EA	0.315	electron affinity (cus atom)	atomic
Q_5	0.255	angular-resolved local order parameter (l = 5)	site
Q_3	0.225	angular-resolved local order parameter (l = 3)	site
DOS	0.219	total density of states (DOS) at the Fermi level (site projected)	site
ME	0.218	Mulliken electronegativity (cus atom)	atomic
WF	0.199	work function	surface
Q_4	0.182	angular-resolved local order parameter (l = 4)	site
$f_{O_{2p}}$	0.164	filling of the O_{2p}-band (coordinated O atoms)	site
IP	0.145	ionization potential (cus atom)	atomic
d_1	0.139	distance to the first nearest-neighbor metal atom	site
Q_2	0.081	angular-resolved local order parameter (l = 2)	site
d_3	0.054	distance to the third nearest-neighbor metal atom	site

[a]The features are sorted according to their linear Pearson correlation coefficient with the adsorption enthalpies in the database.

included in Table 1 is the correlation coefficient of each primary feature with the calculated DFT adsorption enthalpies of our database. Confirming previous works highlighting the importance of these features for other oxide surfaces,[16−19] the CTE and the e_g orbital filling indeed exhibit a very high correlation. However, surprisingly, the width of the *d*-band (W_d) at the cus site that to our knowledge has hitherto never been emphasized as a reactivity descriptor shows an even higher correlation. In contrast, the *d*-band center (ε_d) that so much dominates adsorption enthalpies at TMs and their alloys[9] is only the ninth most correlated feature in our list. In fact, with the continuous range of correlations seen in Table 1, it is not possible to single out any of the primary features as uniquely important. This corroborates our initial statement that for oxides, adsorption enthalpies are unlikely to be a linear function of just one elementary descriptor.

Compressed Sensing. SISSO is a compressed sensing-based method for identifying the key features necessary to describe and predict a property of interest (here adsorption enthalpies).[20−22] The features are constructed by applying a set of algebraic/functional operators (detailed in Section S3 of the Supporting Information) to a list of predefined primary features (cf. discussion above and Table 1). The operators are applied iteratively to the generated feature spaces, with the number of iterations N performed being a hyperparameter of the method (denoted the rung, Φ_N). This leads to a rapidly growing size of the total feature space, which in our case reaches about 10^{12} features at rung Φ_3. SISSO tackles the challenge of identifying the best sparse solution (i.e., the solution containing a small number of linearly combined features) in two steps. First, sure independence screening (SIS) is used to prescreen the vast feature space and select a smaller subspace of top-ranking candidate features by evaluating the correlation of features with the property of interest as well as the correlation of features with the residual error from already selected features. The size of the final subspace is controlled by the SIS parameter, for which we used well-tested values from our previous work[22] as detailed in Section S3 of the Supporting Information. In the second step, a sparsifying operator (SO, here the l_0 constraint) is used to find the best sparse solution. The final desired M number of linearly combined features is also called the descriptor, M being another hyperparameter denoted as the dimensionality of the descriptor.

The target adsorption enthalpies in this work are those of O*, OH*, and OOH*. This represents a multitask optimization problem, which SISSO tackles by identifying the best descriptor for the simultaneous learning of all tasks.[21] The multitask SISSO model then differs for the different adsorbates only in the M + 1 fitting coefficients (one for each feature plus the constant offset). The advantage of this multitask approach is a more stable learning since the entire DFT database can be used as training data in the identification of predictive models for each of the individual adsorbates, and it also allows for capturing features that are mutually relevant for the considered adsorbates.

RESULTS AND DISCUSSION

SISSO Descriptors. In this section, we will first discuss some simple descriptors that are identified based on the entire database and then move on to discuss the best-performing, more complex descriptors and their predictive power for data points not included in the training. In Table 2, we list the top

Table 2. Top Five 1D Φ_1 Descriptors Trained on the Entire Database[a]

correlation	descriptor
0.795	$(W_d - \varepsilon_{O_{2p}})$
0.793	$(Q_4 \times W_d)$
0.786	(Q_4/K_d)
0.786	(IP/K_d)
0.778	$(W_d \times \varepsilon_{O_{2p}})$

[a]The features are sorted according to their linear Pearson correlation coefficient with the adsorption enthalpies in the database.

five one-dimensional (1D) descriptors identified after the first iteration of the feature construction (Φ_1). Astonishingly, these results show that descriptors with an even better correlation than the best primary feature (*d*-band width W_d, cf. Table 1) can readily be obtained by simply combining primary features that themselves have an inferior correlation. For example, the third best descriptor in Table 2 is composed of the fourth best

https://dx.doi.org/10.1021/acscatal.0c04170
ACS Catal. 2021, 11, 734−742

primary feature (d-band kurtosis, K_d) as well as Q_4, the angular-resolved local order parameter for $l = 4$, which is only the nineteenth best primary feature with a very low individual correlation coefficient of 0.182. This highlights that the emphasis on single elementary features in the literature does not necessarily reflect the real usefulness of these features as descriptors, as it may lead one to discard features that only become important in more complex descriptors where they are combined with other features. It is also interesting to note that the best 1D Φ_1 descriptor ($W_d - \varepsilon_{O_{2p}}$) is essentially the CTE where the center of the unoccupied d-band has been replaced by the width of the entire d-band. The two descriptors are highly correlated with each other (correlation of 0.892), which makes good physical sense since a wider d-band is expected to lead to a higher center of the unoccupied part of the d-band. Thus, they capture similar physical insights. The increase in correlation with our DFT database from 0.734 (CTE) to 0.795 ($W_d - \varepsilon_{O_{2p}}$) is significant as revealed by the finding that this corresponds to a lowering of the training RMSE of almost 0.1 eV (from 0.43 to 0.35 eV). We speculate that the better performance of the here identified descriptor could be related to the fact that the d-band width captures more characteristics of the relevant electronic structure since it is calculated over both the occupied and the unoccupied d states. Of course, even higher correlations can be achieved with more complex combinations of primary features as exemplified in the list of the top five 1D Φ_2 descriptors in Table S5 in the Supporting Information. On the other hand, one quickly reaches a combinatorial explosion of possibilities, which is precisely the motivation for employing a systematic compressed sensing approach to identify the best-performing composite descriptors.

In order to assess more generally the performance of these SISSO descriptors, we systematically test all combinations of hyperparameters up to the most complex 8D Φ_3 descriptors. We employ 5-fold cross validation, that is, the database is shuffled and partitioned into five equal-sized subsamples, where furthermore, each contains the same fraction of O*, OH*, and OOH* data points. The training is then carried out based on four of the subsamples while retaining the fifth subsample for validation. This process is repeated five times so that each data point is used for validation exactly once. Figure 3a shows the resulting training and validation RMSE averaged over the five repetitions for each combination of hyperparameters. As seen, both the training and validation errors generally improve drastically when employing more complex descriptors of higher rungs. For Φ_3, we already reach the target corridor of $\sim\pm$0.2 eV in the prediction uncertainty when using 3D descriptors, i.e., for these descriptors, the validation RMSE for the data not included in the training is 0.20 eV. The 4D and 5D descriptors offer additional slight improvements with the RMSE reaching a minimum value of 0.18 eV at dimension 5. Overfitting then sets in at the higher dimensions of these most complex descriptors as evidenced by flat or even slightly increasing validation curves.

For the best 5D Φ_3 descriptors, we also show a violin plot of the distribution of the absolute validation errors in Figure 3b. The majority of the errors (75%) are below 0.21 eV, but a few outliers are also observed with the maximum absolute error (MAE) being 0.65 eV. For comparison, we also performed a corresponding 5-fold cross validation for the two scaling relations shown in Figure 2, resulting in an average validation

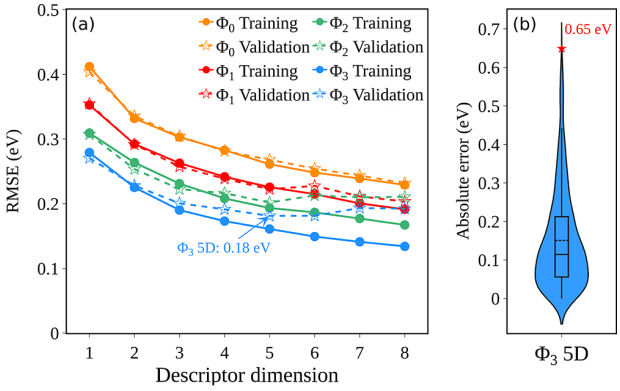

Figure 3. (a) Training and validation RMSE from 5-fold cross validation (averaged over the 5 folds) for all tested SISSO hyperparameters. (b) Violin plot of the distribution of the absolute validation errors (combined from the 5 folds) for the 5D Φ_3 descriptor. The internal solid line marks the median, the internal dashed line marks the mean, the black box marks the 75% and 25% percentiles, the whiskers mark the 95% and 5% percentiles, the red star marks the MAE, and the blue region is the density plot.

RMSE of 0.27 eV and a MAE of 1.26 eV, which is thus significantly worse than the best SISSO descriptors. No significant improvement can be obtained either by fitting the different facets separately, which can also be observed from their similar scatter around the fitted line in Figure 2 (the corresponding Figure S2 in the Supporting Information instead visualizes trends over doping atoms and their position). This confirms the locality of the oxide binding, for which different facets offer similar local geometric motives. Combined with the fact that the scaling approach requires explicit calculation of the O* adsorption enthalpy whereas the SISSO approach requires only primary features calculated from the clean surface, the SISSO descriptors are clearly superior in terms of both accuracy and computational cost. The stable predictive performance with the majority of errors located within the target corridor of $\sim\pm$0.2 eV makes it a promising approach for high-throughput screening. For this purpose, we identify the single best descriptor, see Section S4.1 in the Supporting Information, based on the entire database by fixing the hyperparameters to those best values determined in the cross validation (i.e., 5D Φ_3).

Refined Scaling Relations. As also apparent from the previous section, scaling relations are not that accurate for the prediction of adsorption enthalpies at oxides. Even the training MAE for the here constructed scaling relations is 0.22 eV, which is significantly higher than for corresponding oxygenate scaling relations at TMs (about 0.10 eV[13]). In this section, we show how SISSO can be employed to unravel the underlying reason for this different performance of scaling relations in the two materials classes. Specifically, we elucidate the missing ingredients (primary features) in the standard scaling description by identifying SISSO-refined scaling relations. In practice, this is done by explicitly including the O* adsorption enthalpy itself among the primary features and retraining the SISSO descriptors based on the database of OH* and OOH* adsorption enthalpies alone. For this, we follow the same approach as outlined in the previous section, but since we are here mainly interested in simple, dominant correction terms, we consider only the less complex rungs 0−2.

https://dx.doi.org/10.1021/acscatal.0c04170
ACS Catal. 2021, 11, 734−742

The predictive performance of the new descriptors as evaluated by cross validation is shown in Figure 4, and the

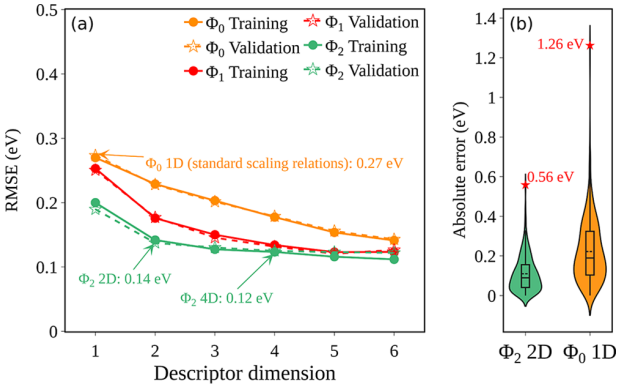

Figure 4. Same as Figure 3 but here identifying SISSO-refined scaling relations by including the O* adsorption enthalpy among the primary features and training and validating only on the OH* and OOH* adsorption enthalpies. Note the dramatic reduction in particular also of the MAE between the standard scaling relations (denoted as Φ_0 1D in the SISSO hierarchy) and already the simple Φ_2 2D refinement.

composition of the simpler 1D and 2D descriptors (as identified by ultimately training on the entire *OH and *OOH database) is given in Table 3. Furthermore, the full

Table 3. RMSE (in eV) of Various Descriptors in Predicting the OH* and OOH* Adsorption Enthalpies in the Database[a]

descriptor	RMSE	first term	second term
1D Φ_0	0.27	(E_{O*})	
2D Φ_0	0.23	(E_{O*})	(Q_3)
1D Φ_1	0.25	(E_{O*}/IP)	
2D Φ_1	0.18	$(E_{O*} - \mathrm{ME})$	(ε_d/K_d)
1D Φ_2	0.20	$(E_{O*} - \mathrm{ME}) - (\varepsilon_d/K_d)$	
2D Φ_2	0.14	$(E_{O*} - \mathrm{ME})\cdot(Q_1 + Q_4)$	$(\mathrm{EA} - \varepsilon_d)\cdot(K_d/d_1)$

[a]The 1D Φ_0 descriptor corresponds to the standard scaling relation ($E_{OH*} = C_1 \times E_{O*} + C_0$ and analogous for E_{OOH*}). The SISSO-refined scaling relations have the form $E_{OH*} = C_1 \times$ first term $+ C_2 \times$ second term $+ C_0$.

overview of the top five descriptors for the dimensions 1 and 2 and the rungs Φ_0, Φ_1, and Φ_2 is given in Tables S8−S13 in the Supporting Information. Note that the simplest 1D Φ_0 descriptor corresponds to the standard OH* vs O* and OOH* vs O* scaling relations from Figure 2. As seen in Figure 4, already the simplest refinements offer substantially improved prediction errors over the standard scaling relations with the validation RMSE (MAE) reaching 0.14 eV (0.56 eV) for the 2D Φ_2 descriptor (see also the comparison of standard and refined scaling relations in Figure S5 in the Supporting Information). The 4D Φ_2 descriptor even lowers the RMSE to 0.12 eV. This overall performance is even better than the general SISSO one discussed in the last section because now, the O* adsorption enthalpy is explicitly used. The learning task is thus simpler than before, at the expense of having to compute E_{O*} with DFT for a new dopant in a potential screening study (whereas only the clean surface DFT calculation would be sufficient for the general SISSO descriptors discussed before).

Considering the composition of the simplest 2D Φ_0 and 1−2D Φ_1 descriptors (Table 3 and Tables S9−S11 in the Supporting Information), we identify the ionization potential (IP) or the Mulliken electronegativity (ME) of the cus atom to which the adsorbates coordinate as the most important corrections to the O* adsorption enthalpy. The only exception is the best 2D Φ_0 descriptor for which Q_3 appears; however, the 2D Φ_0 descriptors involving the IP or ME have close to identical performance, cf. Table S9 in the Supporting Information. Interestingly, the IP and ME themselves do not show any strong correlation (<0.22) with the adsorption enthalpies in our database (cf. Table 1). On the other hand, they are highly correlated with each other (see Figure S4 in the Supporting Information) and are both related to how easily the cus atom accepts or donates charge. We therefore interpret their recurrent presence in the correction terms as an indication that it is this physical information that is missing in the standard scaling description and propose that this is the principal reason why scaling relations do not work very well on oxides. In fact, as we will show later on, it is precisely the inclusion of these SISSO-identified charge correction terms that is crucial to correctly capture promising dopants for OER catalysis. Again, this backs up our initial reflections on the difference between the reactivity of TMs and TM oxides and underlines the generally accepted view that the local charge transfer (among chemists also discussed in terms of the acid/base properties of the sites) is much more important at the oxides.[35−38]

In the 2D Φ_1 (second term) and 1−2D Φ_2 descriptors, additional primary features appear, which are related to the electronic structure (*d*-band center and kurtosis) and local geometry (angular-resolved local order parameter and nearest neighbor distance) of the cus atom. We therefore interpret these properties as the second and third most important missing ingredients.

Screening for OER Catalysts. A particularly interesting application of the above-demonstrated possibilities for low-cost and accurate prediction of adsorption enthalpies is the tailoring of doped TM oxide catalysts for the OER through high-throughput screening. From previous scaling relation-based approaches, it was established that the existence of a universal scaling relation between the critical OER intermediates OH* and OOH* leads to a constraint on the lowest possible theoretical overpotential.[24] In Figure 5a, we plot the here calculated DFT OOH* vs OH* adsorption enthalpies and indicate both this universal scaling relation and the ideal scaling relation that would allow for desirable catalyst operation already at the equilibrium potential for OER of U = 1.23 V vs the reversible hydrogen electrode (more precisely, this is a necessary but not sufficient condition as detailed below).[24] Similar to the OH* vs O* and OOH* vs O* scaling relations in Figure 2, a considerable scatter around the scaling lines is seen. Among the here studied dopants, some clear trends emerge, i.e., independently of the studied facet; the dopants Ru, Ir (and thus also the undoped facets), W, Mo, and Ti tend to lie close to the universal scaling line, whereas the dopants Ni, Co, and Ag tend to lie closer to the ideal scaling line. The remaining dopants Cu, Fe, Mn, and Zn are intermediate cases. Test calculations excluding spin polarization for Ni, Co, and Fe (not shown) do not cause any significant changes to this picture. This is in agreement with a recent study of other oxides that concluded that magnetism is not a good descriptor for OER reactivity.[33] Rather, we

https://dx.doi.org/10.1021/acscatal.0c04170
ACS Catal. 2021, 11, 734−742

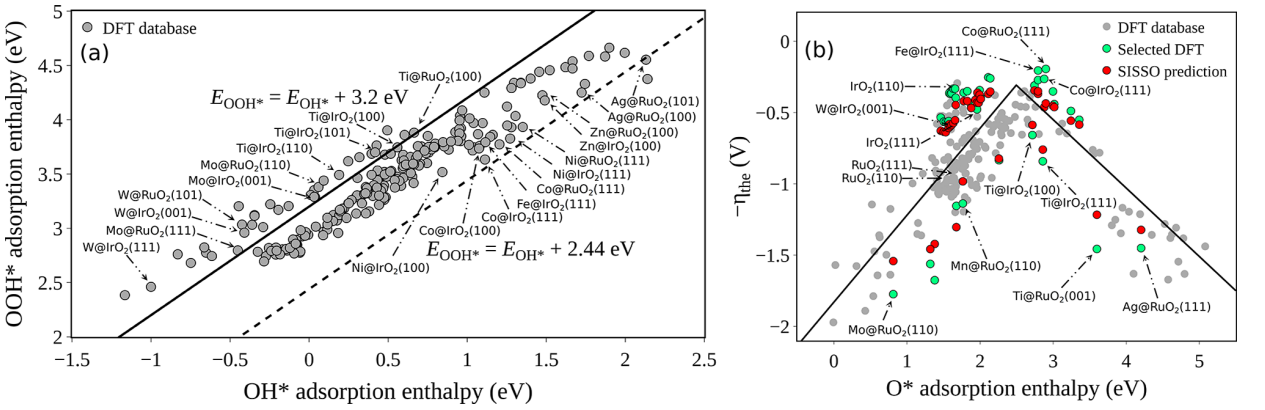

Figure 5. (a) OOH* vs OH* adsorption enthalpies from our DFT database. The solid (dashed) lines indicate the universal (ideal) scaling relations.[24] (b) Negative theoretical overpotential η_{the} of all materials in our database as a function of the O* adsorption enthalpy. The black curve is the volcano predicted from the standard OH* vs O* and OOH* vs O* scaling relations in Figure 2. Selected DFT data points (in green) and corresponding SISSO predictions using refined scaling relations (2D Φ_2, in red) are also indicated. All highlighted catalysts are for substitutional doping in the topmost layer ("Pos1" in Figure 1) with the adsorbates coordinating directly to the dopant atom ("Site1" in Figure S1 in the Supporting Information).

speculate in light of the discussion below that the more favorable scaling properties of some of these dopants are related to local charge transfer specifics, e.g., that they generally prefer lower oxidation states than the formal +4 oxidation state of the Ir or Ru atoms in the host material.

Within the classic volcano picture of OER established by Nørskov and coworkers,[23−25,39] the ideal catalyst should not only follow the ideal scaling line but also possess an ideal absolute O* (or OH*) adsorption enthalpy to satisfy the Sabatier principle. To get a quantitative estimate of the theoretical overpotential of all materials in our database, we carry out the corresponding thermodynamic analysis using the computational hydrogen electrode (CHE) approach[39] for the peroxide OER reaction mechanism consisting of four proton-coupled electron transfer steps[23−25] and using free energy corrections to the intermediates from ref 25. In this analysis, the theoretical overpotential is equated with the potential required to make all four reaction steps exergonic. The results are presented in Figure 5b with further details given in Section S5 of the Supporting Information (here, we also discuss an alternative approach where the volcano is instead expressed as a function of the difference between the O* and OH* adsorption free energies,[24] which is, however, less interesting in our case). It is seen that the scatter of the points around the scaling lines in Figure 5a translates into an uncertainty of about ±0.5 V in the theoretical overpotential as compared to the known scaling-derived volcano curve with its top at the ideal E_{O*} = 2.46 eV. Some of the DFT data points that exhibit particularly large deviations from the volcano are highlighted in green in the figure. Intriguingly, already the quite simple 2D Φ_2 SISSO-refined scaling relation (cf. Table 3) instead quite reliably captures those data points that are outliers to the volcano curve. Compared to the actual DFT-computed theoretical overpotential, the remaining uncertainty of the SISSO-derived overpotential is on average only around the targeted 0.2 V, as visually reflected in Figure 5b by the closeness of the green (DFT) and red (SISSO) data points.

The SISSO-refined scaling relations thus now allow us to differentiate between materials, which, despite very similar O* adsorption enthalpies, may in reality show up to an approx. 1 V difference in the theoretical overpotential (explicit values are provided in the Supporting Information). Indeed, this ability turns out to be crucial for the correct identification of promising dopants. As apparent from Figure 5b, it is in particular Co and Fe that show a favorable deviation from the scaling line and lead to catalysts that exhibit the lowest theoretical overpotentials. This deviation is correctly captured within SISSO, i.e., a SISSO-based computational screening study would have correctly identified these doped systems. In contrast, as their O* adsorption enthalpy does not match the "ideal" value, these systems are located to the right or left of the volcano maximum and therefore would likely have been dismissed as suboptimal in a traditional scaling relation-based screening. As discussed above, we attribute this superior SISSO performance to its ability to appropriately capture the local charge transfer properties of these dopants (with the vertical distance of the red data points to the solid scaling relation line reflecting the amount of this charge transfer). Our interpretation is backed up by explicit comparison of primary features related to charge transfer for materials with similar O* adsorption enthalpy but vastly different theoretical overpotential (see Table S16 in the Supporting Information). This comparison shows that smaller overpotentials (for similar O* adsorption enthalpy) are related to higher Mulliken electronegativity and ionization potential and lower Bader charge of the active metal atom.

Our independent theoretical results are furthermore impressively backed up by experiments, where recent studies have in particular highlighted the favorable electrocatalytic OER activities for Co doping of RuO_2 and IrO_2,[40] Fe/Mn doping of IrO_2,[41] Mn doping of RuO_2,[42] and Ni and Co doping of IrO_2.[43−45] We note that Mn and Ni are also present in many of the here predicted good OER catalysts, even though not exhibiting the lowest theoretical overpotentials. To this end, we recall the approximate nature of the thermodynamic CHE approach that is useful for computational screening but cannot, of course, replace a detailed mechanistic analysis.[6,46] As discussed by Man et al., only trends, i.e., relative differences between computed overpotentials, are in agreement with experiments,[24] which is why the approach is still useful for screening. A more accurate prediction of selected promising catalysts could already be achieved by refined free-energy

https://dx.doi.org/10.1021/acscatal.0c04170
ACS Catal. 2021, 11, 734−742

corrections (i.e., by calculation of the adsorbate vibrational frequencies for the given catalyst), by including implicit or explicit solvation corrections, and by calculation of (solvation- and potential-dependent) kinetic barriers for the OER reaction steps at the given catalyst.[47−49] Ultimately, a full evaluation of the promising catalysts should also include an assessment of their synthesizability and stability under OER reaction conditions.[50]

CONCLUSIONS

In summary, we applied the compressed sensing method SISSO to identify descriptors for the prediction of the adsorption enthalpies of the OER intermediates O*, OH*, and OOH* at the cus sites of various facets of doped IrO_2 and RuO_2 electrocatalysts. The descriptors are constructed as algebraic expressions of electronic and geometric primary features, and their compositions reveal that no single primary feature is uniquely important. Even primary features that themselves show a very poor correlation with the adsorption enthalpies may become important in correction terms that allow for the high predictive performance of the final descriptor. The best validation RMSE reached is 0.18 eV when including only primary features derived from the clean surface and 0.12 eV when additionally including the O* adsorption enthalpy. In the latter case, we term the SISSO descriptors refined scaling relations, as their compositions help us to identify primary features related to the local charge transfer to be the primary correction (and thereby missing ingredient) to standard scaling relations. For the showcased screening of dopants, these corrections turn out as crucial to reliably identify Co and Fe in agreement with recent experimental works. In general, SISSO thus provides a stepping stone for a reliable computational screening of compound materials by offering a systematic approach for the identification of complex composite descriptors.

ASSOCIATED CONTENT

Supporting Information

The Supporting Information is available free of charge at https://pubs.acs.org/doi/10.1021/acscatal.0c04170.

Additional details on DFT, primary features, SISSO, composition of descriptors, and the screening of OER catalysts (PDF)

AUTHOR INFORMATION

Corresponding Author

Mie Andersen − *Chair for Theoretical Chemistry and Catalysis Research Center, Technische Universität München, 85747 Garching, Germany;* orcid.org/0000-0002-9943-1534; Email: mie.andersen@ch.tum.de

Authors

Wenbin Xu − *Chair for Theoretical Chemistry and Catalysis Research Center, Technische Universität München, 85747 Garching, Germany*

Karsten Reuter − *Chair for Theoretical Chemistry and Catalysis Research Center, Technische Universität München, 85747 Garching, Germany; Fritz-Haber-Institut der Max-Planck-Gesellschaft, 14195 Berlin, Germany;* orcid.org/0000-0001-8473-8659

Complete contact information is available at: https://pubs.acs.org/10.1021/acscatal.0c04170

Notes

The authors declare no competing financial interest.

The DFT-calculated adsorption energies and relaxed coordinates can be found on GitHub (https://github.com/wenbin2020/SISSOdescriptorTMOsfiles).

ACKNOWLEDGMENTS

The authors gratefully acknowledge support from the Leibniz Supercomputing Centre of the Bavarian Academy of Sciences and Humanities (www.lrz.de) and the Jülich Supercomputing Centre (www.fz-juelich.de/ias/jsc). Wenbin Xu is grateful for support through the China Scholarship Council (CSC).

REFERENCES

(1) Reuter, K.; Frenkel, D.; Scheffler, M. The Steady State of Heterogeneous Catalysis, Studied by First-Principles Statistical Mechanics. *Phys. Rev. Lett.* **2004**, *93*, 116105.

(2) Hong, W. T.; Risch, M.; Stoerzinger, K. A.; Grimaud, A.; Suntivich, J.; Shao-Horn, Y. Toward the rational design of non-precious transition metal oxides for oxygen electrocatalysis. *Energy Environ. Sci.* **2015**, *8*, 1404−1427.

(3) Zhang, B.; Zheng, X.; Voznyy, O.; Comin, R.; Bajdich, M.; García-Melchor, M.; Han, L.; Xu, J.; Liu, M.; Zheng, L.; García de Arquer, F. P.; Dinh, C. T.; Fan, F.; Yuan, M.; Yassitepe, E.; Chen, N.; Regier, T.; Liu, P.; Li, Y.; De Luna, P.; Janmohamed, A.; Xin, H. L.; Yang, H.; Vojvodic, A.; Sargent, E. H. Homogeneously dispersed multimetal oxygen-evolving catalysts. *Science* **2016**, *352*, 333−337.

(4) Montoya, J. H.; Seitz, L. C.; Chakthranont, P.; Vojvodic, A.; Jaramillo, T. F.; Nørskov, J. K. Materials for solar fuels and chemicals. *Nat. Mater.* **2017**, *16*, 70−81.

(5) Seh, Z. W.; Kibsgaard, J.; Dickens, C. F.; Chorkendorff, I.; Nørskov, J. K.; Jaramillo, T. F. Combining theory and experiment in electrocatalysis: Insights into materials design. *Science* **2017**, *355*, No. eaad4998.

(6) Bruix, A.; Margraf, J. T.; Andersen, M.; Reuter, K. First-principles-based multiscale modelling of heterogeneous catalysis. *Nat. Catal.* **2019**, *2*, 659−670.

(7) Nørskov, J. K.; Scheffler, M.; Toulhoat, H. Density Functional Theory in Surface Science and Heterogeneous Catalysis. *MRS Bull.* **2006**, *31*, 669−674.

(8) Tran, K.; Ulissi, Z. W. Active learning across intermetallics to guide discovery of electrocatalysts for CO_2 reduction and H_2 evolution. *Nat. Catal.* **2018**, *1*, 696−703.

(9) Hammer, B.; Nørskov, J. K. Electronic factors determining the reactivity of metal surfaces. *Surf. Sci.* **1995**, *343*, 211−220.

(10) Abild-Pedersen, F.; Greeley, J.; Studt, F.; Rossmeisl, J.; Munter, T. R.; Moses, P. G.; Skúlason, E.; Bligaard, T.; Nørskov, J. K. Scaling properties of adsorption energies for hydrogen-containing molecules on transition-metal surfaces. *Phys. Rev. Lett.* **2007**, *99*, No. 016105.

(11) Studt, F.; Sharafutdinov, I.; Abild-Pedersen, F.; Elkjaer, C. F.; Hummelshøj, J. S.; Dahl, S.; Chorkendorff, I.; Nørskov, J. K. Discovery of a Ni-Ga catalyst for carbon dioxide reduction to methanol. *Nat. Chem.* **2014**, *6*, 320−324.

(12) Calle-Vallejo, F.; Tymoczko, J.; Colic, V.; Vu, Q. H.; Pohl, M. D.; Morgenstern, K.; Loffreda, D.; Sautet, P.; Schuhmann, W.; Bandarenka, A. S. Finding optimal surface sites on heterogeneous catalysts by counting nearest neighbors. *Science* **2015**, *350*, 185−189.

(13) Calle-Vallejo, F.; Loffreda, D.; Koper, M. T. M.; Sautet, P. Introducing Structural Sensitivity into Adsorption-Energy Scaling Relations by Means of Coordination Numbers. *Nat. Chem.* **2015**, *7*, 403−410.

(14) Vojvodic, A.; Calle-Vallejo, F.; Guo, W.; Wang, S.; Toftelund, A.; Studt, F.; Martínez, J. I.; Shen, J.; Man, I. C.; Rossmeisl, J.; Bligaard, T.; Nørskov, J. K.; Abild-Pedersen, F. On the behavior of Brønsted-Evans-Polanyi relations for transition metal oxides. *J. Chem. Phys.* **2011**, *134*, 244509.

(15) Mehta, P.; Greeley, J.; Delgass, W. N.; Schneider, W. F. Adsorption Energy Correlations at the Metal-Support Boundary. *ACS Catal.* **2017**, *7*, 4707−4715.
(16) Suntivich, J.; May, K. J.; Gasteiger, H. A.; Goodenough, J. B.; Shao-Horn, Y. A perovskite oxide optimized for oxygen evolution catalysis from molecular orbital principles. *Science* **2011**, *334*, 1383−1385.
(17) Zhou, Y.; Sun, S.; Xi, S.; Duan, Y.; Sritharan, T.; Du, Y.; Xu, Z. J. Superexchange Effects on Oxygen Reduction Activity of Edge-Sharing $[Co_xMn_{1-x}O_6]$ Octahedra in Spinel Oxide. *Adv. Mater.* **2018**, *30*, 1705407.
(18) Hong, W. T.; Stoerzinger, K. A.; Lee, Y.-L.; Giordano, L.; Grimaud, A.; Johnson, A. M.; Hwang, J.; Crumlin, E. J.; Yang, W.; Shao-Horn, Y. Charge-transfer-energy-dependent oxygen evolution reaction mechanisms for perovskite oxides. *Energy Environ. Sci.* **2017**, *10*, 2190−2200.
(19) Yamada, I.; Takamatsu, A.; Asai, K.; Shirakawa, T.; Ohzuku, H.; Seno, A.; Uchimura, T.; Fujii, H.; Kawaguchi, S.; Wada, K.; Ikeno, H.; Yagi, S. Systematic Study of Descriptors for Oxygen Evolution Reaction Catalysis in Perovskite Oxides. *J. Phys. Chem. C* **2018**, *122*, 27885−27892.
(20) Ouyang, R.; Curtarolo, S.; Ahmetcik, E.; Scheffler, M.; Ghiringhelli, L. M. SISSO: A compressed-sensing method for identifying the best low-dimensional descriptor in an immensity of offered candidates. *Phys. Rev. Mater.* **2018**, *2*, No. 083802.
(21) Ouyang, R.; Ahmetcik, E.; Carbogno, C.; Scheffler, M.; Ghiringhelli, L. M. Simultaneous learning of several materials properties from incomplete databases with multi-task SISSO. *J. Phys.: Mater.* **2019**, *2*, No. 024002.
(22) Andersen, M.; Levchenko, S. V.; Scheffler, M.; Reuter, K. Beyond scaling relations for the description of catalytic materials. *ACS Catal.* **2019**, *9*, 2752−2759.
(23) Rossmeisl, J.; Qu, Z.-W.; Zhu, H.; Kroes, G.-J.; Nørskov, J. K. Electrolysis of water on oxide surfaces. *J. Electroanal. Chem.* **2007**, *607*, 83−89.
(24) Man, I. C.; Su, H.-Y.; Calle-Vallejo, F.; Hansen, H. A.; Martínez, J. I.; Inoglu, N. G.; Kitchin, J.; Jaramillo, T. F.; Nørskov, J. K.; Rossmeisl, J. Universality in oxygen evolution electrocatalysis on oxide surfaces. *ChemCatChem* **2011**, *3*, 1159−1165.
(25) García-Mota, M.; Vojvodic, A.; Metiu, H.; Man, I. C.; Su, H.-Y.; Rossmeisl, J.; Nørskov, J. K. Tailoring the Activity for Oxygen Evolution Electrocatalysis on Rutile TiO_2(110) by Transition-Metal Substitution. *ChemCatChem* **2011**, *3*, 1607−1611.
(26) Stoerzinger, K. A.; Diaz-Morales, O.; Kolb, M.; Rao, R. R.; Frydendal, R.; Qiao, L.; Wang, X. R.; Halck, N. B.; Rossmeisl, J.; Hansen, H. A.; Vegge, T.; Stephens, I. E. L.; Koper, M. T. M.; Shao-Horn, Y. Orientation-Dependent Oxygen Evolution on RuO_2 without Lattice Exchange. *ACS Energy Lett.* **2017**, *2*, 876−881.
(27) Back, S.; Yoon, J.; Tian, N.; Zhong, W.; Tran, K.; Ulissi, Z. W. Convolutional neural network of atomic surface structures to predict binding energies for high-throughput screening of catalysts. *J. Phys. Chem. Lett.* **2019**, *10*, 4401−4408.
(28) Giannozzi, P.; Baroni, S.; Bonini, N.; Calandra, M.; Car, R.; Cavazzoni, C.; Ceresoli, D.; Chiarotti, G. L.; Cococcioni, M.; Dabo, I.; Dal Corso, A.; de Gironcoli, S.; Fabris, S.; Fratesi, G.; Gebauer, R.; Gerstmann, U.; Gougoussis, C.; Kokalj, A.; Lazzeri, M.; Martin-Samos, L.; Marzari, N.; Mauri, F.; Mazzarello, R.; Paolini, S.; Pasquarello, A.; Paulatto, L.; Sbraccia, C.; Scandolo, S.; Sclauzero, G.; Seitsonen, A. P.; Smogunov, A.; Umari, P.; Wentzcovitch, R. M. QUANTUM ESPRESSO: a modular and open-source software project for quantum simulations of materials. *J. Phys.: Condens. Matter* **2009**, *21*, 395502.
(29) Wellendorff, J.; Lundgaard, K. T.; Møgelhøj, A.; Petzold, V.; Landis, D. D.; Nørskov, J. K.; Bligaard, T.; Jacobsen, K. W. Density functionals for surface science: Exchange-correlation model development with Bayesian error estimation. *Phys. Rev. B* **2012**, *85*, 235149.
(30) Steinhardt, P. J.; Nelson, D. R.; Ronchetti, M. Bond-orientational order in liquids and glasses. *Phys. Rev. B* **1983**, *28*, 784.
(31) Lee, Y.-L.; Kleis, J.; Rossmeisl, J.; Shao-Horn, Y.; Morgan, D. Prediction of solid oxide fuel cell cathode activity with first-principles descriptors. *Energy Environ. Sci.* **2011**, *4*, 3966−3970.
(32) Calle-Vallejo, F.; Inoglu, N. G.; Su, H.-Y.; Martínez, J. I.; Man, I. C.; Koper, M. T. M.; Kitchin, J. R.; Rossmeisl, J. Number of outer electrons as descriptor for adsorption processes on transition metals and their oxides. *Chem. Sci.* **2013**, *4*, 1245−1249.
(33) Hong, W. T.; Welsch, R. E.; Shao-Horn, Y. Descriptors of oxygen-evolution activity for oxides: a statistical evaluation. *J. Phys. Chem. C* **2016**, *120*, 78−86.
(34) Liu, J.; Liu, H.; Chen, H.; Du, X.; Zhang, B.; Hong, Z.; Sun, S.; Wang, W. Progress and Challenges Toward the Rational Design of Oxygen Electrocatalysts Based on a Descriptor Approach. *Adv. Sci.* **2019**, *7*, 1901614.
(35) Metiu, H.; Chrétien, S.; Hu, Z.; Li, B.; Sun, X. Chemistry of Lewis Acid-Base Pairs on Oxide Surfaces. *J. Phys. Chem. C* **2012**, *116*, 10439−10450.
(36) McFarland, E. W.; Metiu, H. Catalysis by Doped Oxides. *Chem. Rev.* **2013**, *113*, 4391−4427.
(37) Laurence, C.; Gal, J.-F. *Lewis basicity and affinity scales: data and measurement*; John Wiley & Sons: 2009.
(38) Moltved, K. A.; Kepp, K. P. The chemical bond between transition metals and oxygen: Electronegativity, d-orbital effects, and oxophilicity as descriptors of metal−oxygen interactions. *J. Phys. Chem. C* **2019**, *123*, 18432−18444.
(39) Nørskov, J. K.; Rossmeisl, J.; Logadottir, A.; Lindqvist, L.; Kitchin, J. R.; Bligaard, T.; Jónsson, H. Origin of the overpotential for oxygen reduction at a fuel-cell cathode. *J. Phys. Chem. B* **2004**, *108*, 17886−17892.
(40) González-Huerta, R. G.; Ramos-Sánchez, G.; Balbuena, P. B. Oxygen evolution in Co-doped RuO_2 and IrO_2: Experimental and theoretical insights to diminish electrolysis overpotential. *J. Power Sources* **2014**, *268*, 69−76.
(41) Wu, Y.; Tariq, M.; Zaman, W. Q.; Sun, W.; Zhou, Z.; Yang, J. Bimetallic Doped RuO_2 with Manganese and Iron as Electrocatalysts for Favorable Oxygen Evolution Reaction Performance. *ACS Omega* **2020**, *5*, 7342−7347.
(42) Chen, S.; Huang, H.; Jiang, P.; Yang, K.; Diao, J.; Gong, S.; Liu, S.; Huang, M.; Wang, H.; Chen, Q. Mn-Doped RuO_2 Nanocrystals as Highly Active Electrocatalysts for Enhanced Oxygen Evolution in Acidic Media. *ACS Catal.* **2020**, *10*, 1152−1160.
(43) Reier, T.; Pawolek, Z.; Cherevko, S.; Bruns, M.; Jones, T.; Teschner, D.; Selve, S.; Bergmann, A.; Nong, H. N.; Schlögl, R.; Mayrhofer, K. J. J.; Strasser, P. Molecular Insight in Structure and Activity of Highly Efficient, Low-Ir Ir-Ni Oxide Catalysts for Electrochemical Water Splitting (OER). *J. Am. Chem. Soc.* **2015**, *137*, 13031−13040.
(44) Moghaddam, R. B.; Wang, C.; Sorge, J. B.; Brett, M. J.; Bergens, S. H. Easily prepared, high activity Ir-Ni oxide catalysts for water oxidation. *Electrochem. Commun.* **2015**, *60*, 109−112.
(45) Zaman, W. Q.; Wang, Z.; Sun, W.; Zhou, Z.; Tariq, M.; Cao, L.; Gong, X.-Q.; Yang, J. Ni-Co Codoping Breaks the Limitation of Single-Metal-Doped IrO_2 with Higher Oxygen Evolution Reaction Performance and Less Iridium. *ACS Energy Lett.* **2017**, *2*, 2786−2793.
(46) Dickens, C. F.; Nørskov, J. K. A theoretical investigation into the role of surface defects for oxygen evolution on RuO_2. *J. Phys. Chem. C* **2017**, *121*, 18516−18524.
(47) Ping, Y.; Nielsen, R. J.; Goddard, W. A., III The Reaction Mechanism with Free Energy Barriers at Constant Potentials for the Oxygen Evolution Reaction at the IrO_2(110) Surface. *J. Am. Chem. Soc.* **2017**, *139*, 149−155.
(48) Gauthier, J. A.; Ringe, S.; Dickens, C. F.; Garza, A. J.; Bell, A. T.; Head-Gordon, M.; Nørskov, J. K.; Chan, K. Challenges in Modeling Electrochemical Reaction Energetics with Polarizable Continuum Models. *ACS Catal.* **2019**, *9*, 920−931.
(49) Oberhofer, H. *Handbook of Materials Modeling: Applications: Current and Emerging Materials*; Andreoni, W.; Yip, S. Eds.; Springer International Publishing: Cham, 2020; pp. 1505−1537, DOI: 10.1007/978-3-319-44680-6_9.

https://dx.doi.org/10.1021/acscatal.0c04170
ACS Catal. 2021, 11, 734−742

(50) Opalka, D.; Scheurer, C.; Reuter, K. Ab Initio Thermodynamics Insight into the Structural Evolution of Working IrO_2 Catalysts in Proton-Exchange Membrane Electrolyzers. *ACS Catal.* **2019**, *9*, 4944−4950.

https://dx.doi.org/10.1021/acscatal.0c04170
ACS Catal. 2021, 11, 734−742

B Paper # 2

Predicting Binding Motifs of Complex Adsorbates Using Machine Learning with a Physics-inspired Graph Representation

Wenbin Xu, Karsten Reuter and Mie Andersen*

Nat. Comput. Sci. 2, 443450 (2022).
DOI:10.1038/s43588-022-00280-7

nature computational science

ARTICLES

https://doi.org/10.1038/s43588-022-00280-7

Predicting binding motifs of complex adsorbates using machine learning with a physics-inspired graph representation

Wenbin Xu[1,2], Karsten Reuter[2] and Mie Andersen[3,4] ✉

Computational screening in heterogeneous catalysis relies increasingly on machine learning models for predicting key input parameters due to the high cost of computing these directly using first-principles methods. This becomes especially relevant when considering complex materials spaces such as alloys, or complex reaction mechanisms with adsorbates that may exhibit bi- or higher-dentate adsorption motifs. Here we present a data-efficient approach to the prediction of binding motifs and associated adsorption enthalpies of complex adsorbates at transition metals and their alloys based on a customized Wasserstein Weisfeiler–Lehman graph kernel and Gaussian process regression. The model shows good predictive performance, not only for the elemental transition metals on which it was trained, but also for an alloy based on these transition metals. Furthermore, incorporation of minimal new training data allows for predicting an out-of-domain transition metal. We believe the model may be useful in active learning approaches, for which we present an ensemble uncertainty estimation approach.

Many surface catalytic reactions of vital importance to our society—such as Fischer–Tropsch, methanol or higher oxygenate syntheses—have complex reaction mechanisms with numerous intermediates ranging from atoms and simple molecules to (possibly oxygenated) C1, C2 or larger fragments. It is well-known that modeling of these latter complex species at transition metal catalysts must account for their ability to exhibit a wide range of adsorption motifs, including mono-, bi- and higher-dentate adsorption modes[1–3]. Density-functional theory (DFT) with van der Waals corrections can, in principle, provide the energetics of such adsorption motifs at moderate cost and satisfactory accuracy[4]. Nevertheless, the identification of the most stable adsorption motifs of adsorbates involved in ethanol synthesis on a simple monometallic catalyst such as Rh(111) is already a formidable task[5–8], and the investigation of broader classes of materials such as transition metal alloys is generally out of reach due to the combinatorial explosion of possible active sites and adsorption motifs.

Machine learning models have already shown their potential for replacing expensive DFT calculations to tackle the screening of large materials spaces for accelerated catalyst discovery[9–13]. However, most works so far have been limited in scope to the consideration of atoms or small molecules with monodentate adsorption motifs. For these simple species, models now routinely achieve the prediction of adsorption enthalpies with a root-mean-square error (r.m.s.e.) of around 0.1–0.2 eV, which is then comparable with the intrinsic DFT accuracy[11,13–15].

Unfortunately, most of these methods cannot easily be extended to complex adsorbates with bi- or higher-dentate adsorption motifs. One notable attempt to treat complex adsorbates is provided in the Open Catalyst Project where the direct prediction of relaxed adsorption enthalpies is achieved by incorporating a graph representation of the initial structure into a graph convolutional neural network[16]. However, approaches that rely purely on connectivity and geometry-based features have revealed poor data efficiency and thus cannot be used without excessively large training databases[14–16]. Moreover, the predictive performance for complex adsorbates in the Open Catalyst Database is still below practical usefulness with a mean absolute error for in-domain prediction of around 0.6 eV (ref. [16]).

In this work we develop and test a data-efficient, physics-inspired machine learning model—based on graph representation, the Wasserstein Weisfeiler–Lehman (WWL) graph kernel[17] and Gaussian process regression (GPR)—that is applicable for both simple and complex adsorbates. We abbreviate the model WWL-GPR. For comparison, we show also results for predictions of simple and complex adsorbates using other popular, fundamentally different machine learning approaches that employ input in vector form instead of graph representation, namely, the sure-independence screening and sparsifying operator (SISSO) approach[18,19], GPR with a radial basis function kernel (RBF-GPR) and extreme gradient boosting (XGBoost)[20]. We train our machine learning models for complex adsorbates on a relatively small database (around 1,700 data points) of DFT adsorption enthalpies calculated at the face-centered cubic (fcc) (211) and (111) facets of four transition metals: copper (Cu), rhodium (Rh), palladium (Pd) and cobalt (Co). The chosen adsorbates and transition metals are of interest for ethanol synthesis[21,22].

Our dataset is smaller than the Open Catalyst Dataset by about a factor of 300, and covers less diverse surfaces and adsorbates, but exhibits a much denser sampling of diverse adsorption motifs for each catalyst–adsorbate combination considered. More importantly, we do not rely on graph representation alone, but augment it with node attributes representing physically motivated properties, for example, *d*-band moments (surfaces), highest-occupied and lowest-unoccupied molecular orbital (HOMO/LUMO) energy levels (adsorbate molecules) and features of the local geometry, all derived from either the clean surfaces or the adsorbates in the gas phase. The model achieves an in-domain prediction of adsorption

[1]Chair for Theoretical Chemistry and Catalysis Research Center, Technische Universität München, Garching, Germany. [2]Fritz-Haber-Institut der Max-Planck-Gesellschaft, Berlin, Germany. [3]Aarhus Institute of Advanced Studies, Aarhus University, Aarhus, Denmark. [4]Department of Physics and Astronomy—Center for Interstellar Catalysis, Aarhus University, Aarhus, Denmark. ✉e-mail: mie@phys.au.dk

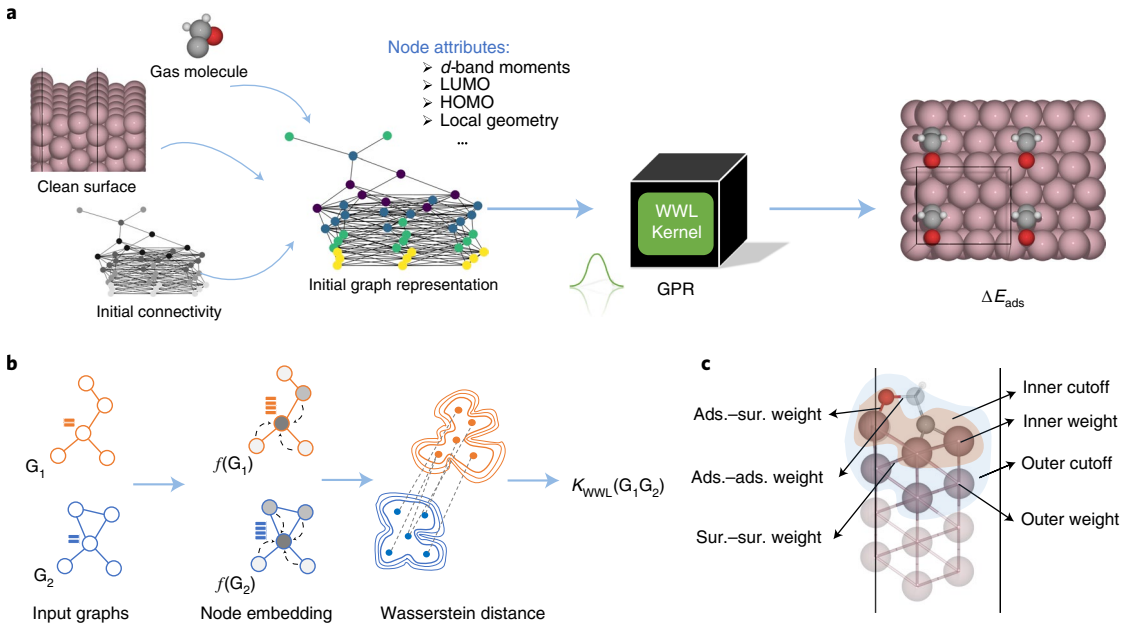

Fig. 1 | Schematic illustration of the WWL-GPR model. a, The adsorption enthalpy of the relaxed structure, ΔE_{ads}, is predicted from a graph representation of the initial structure with node attributes computed from the gas phase molecule and clean surface. The graph similarity is calculated from the WWL graph kernel and input to a GPR model. **b**, The similarity of two input graphs in the WWL kernel, K_{WWL}, is calculated by first generating node embeddings and then computing the Wasserstein distance between their distributions. **c**, Surface adsorption motivated hyperparameters incorporated into the WWL kernel. Sur., surface; Ads., adsorbate.

enthalpies with a r.m.s.e. of about 0.2 eV and also shows good extrapolative performance for two test cases; bimetallic alloys made from elements present in our training data and out-of-domain elements, the latter however only after incorporation of adsorption enthalpies of atomic species on the new element into the training database. Finally, we show that data points with large prediction errors can be quite reliably captured from an ensemble uncertainty estimation approach.

Results

WWL-GPR model. The machine learning task in our work is to directly predict the relaxed adsorption enthalpies corresponding to a range of possible adsorption motifs represented as graphs. Thereby, for a given surface–adsorbate combination of interest, we obtain a spectrum of possible adsorption energies ranging from the most stable to metastable adsorption motifs. Microkinetic models used in catalyst screening often employ only the most stable adsorption energy obtained as input, however, distinct adsorption sites with less favorable adsorption energies could be included as well[23]. Our task is thus quite similar to the task denoted as initial state to relaxed energy (IS2RE) in the Open Catalyst Project, however, we do not directly use the initial state geometry, but only its graph representation. We note that an entirely different approach to this task is to train a machine learning interatomic potential[24,25] to relax the initial structure and thereby predict both the relaxed structure and adsorption enthalpy; however, such approaches are not a topic of this work.

Figure 1a depicts a schematic of our physics-inspired WWL-GPR model. We rely on graph representation, which is a versatile method for representing isolated molecules[26,27], crystal structures[28] or the combined surface–adsorbate system[29–31] in which every atom in the structure is a node with edges representing chemical bonds to neighboring atoms. Graph representation can be used in connection with neural networks[14–16], which generally requires very large training databases. As we are here interested in developing a data-efficient method, we focus on a kernel-based method (GPR) in connection with a customized version of the recently developed WWL graph kernel[17]. Figure 1b illustrates the node embedding scheme, the calculation of the Wasserstein distance (distribution relationship) between the graphs, and the subsequent WWL graph kernel calculation. The WWL graph kernel allows for continuous node attributes, for which we use physically motivated electronic and geometric features calculated from the clean surface and isolated adsorbate. Finally, we incorporate some surface adsorption-motivated hyperparameters into the WWL kernel to learn better representations (see Fig. 1c): edge weights, which differentiate chemical bonds by three classes (adsorbate–adsorbate, surface–surface and adsorbate–surface) as well as inner and outer cutoffs and weights. The cutoffs and weights are used during the computation of the Wasserstein distance to emphasize the importance of various atomic shells around the active site for the adsorption energy prediction. We note that attention algorithms widely used in neural networks serve a similar purpose[15].

Prediction of simple adsorbates. We begin by evaluating the performance of the machine learning models for predicting a database of simple adsorbates with monodentate adsorption motifs (see Methods). We perform fivefold cross-validation, that is, the database is shuffled and partitioned into five equal-sized subsamples stratified by adsorbates. The training is then performed based on four of the subsamples while retaining the fifth subsample for validation. This is repeated five times until all data points have been used once for validation. Figure 2 shows the resulting parity plot of DFT-calculated versus machine learning-predicted adsorption enthalpies for the combined validation set from the five folds as well as violin plots of the absolute error distributions for SISSO and the GPR models. It should be noted here that the SISSO results are obtained using similar hyperparameters to those from our previous work[11,32] (eight-dimensional rung three descriptor). In principle, we would expect a better performance for even more complex models than the r.m.s.e. value of 0.24 eV presented here; see Supplementary Fig. 5. However, the identification of more complex models is

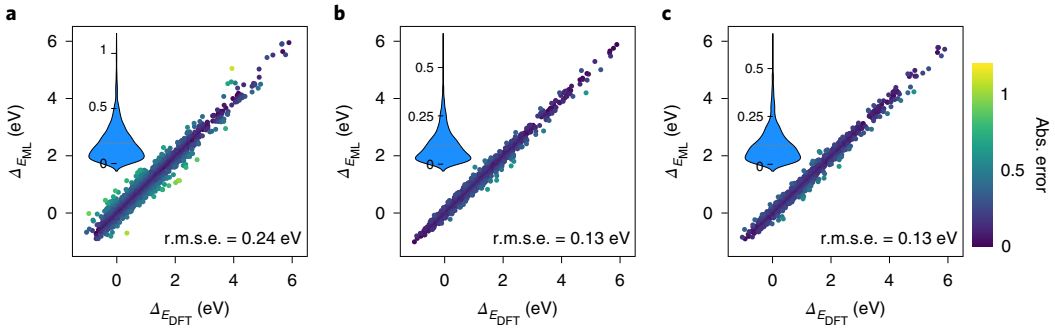

Fig. 2 | Parity plot of DFT-calculated versus machine learning-predicted adsorption enthalpies using SISSO, RBF-GPR and WWL-GPR. a–c, Parity plot of DFT-calculated versus machine learning-predicted adsorption enthalpies from the combined validation set in fivefold cross-validation using SISSO (**a**), RBF-GPR (**b**) and WWL-GPR (**c**) for the simple adsorbates database. The violin plots in the insets illustrate the absolute (Abs.) error distributions (in eV), and the internal dashed lines in the plots mark the mean absolute error. ML, machine learning.

computationally intractable with the SISSO method. Rather than raw performance, the merit of the SISSO approach is that the identified descriptors are (somewhat simple) analytical functions of the features, which are thus easier to interpret than black-box machine learning models. We also note that the reason for the different performance of the descriptors identified in the present work compared with our previous work is that here we train a single model on the entire database (single-task learning) to be able to make a direct comparison to the GPR models, whereas in our previous work separate fitting coefficients were used for each adsorbate (multitask learning). More information about the identified SISSO descriptors is provided in Supplementary Section 3.2.

The model complexity can be more easily tailored for the GPR models, and, after optimization of the relevant hyperparameters (see Supplementary Section 3.5 and Supplementary Table 9), we obtain a r.m.s.e. of 0.13 eV independent of whether we use vector input (RBF-GPR) or graph representation (WWL-GPR). The maximum absolute error (maxAE) also decreases from 1.11 eV (SISSO) to around 0.60 eV in the GPR models. Based on the similar performance of the two GPR models, we can conclude that there is no added value from employing graph representation for the simple adsorbates. The reactivity is apparently already captured by the averaged surface atom features and the adsorbate-specific features used in the RBF-GPR model.

Finally, the XGBoost method represents an ensemble-based machine learning method based on decision trees and gradient boosting, where trees are added one at a time to improve on the residuals of the previous model[20]. Here we find that it performs similarly to the GPR models (see Supplementary Fig. 8), with an r.m.s.e of 0.12 eV. On the basis of this similar performance of state-of-the-art methods, we believe that we are at the limit of the machine learning accuracy achievable for simple adsorbates with the available dataset and feature representation.

Prediction of complex adsorbates. We next turn to a database of complex adsorbates with 41 different adsorbates in mono-, bi- and higher-dentate adsorption motifs on surfaces of Cu, Co, Pd and Rh (see Methods). As we already concluded in the preceding section on simple adsorbates that single-task SISSO is not competitive in terms of performance, we focus here only on the GPR models and XGBoost. The fivefold cross-validation results presented in Fig. 3 show that the graph-based WWL-GPR model has a superior performance (r.m.s.e. of 0.18 eV) for this more challenging database compared with RBF-GPR (r.m.s.e. of 0.47 eV). The maxAE also decreases from 2.23 eV (RBF-GPR) to 0.92 eV in the WWL-GPR model. The XGBoost method clearly outperforms RBF-GPR, with a r.m.s.e. of 0.23 eV, which is possibly related to the advantages of its ensemble-based approach; however, it is still inferior to WWL-GPR. We attribute this to the importance of the graph representation for complex adsorbates, which is present in the WWL-GPR model but missing in the vector-based models. A learning curve for the WWL-GPR model is presented in Supplementary Fig. 6, which shows that an r.m.s.e. of 0.3 eV can be achieved by only training on 30% of the database (~500 data points) and a r.m.s.e. of 0.2 eV is achieved at 70% of the database (~1,200 data points). A visualization of the prediction accuracy for adsorption motifs of one selected adsorbate (CHCO) on one selected surface (Cu(211)) is given in Supplementary Fig. 7.

To visualize what trends the WWL-GPR model has identified in the complex adsorbates database, we present in Fig. 4 a kernel principal component analysis, which is a non-linear dimensionality reduction technique. Specifically, we here present the two dimensions that explain the largest fraction of the variance. Points that are close together in this space are similar in the feature space. The analysis of the entire complex adsorbate database in Fig. 4a shows that the different metals are distinguished as parallel clusters, where for each cluster there is a similar distribution of subclusters containing the individual adsorbates. In Fig. 4b the same analysis is presented for only one metal (here, Rh, but similar results are obtained for the other transition metals). Again, the different adsorbates form clusters, where each point in a cluster corresponds to a separate adsorption motif of the adsorbate. A similar clustering cannot be observed in KPCA plots for the RBF-GPR model (see Supplementary Fig. 9), which is probably related to the fact that this model does not have any structural information on the different adsorbates and their associated adsorption motifs due to the lack of graph representation.

Having established the excellent interpolation performance of the WWL-GPR model, we next assess the predictive performance of the model for extrapolation tasks concerning data that are dissimilar to those in the training database, that is, an out-of-domain prediction. This is highly important for the practical application of the model to catalyst screening. The two tasks we consider are: (1) predictions for a bimetallic catalyst, that is, an alloy of elemental metals present in our database; and (2) predictions for an out-of-domain element when merely incorporating the adsorption enthalpies of atomic species (C, H, and O) at the new element into the database. For these tasks we selected eight adsorbates comprising atomic species and larger molecules, and including some with bidentate adsorption motifs (see Supplementary Table 4).

As it has previously been emphasized in the literature that a careful choice of regularization can substantially improve the robustness of a model in extrapolative, data-poor regimes[33,34], we reoptimized the hyperparameters for the extrapolation tasks. Specifically, we

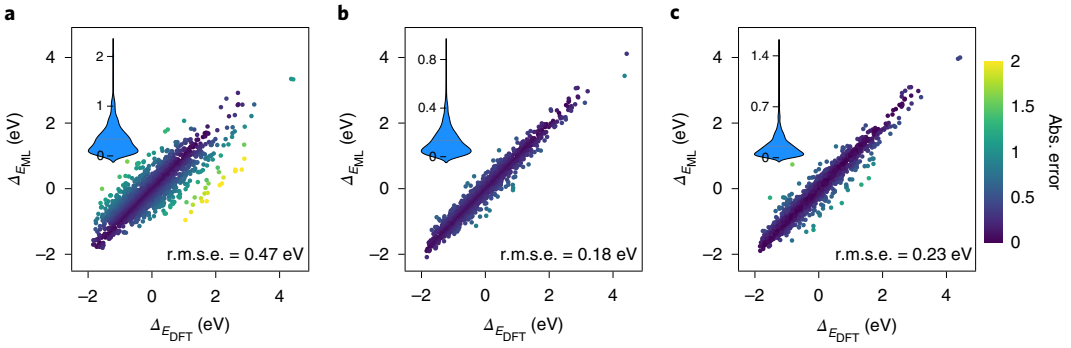

Fig. 3 | Parity plot of DFT-calculated versus machine learning-predicted adsorption enthalpies using RBF-GPR, WWL-GPR and XGBoost. a–c, Parity plot of DFT-calculated versus machine learning-predicted adsorption enthalpies from the combined validation set in fivefold cross-validation using RBF-GPR (**a**), WWL-GPR (**b**) and XGBoost (**c**) for the complex adsorbates database. The violin plots in the insets illustrate the absolute error distributions (in eV), and the internal dashed lines in the plots mark the mean absolute error.

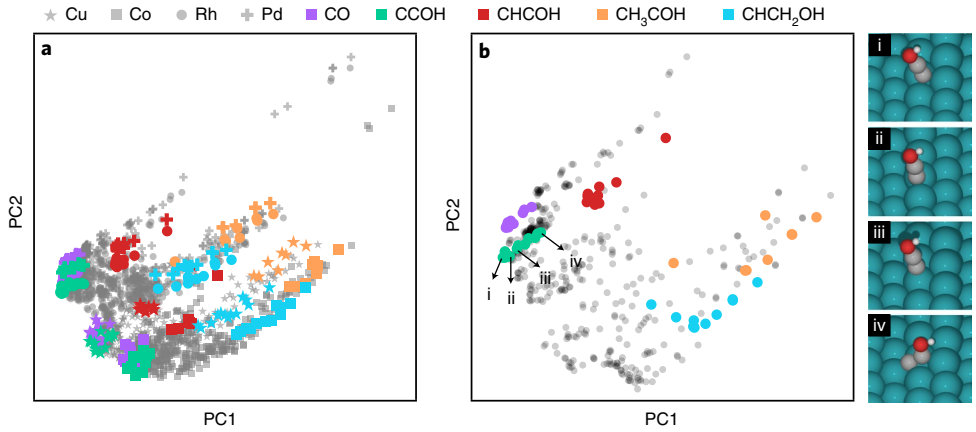

Fig. 4 | Kernel principal component analysis. a,**b**, Two-dimensional kernel principal component (PC) analysis plots for the WWL-GPR model with hyperparameters optimized for interpolation for all metals (**a**) and rhodium (**b**) surfaces only. The locations and structures of selected adsorbates are highlighted. Green, Rh; gray, C; red, O; white, H.

used data for one bimetallic alloy (CuCo) and one out-of-domain element (platinum, Pt) to optimize new hyperparameters by minimizing the loss function ($r.m.s.e._{interpolation} + 2 \times r.m.s.e._{extrapolation}$), where $r.m.s.e._{interpolation}$ is the r.m.s.e. for the original complex adsorbates database (including atomic adsorption enthalpies for Pt) and $r.m.s.e._{extrapolation}$ is the r.m.s.e. of the dataset for CuCo and Pt (only the complex adsorbates for Pt). As the aim is to find hyperparameters well suited for extrapolation, this task was given a higher weight (two) in the loss function than that of the interpolation task (one). Comparing the hyperparameters obtained previously for the complex adsorbates database (see the base case in Supplementary Table 10) with the new hyperparameters optimized specifically for the extrapolation tasks (see the base case in Supplementary Table 11), we see that indeed both the length scale and the regularization term increase for the extrapolation tasks, resulting in a smoother machine learning model, which is consistent with the previous literature observations. The r.m.s.e. values obtained for the new hyperparameters are 0.25 eV for interpolation within the complex adsorbate database, 0.23 eV for the CuCo alloy and 0.30 eV for Pt. Finally, we carry out a true extrapolation test to assess whether the new hyperparameters would also be accurate for yet another bimetallic alloy (here we chose PdRh) and yet another out-of-domain element (here we chose Ru); see Supplementary Table 4. We are able to obtain a very good extrapolation performance with a r.m.s.e. of 0.23 eV for PdRh and 0.23 eV for Ru. We note here that Ru is apparently easier to extrapolate to than Pt (on the basis of the lower r.m.s.e. obtained), which signifies that it must somehow be more similar to the elements present in the complex alloys database. Our results also show that an out-of-domain element is generally harder to predict than an alloy of known elements, even when incorporating some minimal information about the unknown element into the training database through the atomic adsorption enthalpies. We would expect the performance for Pt to improve if more adsorbates were added to the training database.

Uncertainty quantification. Up till now we have demonstrated that our WWL-GPR model can be applied, with r.m.s.e. values of around 0.2–0.3 eV, to flat and stepped metal and bimetallic catalysts, as long as some (at least minimal) training data involving the considered elemental metals are provided; however, apart from knowing which average r.m.s.e. value to expect, it is also useful to be able to directly assess the expected uncertainty on a single predicted data point. For example, uncertainty quantification combined with sensitivity analysis of microkinetic models[35–37] can be used to assess error propagation and the extent to which conclusions drawn from a model are robust to input parameter uncertainty[38,39]. Furthermore, uncertainty quantification is used in active learning approaches, where the training database is iteratively updated through selected DFT calculations, for example, of data points with a high estimated uncertainty[40,41].

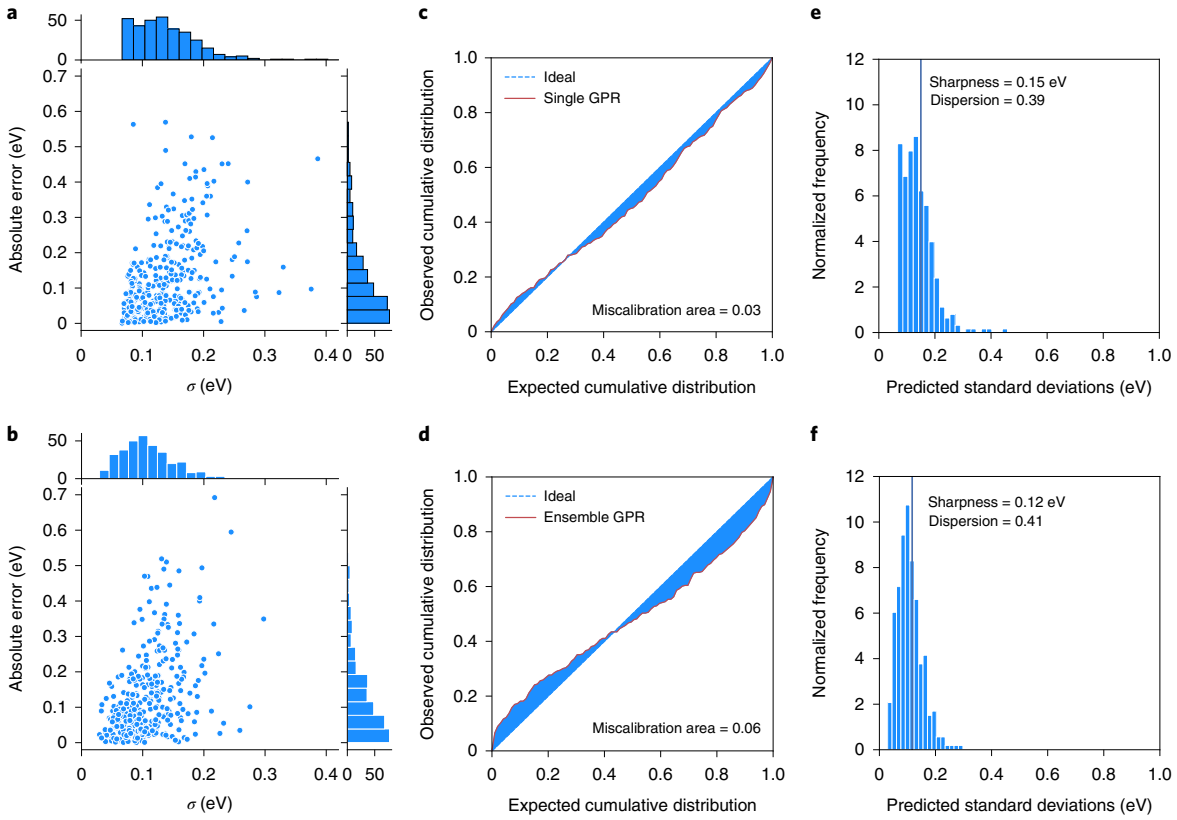

Fig. 5 | Estimated uncertainties versus absolute prediction errors for the single and ensemble models. a–f, The uncertainty versus absolute error, calibration curve and distribution plot of the predicted standard deviations for the single GPR model (**a**, **c** and **e**) and the ensemble GPR model (**b**, **d** and **f**).

In view of these applications, we are here primarily interested in the extent to which a high estimated uncertainty correlates with a high actual error of the model predictions. To assess this point, we use a random 80/20% training/test split of the complex adsorbates database stratified by adsorbate. We compare the intrinsic uncertainty quantification provided in a single GPR model trained on the training set through the standard deviation of the posterior distribution with the uncertainty quantification provided by the standard deviation of an ensemble (100 in total) of GPR models with fixed hyperparameters optimized for interpolation. The ensemble is constructed through bootstrapping of the training set, that is, data points are drawn randomly with replacement. Note that the added computational cost of establishing the ensemble model is negligible because we use a fixed training/test split, and because the kernel between the training and test set only needs to be computed once.

As expected, the prediction accuracies obtained from the single and ensemble models are almost identical (r.m.s.e. of 0.17 eV versus 0.18 eV, respectively). A plot of estimated uncertainties versus absolute prediction errors of the two models is presented in Fig. 5a,b. For comparison, we show also in Fig. 5c–f some distribution-based measures of the quality of an uncertainty quantification that have recently been discussed in the literature: calibration, sharpness and dispersion[42]. A useful uncertainty quantification method should have a small miscalibration area (that is, a good match between the expected and observed cumulative error distribution), a small sharpness value (small error estimates) and a large dispersion value (disperse error estimates). For calibration, sharpness and dispersion, the performances of the single and ensemble models are quite similar, with the single model having a slightly better calibration and the ensemble model having a slightly better sharpness and dispersion. However, with our primary interest being active learning, it is much more intriguing to see that the ensemble model does a better job than the single model at assigning a high uncertainty to data points with a high actual prediction error. In particular, the group of points with an estimated uncertainty higher than 0.2 eV in the ensemble model includes the largest prediction errors, whereas this is not the case for the single model, which actually assigns quite a low uncertainty to some of the largest prediction errors. We therefore conclude that the ensemble model is best suited for active learning approaches. We note here that we do not expect any quantitative match between the absolute error and the uncertainty in Fig. 5, partly as these are not directly comparable quantities (one is a standard deviation and the other an absolute error), and partly because it has been shown that specific calibration measures[43,44] are required for quantitatively accurate uncertainty quantification in both single and ensemble GPR models.

Discussion

We begin by discussing the origin of the superior performance of the WWL-GPR model over the vector-based RBF-GPR and XGBoost models. First of all, we note that it is not surprising that for complex adsorbates, simply accounting for the surface and adsorbate in terms of features averaged over the atoms directly involved in the bonding, as well as the global features of the adsorbate (for example, HOMO/LUMO levels) and clean surface (for example work function), as done in the vector-based models, is insufficient. By contrast, the graph representation provides direct access to structural information on the system, that is, the number and types of atoms in the adsorbate and how these atoms connect to each other and to the surface, possibly in complex bi- or higher-dentate adsorption motifs. Atom-specific features related to the local electronic or geometric structure can be directly used as node attributes (for

example, through SOAP descriptors), and we can introduce surface adsorption-motivated hyperparameters as discussed above and illustrated in Fig. 1c. The main remaining limitation of our model is that it cannot be expected to handle cases where the adsorbate dissociates or the surface reconstructs upon the adsorption event, as it—by contrast to machine learning force fields—does not predict the entire potential energy surface of the system, but only discrete minima corresponding to the adsorbed states. Furthermore, it relies on user-specified features, which would have to be adjusted for the consideration of other materials classes, for example, metal oxides[32].

Based on the demonstrated extrapolation performance, we trust that our WWL-GPR model could be useful for catalyst screening purposes, for example, for exploring reactions with complex adsorbates on alloy surfaces. Here the complexity encountered from the many possible adsorption motifs of each adsorbate on each type of alloy surface makes direct DFT investigations computationally intractable, while reliable machine learning force fields or density-functional tight-binding methods for the simultaneous treatment of many different adsorbates and/or alloy surfaces are still difficult to obtain[2,16].

We envision that it could be particularly interesting to apply our model in the context of an active learning strategy, where the training database is iteratively expanded towards catalytically interesting and/or previously poorly explored regions of the catalyst space. Key advantages of our data-efficient GPR model in this regard are the low training cost (compared to, for example, deep neural networks) and the demonstrated uncertainty quantification. For active learning purposes, we also recommend using the model with different hyperparameter settings depending on the exploitative or explorative nature of the task at hand. Specifically, we can confirm the findings from past literature reports that hyperparameters characterized, among others, by larger length scale and regularization terms are beneficial for accurate predictions in data-poor regions of the catalyst space.

Methods

DFT databases. The machine learning models are trained and tested on two different databases, termed simple adsorbates and complex adsorbates. The former is taken from refs. [11,23]. After a post-processing step, the database contains 1,422 data points and includes the adsorption enthalpies of eight simple adsorbates with monodentate coordination; C, H, O, CO, OH, CH, CH_2 and CH_3. The considered surfaces include the fcc(100), fcc(110), fcc(111) and fcc(211) facets of pure Ni, Cu, Ru, Rh, Pd, Ag, Ir, Pt and Au, the body-centered cubic (bcc) (210) facet of Fe as well as the stepped hexagonal close-packed (hcp) (0001) facet of Co. For alloy catalysts, the database contains the adsorbates on the four single-atom alloys Ag@Cu, Pt@Rh, Pd@Ir and Au@Ni (that is, single-atom Ag, Pt, Pd or Au dispersed in the surface of another host metal), and the four AB bimetallic alloys AgPd, IrRu, PtRh and AgAu.

The complex adsorbates database contains 1,679 data points and includes 41 different small and large adsorbates involved in ethanol synthesis on fcc(111) and fcc(211) facets of Cu, Rh, Pd and Co. Examples of complex adsorbates are CHCO, CCHOH, CH_2CH_2O and CH_3CH_2OH; the full list of adsorbates is provided in Supplementary Table 3. Furthermore, selected adsorbates are calculated at the CuCo(111), PdRh(111), Pt(111), Ru(111), Pt(211) and Ru(211) surfaces for model testing purposes. The adsorbates contain up to nine atoms and cover mono-, bi- and higher-dentate adsorption modes. The database is constructed using an automated workflow and DFT settings that are compatible with the simple adsorbates database (Quantum Espresso code[45] and the Bayesian error estimation functional with van der Waals correlation (BEEF-vdW) functional[46]). Further computational details and overviews of both databases are given below and in Supplementary Section 1.

Database construction and workflow. The initial geometries of the surface–adsorbate systems are generated using the CatKit software[30]. CatKit employs a graph representation of the surface atoms to enumerate mono- and bidentate adsorption sites, where the latter are defined by a neighboring node–edge pair of the graph. For each adsorbate, a manual tagging of the bonding atoms for mono- and bidentate adsorption motifs is required (see Supplementary Table 3). CatKit then adds the adsorbates at the enumerated adsorption sites by employing some simple geometric procedures to produce good estimates for the angles and bond lengths in the system. We note that CatKit does not generate all possible adsorption motifs (which would be computationally intractable), but only those that are judged as most plausible. This adds a human bias into the generation of the database. Furthermore, not all initial geometries generated are actually stable, but could transform into other structures during the DFT relaxation.

To overcome some of these limitations, we added the following steps to our computational workflow. During the DFT relaxation, we monitor the graph representation of the system and assign it to the following four cases: (1) if the graph representation is unchanged, the data point is simply added to our database (32.3% of cases); (2) if the structure transforms into another graph that is already covered in the CatKit-enumerated structures (28.4% of cases), only the calculation with the most favorable adsorption enthalpy is added to the database to avoid duplicates; (3) the calculation is discarded if the structure transforms into a non-valid graph, that is, a graph that is incompatible with our direct graph-based machine learning model (for example, adsorbate dissociation, surface reconstruction) (23.4% of cases); (4) if the structure transforms into a valid graph that was not enumerated by CatKit (15.9% of cases), the data point is added to the database with updated initial graph representation and the new adsorption motif is tested also for the other surfaces of interest. The last case (4), as well as large adsorbates whose initial adsorption motifs cannot be well controlled by CatKit, are the source of all higher-dentate adsorption motifs in our database (see Supplementary Fig. 3 for examples). Our workflow is implemented with AIIDA[47], which is a scalable computational infrastructure providing advanced automation to allow interfacing with external simulation software. In our case this entails customized python scripts[48] interfacing with CatKit, the Atomic Simulation Environment software[49] and the Quantum Espresso DFT code.

DFT computational details. For the DFT calculations of the complex adsorbates database, the following settings were used in full compliance with the simple adsorbates database. We used the Quantum ESPRESSO code[45] with a plane-wave basis set, the BEEF-vdW functional and ultrasoft pseudopotentials. Pseudopotentials for Cu, Rh, Pd and Pt were generated using the 'atomic' code by A. Dal Corso (v.5.0.2 svn rev. 9415)[50], for Co using the Vanderbilt code version 7.0.0 (ref. [51]) and for Ru using the Vanderbilt code v.7.3.5. To relieve the interaction between the adsorbates, we modeled the fcc(211) slab in a (3×1) cell and the fcc(111) slab in a (3×3) cell. In both cases this corresponds to nine atoms per atomic layer. The CuCo(111) and PdRh(111) alloy surfaces were modeled in a (4×2) cell and contain 16 atoms per layer. We used a (4×4) *k*-point grid for the pure metal slabs and a (3×3) grid for the alloy slabs. All slabs contained four atomic layers, where the bottom two layers were kept fixed in their bulk-truncated positions, whereas the top layers and the adsorbates were relaxed until the maximum force on each atom fell below 0.05 eV $Å^{-1}$ (see Supplementary Fig. 1 for images of the used slab geometries). All DFT calculations were performed as periodic slab calculations employing a vacuum region of 20 Å perpendicular to the surface and a dipole correction. Spin polarization was taken into account for the calculations involving Co. The cutoff energy was set to 500 eV and 5,000 eV for the orbitals and charge density, respectively, and a Fermi-level smearing of 0.1 eV was used. The resulting adsorption enthalpies are formation energies referenced to gaseous CH_3OH, CO and H_2O.

The features that require DFT calculations were obtained as follows. For the clean surfaces involved in both the simple and complex adsorbate databases, we first performed a geometry relaxation as outlined above. The projected density of states (PDOS) was calculated using the smearing-free tetrahedron method and an energy spacing of 0.01 eV. We used a (14×14) *k*-point grid for the pure metal fcc and bcc slabs, a (7×21) grid for the SG225 fcc alloys, a (14×21) for the SG221 fcc alloys, a (7×14) grid for the Co hcp slab, and a (7×42) for the hcp alloy structures. We used a (12×12) *k*-point grid for the CuCo(111) and PdRh(111) alloy surfaces involved in the extrapolation tasks.

For the calculation of band moments, we integrated empty bands up to the energy above the Fermi level where the PDOS had fallen below a value of 0.01 $Å^{-3}eV^{-1}$. The features involving the density of states at the Fermi level were calculated using a smearing of 0.1 eV in the PDOS calculation, and the PDOS was averaged over the interval ±0.1 eV around the Fermi level. For the calculation of adsorbate-specific features, we carried out a structural optimization of the isolated adsorbate positioned in a cubic supercell with a side length of 15 Å. We used a Fermi-level smearing of 0.01 eV and the Brillouin zone integration was performed using the Gamma point only.

Further details on machine learning models. The WWL-GPR model is compared with three other machine learning models (SISSO, RBF-GPR and XGBoost) that do not use graph representation, but input in vector form with features of the clean surface and the isolated adsorbates. The features used in the vector-based models are specific to the surface, site or adsorbate considered, where site-specific features are calculated by averaging over the metal atoms to which the adsorbate coordinates (clean surface features) or the bonding atoms of the adsorbate (isolated adsorbate features). The WWL-GPR model also uses atom-specific features as node attributes, for example, electronic properties of individual surface atoms or features of the local geometry of the clean surface and isolated adsorbate through Smooth Overlap of Atomic Positions (SOAP) descriptors[52]. All of the details on the features used in the compared machine learning models are provided in Supplementary Section 2.

Supplementary Section 3 provides more information about each of the models, including a more in-depth discussion on the hyperparameters. When comparing the RBF-GPR and WWL-GPR models, it is interesting to note that although the WWL-GPR model finds that the optimal cutoff values are one node distance for both inner and outer cutoff for the simple adsorbates database (that is, mostly the atoms directly involved in surface–adsorbate bonding are judged important), the optimal inner and outer cutoffs (weights) are one (0.60) and two (0.06) node distances, respectively, for the complex adsorbates database, see Supplementary Table 9 (that is, also atoms neighboring the immediately bonding atoms are judged important, although with smaller weights). The effect of more distant atoms is not taken into account in the vector-based models, which then possibly relates to their decreased performance for complex adsorbates. Note also that during the node embedding scheme of the WWL graph kernel, the node attribute of every atom is updated with information about the node attributes of the neighboring atoms, see Supplementary Section 3.3.1.2. That is, even if weights beyond the outer cutoff are zero, the atoms there can still have a non-negligible influence on the kernel value.

It should be emphasized that the WWL-GPR model leverages only features from the initial guess geometry, specifically, the graph connectivity, and electronic and geometric features calculated from the clean surface and isolated adsorbate. From a computational screening point of view this is essential for keeping the computational cost of model predictions low. The computationally most intensive part of the model prediction is the DFT calculation of the clean surface to obtain the node attributes (for example *d*-band moments) for the surface atoms. However, given that we target 41 different adsorbates in various possible adsorption motifs for each surface, this is still a low-cost-per-machine learning prediction.

For SISSO, we previously used an approach to target simple adsorbates where the free parameters of the identified models were fitted to each adsorbate separately[11,32]. A similar approach has been taken in most other works targeting simple adsorbates[12,14,53,54]. In the present work we instead fit a single model to all adsorbates, and the different adsorbates are then instead distinguished from each other via adsorbate-specific features such as HOMO/LUMO energy levels. Further information about SISSO is given in Supplementary Section 3.2.

Data availability

The DFT-calculated adsorption energies and relaxed coordinates of the simple and complex adsorbates databases as well as all calculated features are available at https://github.com/Wenbintum/WWL-GPR and Zenodo[48]. Source Data are provided with this paper.

Code availability

The source code of WWL-GPR is publicly available on GitHub at https://github.com/Wenbintum/WWL-GPR and Zenodo[48]. We provide predefined tasks for tutorial purposes and for reproducing the results presented in this work. The RBF-GPR is implemented with Scikit-learn[55], which is available at https://scikit-learn.org. The SISSO code[18] is available at https://github.com/rouyang2017/SISSO, and the XGBoost code[20] is available at https://github.com/dmlc/xgboost.

Received: 27 January 2022; Accepted: 17 June 2022;
Published online: 25 July 2022

References

1. Cao, A. et al. Mechanistic insights into the synthesis of higher alcohols from syngas on CuCo alloys. *ACS Catal.* **8**, 10148–10155 (2018).
2. Chang, C. & Medford, A. J. Application of density functional tight binding and machine learning to evaluate the stability of biomass intermediates on the Rh(111) surface. *J. Phys. Chem. C* **125**, 18210–18216 (2021).
3. Wang, Z., Li, Y., Boes, J., Wang, Y. & Sargent, E. CO_2 Electrocatalyst design using graph theory. Preprint at https://doi.org/10.21203/rs.3.rs-66715/v1 (2020).
4. Nørskov, J. K., Abild-Pedersen, F., Studt, F. & Bligaard, T. Density functional theory in surface chemistry and catalysis. *Proc. Natl Acad. Sci. USA* **108**, 937–943 (2011).
5. Choi, Y. & Liu, P. Mechanism of ethanol synthesis from syngas on Rh(111). *J. Am. Chem. Soc.* **131**, 13054–13061 (2009).
6. Michel, C., Auneau, F., Delbecq, F. & Sautet, P. C–H Versus O–H bond dissociation for alcohols on a Rh(111) surface: a strong assistance from hydrogen bonded neighbors. *ACS Catal.* **1**, 1430–1440 (2011).
7. Filot, I. A. W. et al. First-principles-based microkinetics simulations of synthesis gas conversion on a stepped rhodium surface. *ACS Catal.* **5**, 5453–5467 (2015).
8. Gu, T., Wang, B., Chen, S. & Yang, B. Automated generation and analysis of the complex catalytic reaction network of ethanol synthesis from syngas on Rh(111). *ACS Catal.* **10**, 6346–6355 (2020).
9. Tran, K. & Ulissi, Z. W. Active learning across intermetallics to guide discovery of electrocatalysts for CO_2 reduction and H_2 evolution. *Nat. Catal.* **1**, 696–703 (2018).
10. Noh, J., Back, S., Kim, J. & Jung, Y. Active learning with non-ab initio input features toward efficient CO_2 reduction catalysts. *Chem. Sci.* **9**, 5152–5159 (2018).
11. Andersen, M., Levchenko, S. V., Scheffler, M. & Reuter, K. Beyond scaling relations for the description of catalytic materials. *ACS Catal.* **9**, 2752–2759 (2019).
12. Wang, S.-H., Pillai, H. S., Wang, S., Achenie, L. E. & Xin, H. Infusing theory into deep learning for interpretable reactivity prediction. *Nat. Commun.* **12**, 1–9 (2021).
13. Fung, V., Hu, G., Ganesh, P. & Sumpter, B. G. Machine learned features from density of states for accurate adsorption energy prediction. *Nat. Commun.* **12**, 88 (2021).
14. Back, S. et al. Convolutional neural network of atomic surface structures to predict binding energies for high-throughput screening of catalysts. *J. Phys. Chem. Lett.* **10**, 4401–4408 (2019).
15. Gu, G. H. et al. Practical deep-learning representation for fast heterogeneous catalyst screening. *J. Phys. Chem. Lett.* **11**, 3185–3191 (2020).
16. Chanussot, L. et al. Open Catalyst 2020 (OC20) dataset and community challenges. *ACS Catal.* **11**, 6059–6072 (2021).
17. Togninalli, M., Ghisu, E., Llinares-López, F., Rieck, B. & Borgwardt, K. Wasserstein Weisfeiler–Lehman graph kernels. In *Adv Neural Inf Process Syst.* Vol. 32 (NeurIPS, 2019).
18. Ouyang, R., Curtarolo, S., Ahmetcik, E., Scheffler, M. & Ghiringhelli, L. M. SISSO: a compressed-sensing method for identifying the best low-dimensional descriptor in an immensity of offered candidates. *Phys. Rev. Mater.* **2**, 083802 (2018).
19. Ouyang, R., Ahmetcik, E., Carbogno, C., Scheffler, M. & Ghiringhelli, L. M. Simultaneous learning of several materials properties from incomplete databases with multi-task SISSO. *J. Phys. Mater.* **2**, 024002 (2019).
20. Chen, T. & Guestrin, C. XGBoost: a scalable tree boosting system. In *Proc. 22nd ACM SIGKDD International Conference on Knowledge Discovery and Data Mining* 785–794 (ACM, 2016).
21. Medford, A. J. et al. Activity and selectivity trends in synthesis gas conversion to higher alcohols. *Top. Catal.* **57**, 135–142 (2014).
22. Schumann, J. et al. Selectivity of synthesis gas conversion to C_{2+} oxygenates on fcc(111) transition-metal surfaces. *ACS Catal.* **8**, 3447–3453 (2018).
23. Deimel, M., Reuter, K. & Andersen, M. Active site representation in first-principles microkinetic models: data-enhanced computational screening for improved methanation catalysts. *ACS Catal.* **10**, 13729–13736 (2020).
24. Deringer, V. L., Caro, M. A. & Csányi, G. Machine learning interatomic potentials as emerging tools for materials science. *Adv. Mater.* **31**, 1902765 (2019).
25. Gasteiger, J., Becker, F. & Günnemann, S. Gemnet. Universal directional graph neural networks for molecules. In *Conference on Neural Information Processing Systems* Vol. 34 (NeurIPS, 2021).
26. Wen, M., Blau, S. M., Spotte-Smith, E. W. C., Dwaraknath, S. & Persson, K. A. BonDNet: a graph neural network for the prediction of bond dissociation energies for charged molecules. *Chem. Sci.* **12**, 1858–1868 (2021).
27. Tang, Y.-H. & de Jong, W. A. Prediction of atomization energy using graph kernel and active learning. *J. Chem. Phys.* **150**, 044107 (2019).
28. Xie, T. & Grossman, J. C. Crystal graph convolutional neural networks for an accurate and interpretable prediction of material properties. *Phys. Rev. Lett.* **120**, 145301 (2018).
29. Montoya, J. H. & Persson, K. A. A high-throughput framework for determining adsorption energies on solid surfaces. *npj Comput. Mater.* **3**, 14 (2017).
30. Boes, J. R., Mamun, O., Winther, K. & Bligaard, T. Graph theory approach to high-throughput surface adsorption structure generation. *J. Phys. Chem. A* **123**, 2281–2285 (2019).
31. Deshpande, S., Maxson, T. & Greeley, J. Graph theory approach to determine configurations of multidentate and high coverage adsorbates for heterogeneous catalysis. *npj Comput. Mater.* **6**, 79 (2020).
32. Xu, W., Andersen, M. & Reuter, K. Data-driven descriptor engineering and refined scaling relations for predicting transition metal oxide reactivity. *ACS Catal.* **11**, 734–742 (2020).
33. Rupp, M. Machine learning for quantum mechanics in a nutshell. *Int. J. Quantum Chem.* **115**, 1058–1073 (2015).
34. Deringer, V. L. et al. Gaussian process regression for materials and molecules. *Chem. Rev.* **121**, 10073–10141 (2021).
35. Bruix, A., Margraf, J. T., Andersen, M. & Reuter, K. First-principles-based multiscale modelling of heterogeneous catalysis. *Nat. Catal.* **2**, 659–670 (2019).
36. Meskine, H., Matera, S., Scheffler, M., Reuter, K. & Metiu, H. Examination of the concept of degree of rate control by first-principles kinetic monte carlo simulations. *Surf. Sci.* **603**, 1724–1730 (2009).
37. Medford, A. J. et al. Assessing the reliability of calculated catalytic ammonia synthesis rates. *Science* **345**, 197–200 (2014).
38. Sutton, J. E., Guo, W., Katsoulakis, M. A. & Vlachos, D. G. Effects of correlated parameters and uncertainty in electronic-structure-based chemical kinetic modelling. *Nat. Chem.* **8**, 331 (2016).

39. Döpking, S. & Matera, S. Error propagation in first-principles kinetic monte carlo simulation. *Chem. Phys. Lett.* **674**, 28–32 (2017).
40. Flores, R. A. et al. Active learning accelerated discovery of stable iridium oxide polymorphs for the oxygen evolution reaction. *Chem. Mater.* **32**, 5854–5863 (2020).
41. Kunkel, C., Margraf, J. T., Chen, K., Oberhofer, H. & Reuter, K. Active discovery of organic semiconductors. *Nat. Commun.* **12**, 1–11 (2021).
42. Tran, K. et al. Methods for comparing uncertainty quantifications for material property predictions. *Mach. Learn. Sci. Technol.* **1**, 025006 (2020).
43. Palmer, G. et al. Calibration after bootstrap for accurate uncertainty quantification in regression models. *npj Comput. Mater.* **8**, 1–9 (2022).
44. Kuleshov, V., Fenner, N. & Ermon, S. Accurate uncertainties for deep learning using calibrated regression. In *International Conference on Machine Learning* 2796–2804 (MLR Press, 2018).
45. Giannozzi, P. et al. QUANTUM ESPRESSO: a modular and open-source software project for quantum simulations of materials. *J. Phys. Condens. Matter* **21**, 395502 (2009).
46. Wellendorff, J. et al. Density functionals for surface science: exchange-correlation model development with Bayesian error estimation. *Phys. Rev. B* **85**, 235149 (2012).
47. Huber, S. P. et al. AiiDA 1.0, a scalable computational infrastructure for automated reproducible workflows and data provenance. *Sci. Data* **7**, 300 (2020).
48. Xu, W., Reuter, K. & Andersen, M. *Predicting Binding Motifs of Complex Adsorbates Using Machine Learning with a Physics-Inspired Graph Representation* (Zenodo, 2022); https://doi.org/10.5281/zenodo.6640198
49. Larsen, A. H. et al. The atomic simulation environment—a Python library for working with atoms. *J. Phys. Condens. Matter* **29**, 273002 (2017).
50. Dal Corso, A. Pseudopotentials periodic table: from H to Pu. *Comput. Mater. Sci.* **95**, 337–350 (2014).
51. Garrity, K. F., Bennett, J. W., Rabe, K. M. & Vanderbilt, D. Pseudopotentials for high-throughput DFT calculations. *Comput. Mater. Sci.* **81**, 446–452 (2014).
52. Bartók, A. P., Kondor, R. & Csányi, G. On representing chemical environments. *Phys. Rev. B* **87**, 184115 (2013).
53. Esterhuizen, J. A., Goldsmith, B. R. & Linic, S. Theory-guided machine learning finds geometric structure–property relationships for chemisorption on subsurface alloys. *Chem* **6**, 3100–3117 (2020).
54. Andersen, M. & Reuter, K. Adsorption enthalpies for catalysis modeling through machine-learned descriptors. *Acc. Chem. Res.* **54**, 2741–2749 (2021).
55. Pedregosa, F. et al. Scikit-learn: machine learning in Python. *J. Mach. Learn. Res.* **12**, 2825–2830 (2011).

Acknowledgements

The authors gratefully acknowledge support from the Max Planck Computing and Data Facility (MPCDF) and the Jülich Supercomputing Centre (www.fz-juelich.de/ias/jsc). W.X. is grateful for support through the China Scholarship Council (CSC). M.A. acknowledges funding from the European Union's Horizon 2020 research and innovation programme under the Marie Skłodowska-Curie (grant agreement no. 754513), the Aarhus University Research Foundation, the Danish National Research Foundation through the Center of Excellence 'InterCat' (grant agreement no. DNRF150) and VILLUM FONDEN (grant no. 37381).

Author contributions

W.X. performed the DFT calculations, workflow and machine learning methods development. K.R. and M.A. conceived and supervised the project. All authors contributed to analyzing the data and writing the manuscript.

Competing interests

The authors declare no competing interests.

Additional information

Supplementary information The online version contains supplementary material available at https://doi.org/10.1038/s43588-022-00280-7.

Correspondence and requests for materials should be addressed to Mie Andersen.

Peer review information *Nature Computational Science* thanks Gyoung Na, Hongliang Xin and the other, anonymous, reviewer(s) for their contribution to the peer review of this work. Handling editor: Kaitlin McCardle, in collaboration with the *Nature Computational Science* team. Peer reviewer reports are available.

Reprints and permissions information is available at www.nature.com/reprints.

Publisher's note Springer Nature remains neutral with regard to jurisdictional claims in published maps and institutional affiliations.